

Modelling of a piled raft foundation as a plane strain model in PLAXIS 2D

A geotechnical case study of Nordstaden 8:27

Master of Science Thesis in the Master's Programme Infrastructure and Environmental Engineering

JOEL ALGULIN
BJÖRN PEDERSEN

Department of Civil and Environmental Engineering
Division of GeoEngineering
Geotechnical Engineering Research Group
CHALMERS UNIVERSITY OF TECHNOLOGY
Göteborg, Sweden 2014
Master's Thesis 2014:131

Modelling of a piled raft foundation as a plane strain model in PLAXIS 2D

A geotechnical case study of Nordstaden 8:27

*Master of Science Thesis in the Master's Programme Infrastructure and
Environmental Engineering*

JOEL ALGULIN

BJÖRN PEDERSEN

Department of Civil and Environmental Engineering
Division of GeoEngineering
Geotechnical Engineering Research Group
CHALMERS UNIVERSITY OF TECHNOLOGY

Göteborg, Sweden 2014

Modelling of a piled raft foundation as a plane strain model in PLAXIS 2D

A geotechnical case study of Nordstaden 8:27

Master of Science Thesis in the Master's Programme Infrastructure and Environmental Engineering

JOEL ALGULIN

BJÖRN PEDERSEN

© JOEL ALGULIN & BJÖRN PEDERSEN, 2014

Examensarbete / Institutionen för bygg- och miljöteknik,
Chalmers tekniska högskola 2014:131

Department of Civil and Environmental Engineering

Division of GeoEngineering

Geotechnical Engineering Research Group

Chalmers University of Technology

SE-412 96 Göteborg

Sweden

Telephone: + 46 (0)31-772 1000

Cover:

Pore pressure distribution below cross-section K after ten years of consolidation and an additional construction of two floors.

Chalmers Reproservice

Göteborg, Sweden 2014

Modelling of a piled raft foundation as a plane strain model in PLAXIS 2D
– A geotechnical case study of Nordstaden 8:27

Master of Science Thesis in the Master's Programme Infrastructure and Environmental Engineering

JOEL ALGULIN

BJÖRN PEDERSEN

Department of Civil and Environmental Engineering

Division of GeoEngineering

Geotechnical Engineering Research Group

Chalmers University of Technology

ABSTRACT

The aim of this report has been to, through a case study, investigate if a composite foundation, consisting of a piled raft, is possible to model in a satisfying way with the finite element computer software PLAXIS 2D, as well as investigate if an additional construction of storeys would be possible on the existing foundation. For the case study, a building in the shopping centre Nordstan in Gothenburg has been used. Documentation in form of construction drawings, soil tests and reports regarding the foundation of Nordstan has been used for the calculations. The soil model Soft Soil has been used since it is suitable for modeling deformations of clay, like the one present at the site of the case study. The structural element embedded pile row, which provides the opportunity to set the out-of-plane distance in spite of the two-dimensional modelling, has been used to model the piles. Different loading scenarios have been used in order to predict settlements for addition of different number of storeys. Comparisons between the soil models Soft Soil and Soft Soil Creep have been performed as well as comparisons between rafts with and without piles. In the conclusion it is stated that it seems possible to model the case study in a way that gives reasonable results regarding settlements, which indicates that a two-dimensional model can be a good and time efficient way to get a rough estimation of the capacity of a piled raft foundation. The embedded pile row element has a reasonable behaviour in the calculations, but comparisons to real testing of piles are needed. For further studies new soil tests are also needed. The results indicate that construction of additional storeys meets the demands regarding differential settlements and that deformations at connections to surrounding streets more likely will set the limits of design.

Key words: Piled raft, Plaxis 2D, Excavation, Settlements, Vertical soil deformations, Soft Soil, Gothenburg, Nordstan, Östra Nordstaden, Embedded pile row

Modellering av en samverkansgrundläggning som ”plane strain” model i PLAXIS 2D
– En geoteknisk fallstudie av Nordstaden 8:27

Examensarbete inom masterprogrammet Infrastructure and Environmental Engineering

JOEL ALGULIN
BJÖRN PEDERSEN

Institutionen för bygg- och miljöteknik
Avdelningen för geologi och geoteknik
Forskargruppen för geoteknik
Chalmers tekniska högskola

SAMMANFATTNING

Denna rapports ändamål har varit att, genom en fallstudie, undersöka huruvida en samverkansgrundläggning, bestående av en platta på pålar, går att modellera på ett bra sätt i det finita element-datorprogrammet PLAXIS 2D samt om en eventuell tillbyggnad av våningar skulle vara möjlig på den befintliga grundläggningen. Som fallstudie har en byggnad i köpcentret Nordstan i Göteborg använts. Dokumentation i form av konstruktionsritningar, jordtester samt rapporter om Nordstans grundläggning har använts för beräkningar. Jordmodellen Soft Soil har använts eftersom den är lämplig för att modellera sättningsbeteende i lerjordar likt den som finns vid fallstudien. Konstruktionselementet ”embedded pile row”, vilket ger möjlighet att ställa in avstånd i djupled trots tvådimensionell modellering, har använts för att modellera pålarna. Olika lastscenarion har använts i beräkningar för att förutsäga sättningar för olika antal våningar vid en eventuell tillbyggnad. Jämförelse mellan jordmodellerna Soft Soil och Soft Soil Creep har utförts liksom en jämförelse mellan plattor med och utan pålar. I rapportens slutsatser framkommer att fallstudien verkar gå att modellera på ett sätt som ger rimliga resultat i form av sättningar, vilket indikerar att en tvådimensionell modell kan vara ett bra och tidseffektivt sätt att få en grov uppfattning av en samverkansgrundläggnings kapacitet. Pålelementet har ett rimligt beteende i beräkningarna, men behöver jämföras med verkliga påltester. För fortsatta studier behövs det även utföras nya jordtester. Resultat indikerar att eventuell tillbyggnad klarar kraven för differentialsättningar och att sättningar vid förbindelser med omkringliggande gator snarare kommer bli dimensionerande.

Nyckelord: Samverkansgrundläggning, Plaxis 2D, Schaktning, Sättningar, Vertikala jorddeformationer, Soft Soil, Göteborg, Nordstan, Östra Nordstaden, Embedded pile row

Contents

ABSTRACT	I
SAMMANFATTNING	II
CONTENTS	III
PREFACE	VII
NOTATIONS	VIII

1	INTRODUCTION	1
1.1	Background	1
1.2	Aim	1
1.3	Limitations	2
1.4	Methodology	2
2	BUILDING FOUNDATIONS ON SOFT COHESIVE SOIL	3
2.1	Raft foundation	3
2.1.1	Contact pressure and settlements	3
2.2	Compensated foundations	4
2.3	Piled foundations	5
2.3.1	Friction piles	6
2.3.2	Negative skin friction - Down drag	6
2.3.3	Neutral plane	6
2.3.4	Settlements for piled foundations	7
2.4	Composite foundation - Piled raft	9
2.4.1	The creep pile principle	10
2.5	Magnitude of allowable settlements for foundations on soft cohesive soil	11
3	CASE STUDY OF NORDSTADEN 8:27	12
3.1	History of the area	12
3.2	Geotechnical conditions	13
3.2.1	Geology	13
3.2.2	Hydrogeological conditions	14
3.2.3	Soil properties - parameter evaluation	14
3.3	Foundation of Nordstan	22
3.4	Principles behind the foundation method of building 6	26
3.4.1	Bearing capacity of the soil	27
3.4.2	Bearing capacity of the piles	28
3.4.3	Settlements readings	29
3.5	Loads acting on the foundation	29
4	NUMERICAL ANALYSES. MODELLING IN PLAXIS 2D	31

4.1	Introduction to PLAXIS 2D	31
4.2	Soil models	32
4.2.1	Linear elastic (simplification of top layers)	32
4.2.2	Soft Soil (SS)	32
4.2.3	Soft Soil Creep (SSC)	33
4.3	Structural elements	35
4.3.1	Plate element	35
4.3.2	Embedded pile row element	36
4.4	Loads in PLAXIS 2D	39
5	VERIFICATION OF SOIL PARAMETERS AND SOIL MODELS	40
5.1	Soil tests performed in PLAXIS 2D	40
5.1.1	Axisymmetric model, Stepwise oedometer test	40
5.1.2	Triaxial soil test	41
5.2	Evaluating results	42
5.2.1	Stepwise oedometer simulations	42
5.2.2	Triaxial test simulations	46
6	MODELLING	47
6.1	Geometry and simplifications	47
6.2	Soil Model	50
6.3	Structural elements	51
6.3.1	Embedded pile row element	51
6.3.2	Plate element	52
6.4	Loads	53
6.4.1	Load scenarios	53
6.5	Mesh optimization	54
6.6	Phases	54
6.7	Validation analysis	55
6.8	Sensitivity analysis	55
7	RESULTS	57
7.1	Results from PLAXIS analyses	57
7.1.1	Excess pore water pressure	58
7.1.2	Settlements	60
7.1.3	Pile interaction	69
7.2	Sensitivity analyses results	71
7.3	Hand calculations	78
7.3.1	Stress distribution	78
7.3.2	Design demands	79
8	DISCUSSION	81

9	CONCLUSIONS	83
10	REFERENCES	84

Preface

This Master of Science Thesis has been conducted at the unit for geotechnical engineering at ELU, Gothenburg, between January 7th and June 18th in 2014. The project was initiated by ELU employees Bo Jansson and Lars Hall.

The authors would like to mention a number of people who have been of great help and made this project possible:

We would like to thank our supervisor at ELU, Lars Hall, and ELU employee Therese Hedman for support during the spring in 2014. Furthermore we would like to thank the rest of the employees at ELU, especially Bo Jansson, Hans Lindewald, Mehras Shahrestanakizadeh, Fredrik Olsson, Anders Beijer and Anna Iversen.

We would also like to thank Torbjörn Pettersson at Vasakronan, Malin Klarquist at the Urban Planning Department of Gothenburg and Björn Petersson at WSP for providing us with useful information about the building Nordstaden 8:27. Likewise we would like to thank Professor Emeritus Sven Hansbo, responsible for the foundation of the case study building, for explaining questions regarding his, at the time unconventional, foundation method.

Lastly we would like to direct our appreciation to Professor Minna Karstunen at Chalmers University of Technology for providing us with feedback as well as always taking time to answer question and discuss different kinds problems encountered during the process.

Gothenburg, June 2014

Joel Algulin and Björn Pedersen

Notations

Roman upper case letters

A	cross section area of pile
B	width of raft
C_v	coefficient of consolidation
C_c	compression index
C_s	swelling index
C_α	creep index
D	depth of raft below closest adjacent surface
E	Young's modulus
E_{ck}	characteristic Young's modulus for concrete
EA	normal stiffness
EA_1	normal stiffness for plate element in PLAXIS 2D
EI	flexural rigidity
G_s	specific gravity
K_0^{NC}	earth pressure coefficient for normally consolidated soil
K_0^{OC}	earth pressure coefficient for over consolidated soil
L	length of raft
L_p	length of pile
L_{pilei}	length of pile part i in Figure 3.18
$L_{spacing}$	pile spacing perpendicular to the model plane
N	bearing capacity of pile toe
O	circumference of pile
OCR	over consolidation ratio
R	bearing capacity of pile
R_i	bearing capacity of pile part i in Figure 3.18
T_{max}	skin resistance of embedded pile row element
$T_{top, max}$	skin resistance at pile top for embedded pile row element
$T_{bot, max}$	skin resistance at pile bottom for embedded pile row element

Roman lower case letters

b	width of plate element
c'	cohesion for Mohr Coulomb criteria
c_u	corrected undrained shear strength
d_{eq}	equivalent thickness of plate element
d_i	diameter at pile part i in Figure 3.18
d_{pile}	diameter of pile
e	void ratio
e_0	initial void ratio
h	height of plate element
h_p	depth from +3.5 in Figure 3.18
k	permeability
k_y	vertical permeability
k_x	horizontal permeability
m_v	coefficient of volume compressibility
p'	mean effective stress
p'_p	effective preconsolidation pressure
POP	over consolidation formulated as $POP = \sigma'_c - \sigma'_0$
$q_{excavated\ soil}$	weight of excavated soil
q_{ground}	bearing capacity of the ground
$q_{newbuilding}$	load from new building
q_{piles}	bearing capacity of piles/area per pile
q_{water}	uplifting water pressure
r_{ou}	dry density of timber
r_u	real density of timber
u	moisture content
u_i	circumference at pile part i in Figure 3.18
u_{pile}	expression for circumference of lower pile part in Figure 3.18
w_{plate}	weight of plate element material
w_L	liquid limit
w_N	natural water content
x	length along raft from left to right
z	depth from level y

Greek lower case letters

α	adhesion factor
α_{rp}	ratio of load carried by piles for a piled raft
γ_{pile}	unit weight of pile material
γ_{soil}	unit weight of soil
γ_w	unit weight of pore water
ε	one-dimensional strain
ε_{0v}	initial volumetric strain
ε_{0v}^e	initial volumetric strain during elastic response
ε_v	volumetric strain
ε_v^c	change of creep rate in time
ε_v^e	volumetric strain during elastic response
κ^*	modified swelling index
λ^*	modified compression index
μ^*	modified creep index
μ	correction factor for undrained shear strength
ν	Poisson's ratio
$\nu_{concrete}$	Poisson's ratio of concrete
σ_0'	in-situ effective earth pressure
σ_1'	effective vertical earth pressure
σ_3'	effective horizontal earth pressure
σ_c'	effective preconsolidation pressure
σ_{creep}'	effective creep pressure
σ_m	bearing capacity of raft
τ	reference time for oedometer test
τ_{fu}	undrained shear strength of the soil
ϕ'	friction angle
ψ	dilatancy angle

1 Introduction

In 1970's the shopping centre Nordstan was completed. Professor Sven Hansbo implemented a new method when designing the foundation of the building. The foundation method constitutes of a composite foundation with a piled raft, combined with effects of uplifting water pressure and compensated weight of excavated soil. Today, about 40 years later, the property owner, Vasakronan, is looking at the possibility of expanding the building, by adding floors. To investigate if this is possible, they have hired the consultancy company ELU.

This Master thesis was initiated with the belief that the foundation of Nordstan was designed according to the creep pile principle. That kind of foundation method is rather unusual today, which made ELU interested in the design and theory behind the foundation method as well as whether or not it was possible to construct additional floors.

1.1 Background

The shopping centre Nordstan is situated in the northern part of central Gothenburg. It is one of the largest shopping centres in Europe and consists of nine buildings, numbered 1-9 according to Figure 1.1, with a total gross floor of approximately 300 000 m². The buildings are connected by streets and a roof. They also share a common basement, where there are streets and loading docks. Nordstan was built between 1965 and 1976 (Fritz, 1997).



Figure 1.1 Overview of Nordstan shopping centre, including object numbering of the buildings. (Svensson, 1993)

The building Nordstaden 8:27, which is in focus of the case study of this report, is also known by the object number 6. The building is owned by Vasakronan and the storeys of the house mainly consist of bank offices and department stores.

1.2 Aim

The aim of this project is to investigate the foundation principle of a piled raft and how well this can be modelled with numerical analysis, using a plane strain model in the computer software PLAXIS 2D. A case study model has been made of the building Nordstaden 8:27.

The aim of the case study model in PLAXIS 2D, can be divided into the objectives listed below:

- Determine to what extent it is possible to model a piled raft, with the complexity of Nordstan, as a plane strain problem in PLAXIS 2D.
- Determine to what extent the structural element embedded pile row is working when modelling a piled raft.
- Determine what geotechnical effects increasing loads, due to additional construction, would have in terms of settlements.

1.3 Limitations

When constructing on soft soil, deformations generally sets the limits for how large loads can be applied to the foundation and is therefore the focus of this thesis.

The numerical calculations have been limited to 2D and only the building itself have been taken into consideration for the numerical modelling. No consideration has been taken to for example surrounding streets and buildings.

Construction drawings from before construction have been used as a basis for the modelling and no consideration has been taken to any reconstruction. The property owner states that the loads on acting on the foundation should be more or less the same today as after reconstruction of the building¹.

1.4 Methodology

In order to perform this investigation a literature survey regarding foundation methods, commonly used on soft soil, have been carried out. Also a literature survey of the foundation of the building, in the case study of Nordstaden 8:27, has been carried out through articles, construction drawings, existing soil tests and documentation of the building process. There was little documentation found regarding the details of the design of building 6. However, such documentation was found for building 5, which foundation was designed in a similar manner (Hansbo, Hoffman and Mosesson, 1973).

Numerical analyses, with the finite element computer software PLAXIS 2D, have been performed with focus on the real case scenario from Nordstan. The soil models used in the case study model have been calibrated to match with existing soil tests. A literature survey on different soil models and structural elements in PLAXIS has also been made.

Elevation values mentioned in this thesis are corresponding to the local coordinate system of Gothenburg used during the 20th century. In this system the datum line is situated about 10 m below sea level.

¹ Torbjörn Petterson, technical manager at Vasakronan, interviewed 14-02-20

2 Building foundations on soft cohesive soil

This chapter contains information about different foundation methods for constructing buildings on clay.

The main purpose of a foundation is to transmit loads to the underlying soil. This results in a soil-structure interaction. The foundation method which is most suitable depends on the properties of the soil and the functional requirements of the building.

Since structural parts of a building often have higher stiffness and strength than underlying soil, support is generally done by the use of shallow foundations (Hansbo, 1989). An example of this is enlarged ground plates (or slabs) which distributes the loads over a larger area. However, if the soil stratum near the surface is not capable to give sufficient support, deep foundations as piles or caissons may be used to transfer the loads to larger depths, where the soil often has higher strength and stiffness (Craig and Knappet, 2012).

2.1 Raft foundation

A large single slab which supports the structure as a whole is called a raft. Raft foundations are used to distribute structural loads when the bearing capacity of the underlying soil is low. A slab can cover the entire bottom area of the building or several smaller ones can be strategically placed below pillars or walls (Hansbo, 1989). A single raft is preferable in order to reduce differential settlements or when there are local parts of the soil where the strength deviates. The raft can have an even thickness or have stiffer parts where structural loads from walls or pillars are transmitted. It can be designed with a stiffness large enough for the contact pressures to be assumed equally distributed throughout the plate. Otherwise the distribution will depend on the relative stiffness between plate and soil (Bergdahl, Malmberg and Ottosson, 1993).

2.1.1 Contact pressure and settlements

The distribution of the contact pressure depends on the mechanical properties of the soil in combination with the stiffness of the foundation plate. The flexural rigidity of a slab, resting on soil, is often very large compared to the deformability of the material below (Hansbo, 1989).

As to be expected, the settlements are uniform for a completely rigid foundation slab. However the contact pressure is not. When a rigid foundation slab is placed directly on cohesive soil, and a uniform load is applied, the contact pressure at the edges reaches high values that causes plastic deformation, see Figure 2.1. The shear stress under the edge of the foundation reaches, but cannot exceed, the shear strength of the clay, i.e. the contact pressure at the edges reaches a limit based on the shear strength of the clay. As the load on the foundation slab gradually increases, the zone of plastic deformation grows towards the centre of the slab. Thus, the contact pressure distribution depends on the shear strength of the clay as well as the applied load (Hansbo, 1989).

The contact stress distribution for a flexible raft is uniform and the settlement distribution is largest in the middle, according to Figure 2.2 (Holtz, 1991).

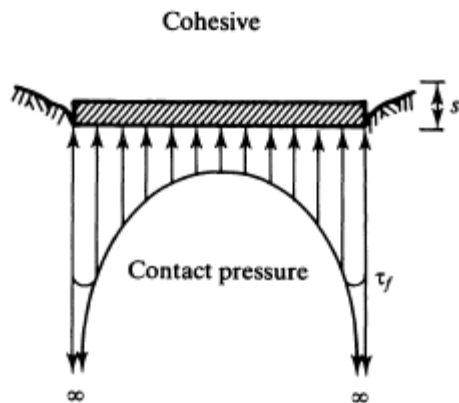


Figure 2.1 Contact stress distribution and settlements for a rigid raft (Holtz, 1991).

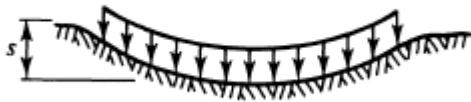


Figure 2.2 Contact stress distribution and settlements for a flexible raft (Holtz, 1991).

A gradual equalization of the contact pressure can be expected over time. With this in mind, the errors are presumed to be negligible when designing a foundation slab with evenly distributed pressure (Jendeby, 1986a).

2.2 Compensated foundations

Excavations are often performed to such a large depth that the weight of the excavated soil exceeds the weight of the building. The building is constructed with a single slab and “floats” on the soil like a raft on water. This kind of foundation can be suitable when constructing buildings on thick homogenous layers of silt or clay (Hansbo, 1989).

When constructing these kinds of foundations on clay the slab is often situated below the groundwater table, which adds an uplifting water pressure on the slab. Even if the slab is made of watertight concrete there is still a small permeability in the same magnitude as clay. This results in a water flow directed upwards through the slab and consequently a lowering of the pore water pressure in the clay. This risk can be eliminated if a highly permeable layer of sand or gravel were to be placed between the “watertight” slab and a layer of concrete casted directly on the clay. Groundwater will then be able to flow freely through this layer and the water level will be at least the same as in the surrounding clay. If the building, or parts of it, is encircled by sheet pile walls, different parts of the pore water pressure can be controlled. This makes it possible to reduce differences in effective stress on the slab. Water pressure can be controlled, with respect to the size of the loads on different parts of the slab, in order to not fall short of respectively exceed a certain value (Hansbo, 1989).

2.3 Piled foundations

When designing foundations with piles, the two main aspects to take into consideration are bearing capacity and settlements. For a foundation on clay, settlements are almost exclusively the limiting factor (Jendeby, 1986a).

The main reason for using piles in a foundation design is to transfer applied loads to a greater depth of the soil. Deeper layers of the soil, due to their stress history, normally have higher strength and stiffness compared to more shallow layers and therefore would have greater resistance to settlement.

When a pile is subjected to a vertical force at the top of the pile, the pile head, shear stresses are mobilised in the ground that surrounds the pile. If the created shear stress exceeds the shear strength of the soil, ground failure will occur. Two different parameters decide the capacity:

1. Shear stress that is developed in the soil around the pile toe
2. Shear stress that is developed at the interface between the shaft and the surrounding soil.

This leads to two types of pile classification; end bearing piles and shaft bearing piles, see Figure 2.3. However, this classification describes special cases. In the normal case, the pile resistance depends on both end and shaft resistance (Alén, 2012).

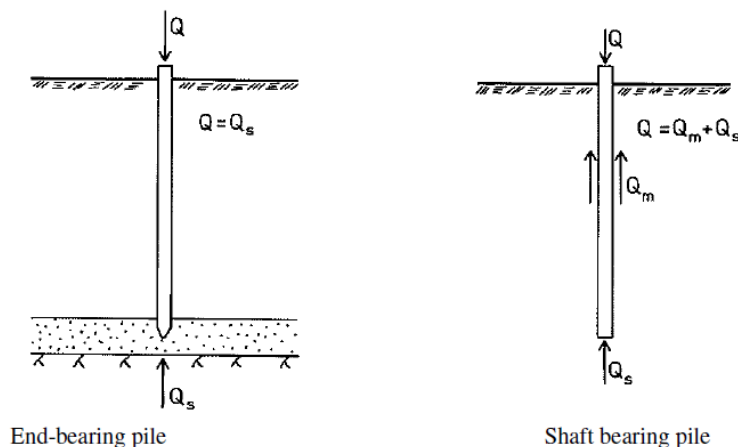


Figure 2.3 Principal sketches of how a shaft respective end bearing pile work (Alén, 2012).

The usual long and slender dimension of a pile makes axial loading the most beneficial way to use them. The failure load of a pile is defined as the load acting on a pile when the soil no longer can carry the transmitted load. The creep load of a pile is defined as the biggest load that can be applied to the pile, without achieving a substantial increase of settlements (Holm and Olsson, 1993).

Piled foundations are, almost exclusively, constructed as a group of piles. A group has the dual effect of both carrying the load down to deeper layers of the soil as well as reinforcing the soil. A failure of the group can either occur as a failure of a single pile or as a failure of the whole reinforced block of soil. Block failure is in general more likely to happen with close spacing of the piles (Flemming et al., 1992).

The capacity of a single pile in a group may be lower than a single isolated pile. This is due to the fact that the capacity of each single pile within a group may be affected

by the remoulding of surrounding soil, when other piles are installed in close proximity (Flemming et al., 1992).

2.3.1 Friction piles

A friction pile utilises the shaft bearing principle, according to Figure 2.3 above. A foundation which includes friction piles can act differently depending on the duration of the load. Thus, the bearing capacity should be controlled with regards to both short-term and long-term loads. For the settlements calculation, only the long-term load is considered in a normal case (Eriksson et al., 2004).

2.3.2 Negative skin friction - Down drag

Due to settlements, soil surrounding the pile can start to move downward relative the pile. This creates negative skin friction. The negative skin friction acts as down drag, an extra load on the pile. Thus, it is the relative movement between the pile and the soil that determines the size of the additional load. The action effect in the pile equals the sum of the negative skin friction and the loading at the pile head (Alén, 2012). The shaft friction is considered to be fully developed with a relative movement of 2-5 mm. Common practice is to take the effect into consideration along the part of the pile where the soil settles 5 mm more than the pile (Eriksson et al., 2004).

A simplified evaluation of the risk of down drag can be made by using the same relationship as when evaluating the risks for long term settlements, creep, described in equation 3.8. With this approach, negative skin friction is considered along the pile, where the vertical stress is bigger than the creep limit.

2.3.3 Neutral plane

The neutral plane is defined as where the relative movement between the soil and the pile is zero, i.e. the pile and the soil settle equally (Fellenius, 2004). For this to happen, the pile needs to be in equilibrium state. The equilibrium state is when the sum of all external loads on the pile as well as the down drag equals the bearing capacity of the pile. This means that on a certain depth, the down drag of the pile changes into friction resistance (Eriksson et al., 2004). This is illustrated in Figure 2.4.

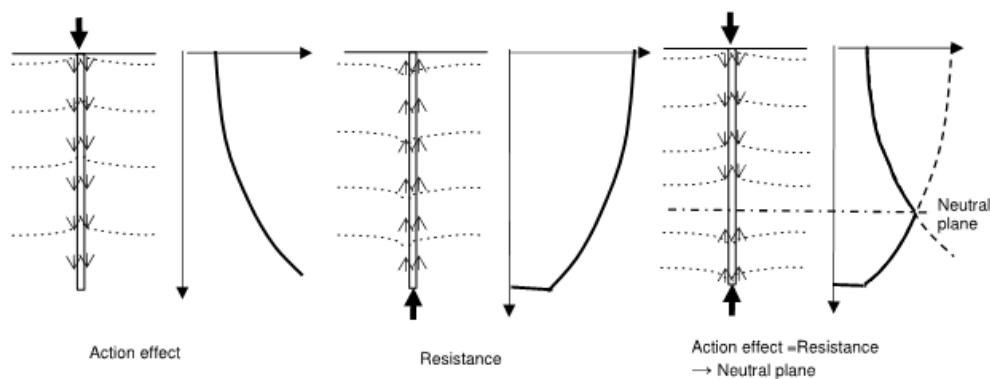


Figure 2.4 Description of the neutral plane for shaft bearing piles (Alén, 2012).

The neutral plane principle is based upon an assumption of ongoing settlements in the ground, i.e. the pile is subjected to negative skin friction, or down drag. In a real case scenario, this might not be the case. However, as described above, relative movements as small as 2-5 mm are required to develop full friction between the soil and the pile shaft. If despite that, no settlements would occur below a certain depth, no additional loading by down drag can occur below that depth. This creates a zone of equal strain that “pushes” the neutral plane further down, see Figure 2.5. Thus, the concept of the neutral plane is on the safe side (Alén, 2012).

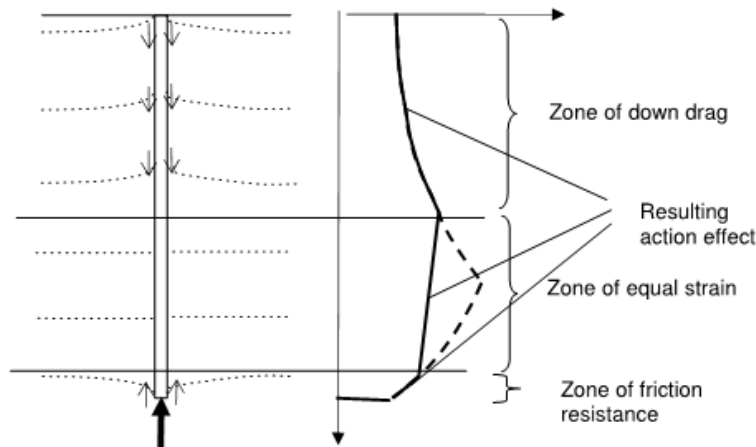


Figure 2.5 Behaviour of the neutral plane due to zone of equal strain (Alén, 2012).

2.3.4 Settlements for piled foundations

Settlements of a pile foundation are caused by an increase of effective stress in the soil. The neutral plane governs the settlement analysis of a piled foundation. When calculating settlements on a piled foundation, the applied loads can be transferred to an “equivalent footing” placed at the location of the neutral plane, i.e. the loading from the upper levels are transmitted through the piles and distributed downwards from the neutral plane. The settlement of the whole piled foundation is considered to be the same as for the equivalent footing, Figure 2.6 (Fellenius, 2004).

For a large group of piles, the reinforcing effect of the piles to the surrounding soil must be taken into consideration, when calculating settlements for the equivalent footing. This can be done by combining the stiffness moduli of the soil and piles into a combined modulus. The new modulus is applied between the neutral plane level and the pile toe level. The combined modulus is usually so large that the settlements between the neutral plane level and the pile toe level can be neglected. Therefore, a simplified approach can be made by placing the equivalent footing at the pile toe level (Fellenius, 2004).

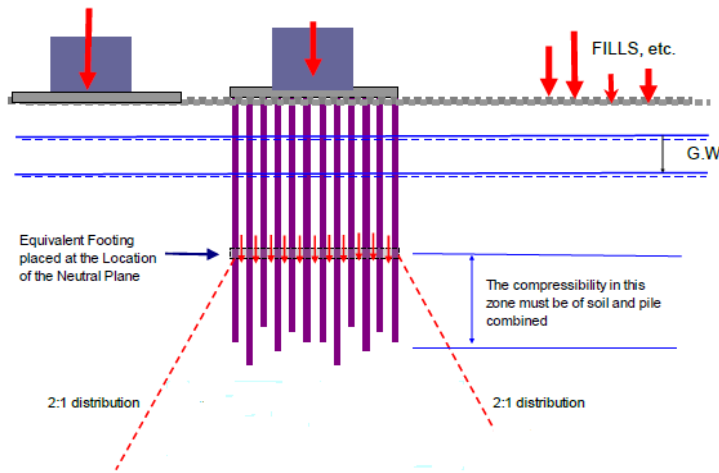


Figure 2.6 Placement of the simplified equivalent footing (Fellenius, 2004).

Bearing capacity of friction piles

Settlement calculations are based on the bearing capacity of the piles. In Sweden, the geotechnical bearing capacity for friction piles is usually decided with the α -method (Eriksson et al., 2004). In soft soils, α stands for the relationship between the undrained shear stress that can be developed between the shaft area and the surrounding soil, and the shear strength of the soil. According to Alén (2012) α can be set to 1.2 for timber piles with an upward increasing section area. As illustrated above, the resistance of a pile, R , is decisive for where the neutral plane is located. R is described by equation 2.1 (Eriksson et al., 2004).

$$R = \int_0^{L_p} \alpha * c_u * O \, dz + N * A * c_u \quad (2.1)$$

where:

L_p = length of the pile

α = adhesion factor

O = pile circumference

c_u = corrected undrained shear strength

N = bearing capacity factor for the pile toe

A = pile cross section area

For toe resistance to be fully developed, a considerable larger deformation than 2-5 mm is needed. An approximated value is 10 % of the pile width. Thus, due to the large deformations required, it might not be possible to account for the complete end resistance of the pile, when using the formula above. Therefore, the end bearing resistance of a friction pile in soft soil is usually neglected (Alén, 2012).

2.4 Composite foundation - Piled raft

According to Eriksson et al. (2004) there are three different design methods for piled rafts:

- The “conventional case”. Foundations where all load is carried by friction piles. In a case like this, the piles have to acquire sufficient bearing capacity as well as reduce the settlements.
- Foundations where the load distribution is divided between the friction piles and the contact pressure from the soil on a foundation slab. Used when the weight of the excavated soil only covers part of the applied load. The piles main function here is to reduce settlements. The creep pile principle can be applied for such foundations.
- Foundations where all applied load can be carried by the contact pressure against the foundation slab. In such cases, the friction piles are placed under concentrated loads and their primary function are to decrease the dimensions of the overlying constructions, such as the foundation slab. This is suitable when all applied loads can be compensated by excavating soil.

Most foundations constructed on clay are within the limits from a bearing capacity perspective without the use of piles (Jendenby, 1986b). The main reason for adding pile elements to the raft is usually not to carry the major part of the loads but to reduce average and differential settlements (Kulhawy and Prakoso, 2001). Therefore, the piles are designed to act both as soil reinforcing and settlement reducing elements, as well as to take care of concentrated loads acting on the raft. The distribution and number of piles is decided upon these criteria. This enables the design of the foundation to be optimized and the number of piles to be reduced, which generally is the most cost effective approach (Hansbo and Källström, 1983).

The load sharing mechanism of a piled raft, as well as its stiffness and resistance, is regulated by the soil structure interactions between the load bearing components of the foundation, i.e. the piles, the raft and the soil (Giretti, 2009). The raft is often designed to carry loads of the same size as the preconsolidation pressure (Jendenby, 1986a).

As illustrated in Figure 2.7, a piled raft foundation can be assumed to have four kinds of interactions. Each interaction is governed by the parameters of the three elements, for example stiffness, shear strength of the soil, pile spacing and pile length. The pile-soil and pile-raft interactions are described in earlier in this chapter. The pile-pile interaction can be defined as additional settlements of a pile, caused by a loaded adjacent pile, and the pile-raft interaction can be defined as additional settlement of the raft caused by supporting piles (Nguyen, Jo and Kim, 2013).

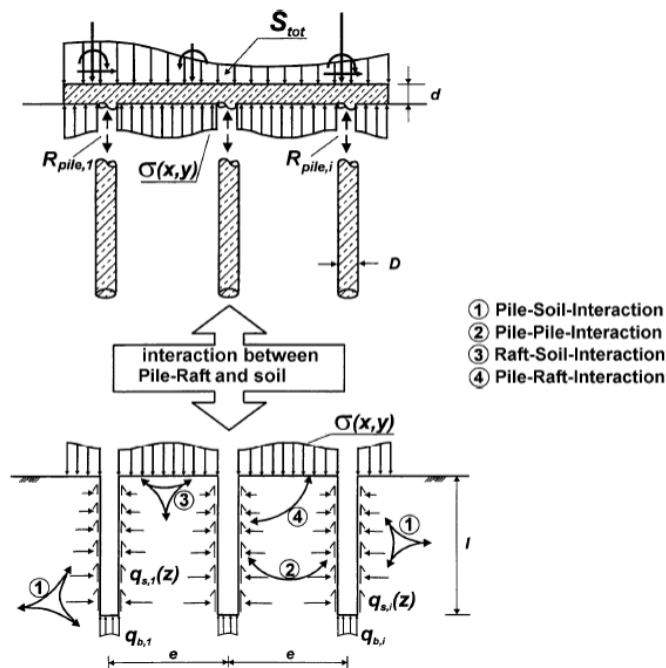


Figure 2.7 The four different interactions of a piled-raft foundation (Katzenbach, Gutberlet and Bachmann, 2007).

2.4.1 The creep pile principle

The use of a relatively high safety factor when designing a piled foundation could result in a scenario where the surrounding soil settles more than the foundation, which would mean that no contribution from contact pressure between soil and raft could be accounted for. The principle of a piled raft foundation is to distribute the loads between the raft and the piles. To achieve this, the design of the factor of safety of the piles is close to unity, which means that the neutral plane is designed to be located at or close to the bottom of the raft (Fellenius, 2004). With the piled raft method, the piles can be designed to make the potential settlements of the foundation be the same as the settlements of the surrounding soil. This is done through a better utilisation of the piles, by designing them to be exposed of a load equal to their creep load, causing a state of creep failure (Fredriksson and Rosén, 1988).

The design should ensure that the contact stress is uniformly distributed across the raft (Fellenius, 2004). The ability of a construction to distribute forces horizontally is especially governed by the stiffness of the construction (Eriksson et al., 2004). Since there is pressure acting on the raft, it will generally have to be thicker and more reinforced than in a conventional piling case.

The theory behind the principle is to take advantage of the compensation in effective stress created by the excavated soil. A certain percentage (Q_1) of the total applied load (Q), can be carried without piles, due to the compensation. The remaining part of the load ($Q - Q_1$) has to be carried by the pile system. For example, if a raft can carry 80% of the load without causing substantial settlements, the piles has to carry the remaining 20% of the load. Thus, the purpose of using the creep pile principle is to maximize the pile capacity in order to control that a certain part of the load will be carried by the raft. The pile spacing is chosen to regulate the amount of load carried by piles (Hansbo and Jendenby, 1998).

The load-settlement behaviour for different design approaches, concerning a piled raft, is presented in Figure 2.8. Curve 0 represents the behaviour of a raft acting alone. Curve 1 represents the conventional design approach. Curve 2 illustrates the “creep pile principle”, in which the piles are designed with a lower factor of safety. Curve 3 represents the use of full utilization of the piles at the design load, by strategically placing the piles as settlement reducers. The reduction in number of piles for curve 2 and 3, results in a larger amount of load carried by the raft. Fewer piles results in a more economical design (Poulos, 2001).

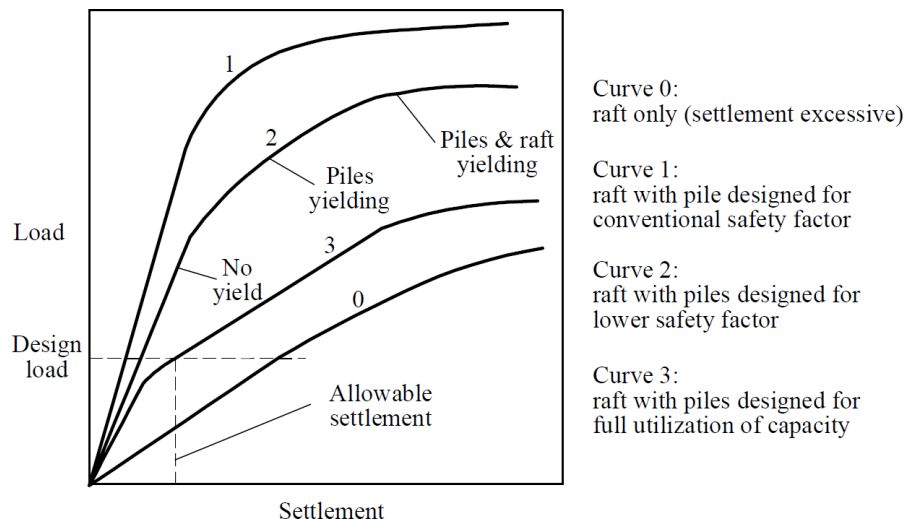


Figure 2.8 Load-settlement behaviour for a piled raft, comparing different design approaches (Poulos, 2001).

2.5 Magnitude of allowable settlements for foundations on soft cohesive soil

A settlement analysis should involve more than just an upper boundary. Both total amount of settlements as well as differential settlements needs to be evaluated. The magnitude of acceptable settlements varies with the size and type of structure (Fellenius, 2006).

The differential settlement ratio is calculated as the difference in settlement of two edges of a section, divided by the length between them. In Appendix E, allowable settlement limits for structures, according to Holtz (1991), are presented. It underlines that the settlement demands varies depending on the type of structure and its function.

3 Case study of Nordstaden 8:27

This chapter contains information about the case study building and its surroundings. It also contains information about geotechnical conditions at the site, in form of evaluations made from test documentation.

3.1 History of the area

The district Östra Nordstaden is situated north of Stora Hamnkanalen and east of Östra Hamngatan and was earlier a district of emigrant hotels, storehouses and brasseries. This is also the place where “Chalmer’s crafting school” once started in the first half of the 19th century. Most of the buildings were from the late 18th or early 19th century. Since the 1970’s, this area is totally dominated by the shopping centre Nordstan. (Fritz, 1997).

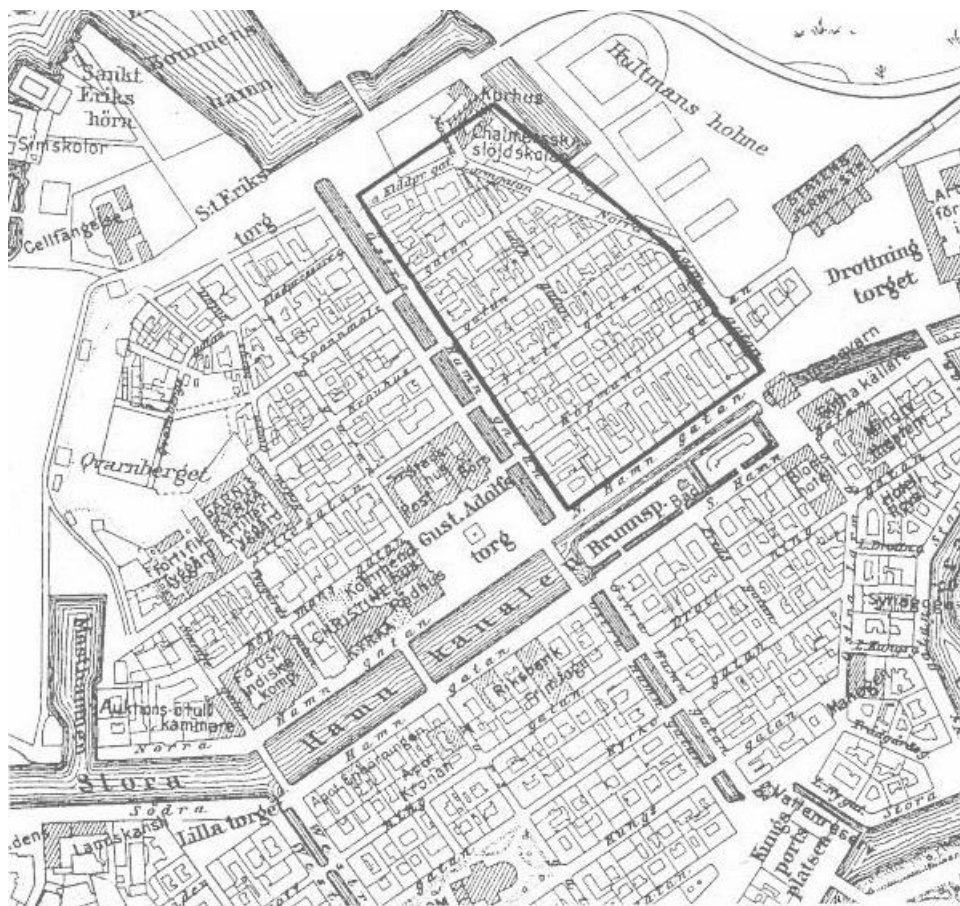


Figure 3.1 Map of Östra Nordstaden from around 1860. The location where Nordstan shopping centre later was erected is marked by thick lines. The top corner of this marking is where Chalmers Crafting School was located at the time (Fritz, 1997).

In the middle of the 20th century, the existing buildings were in a rather bad condition (Fritz, 1997). It was deemed not economically justified to reconstruct or restore them. In November 1959 it was therefore decided that, in order to prevent the ongoing deterioration into slum of the northern part of central Gothenburg, a redevelopment of Östra Nordstaden was to take place. The old buildings were to be torn down and a modern shopping centre to be erected in their place (Hansbo, Hoffman and Mosesson,

1973). The first buildings, 1 and 2, were constructed during the years 1965-68, while buildings 3 to 9 were constructed during the years 1970-76.

3.2 Geotechnical conditions

The geological data used for the case study of this thesis come from investigations performed by AB Flygfältsbyrå and Jacobson & Widmark AB (J&W AB) in 1966, during planning of the reconstruction. The tests consist of in-situ testings as Field Vane Tests (FVT) and Cone Penetration Tests (CPT), as well as standard laboratory tests, consisting of stepwise oedometer tests and fall cone tests. Oedometer tests were performed on soil from two boreholes, 1 and 17b, in the area and down to a depth of 25 meters. Boreholes used for the tests are presented in Figure 3.2.

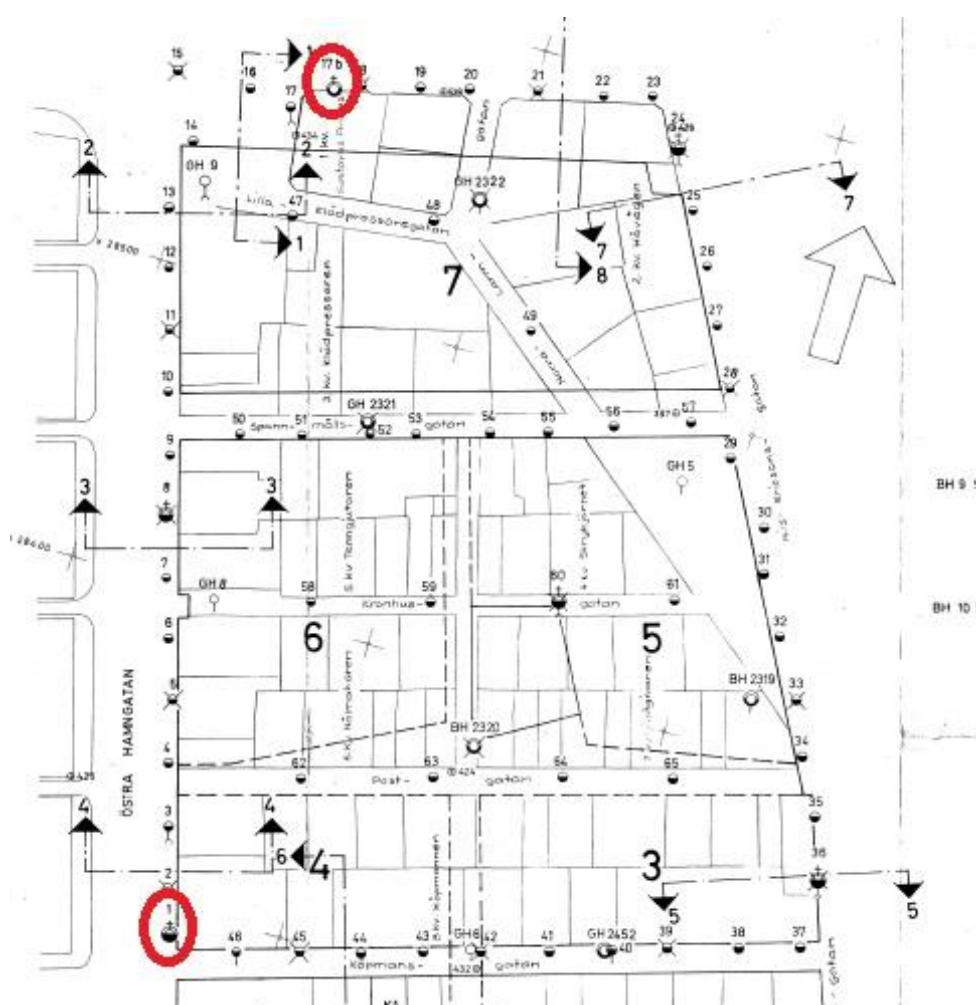


Figure 3.2 Plan of boreholes from the investigation performed by AB Flygfältsbyrå and J&W AB. Boreholes 1 and 17b, where samples for the oedometer tests have been taken, are marked by ellipses.

3.2.1 Geology

The ground level at building 6 is approximately at +12.1. It consists of 1.5-3 m fill on top of a deep layer of clay. In the southwest corner the depth of the clay layer is 49 m.

Below there is a 2 m thick layer of frictional soil resting on the bedrock. In the other three corners the clay and friction soil layers has a thickness of approximately 90 and 10 m respectively. Sampling of soil has been made to a depth of 40 m (Svensson, 1993).

3.2.2 Hydrogeological conditions

The mean groundwater level for the area is approximately at level +10.1. There is a hydrostatic overpressure of 20-30 kPa at a depth of 20 m. There is however no information on what level this overpressure starts (Svensson, 1993).

3.2.3 Soil properties - parameter evaluation

This chapter presents parameters evaluated from the obtained tests as well as assumptions made regarding other parameters that will be of importance for this thesis.

Unit weight - γ_{soil}

The volume weight is uniform with depth and has an approximate value of 1.6 t/m³. The data is transformed into unit weight, γ_{soil} [kN/m³]. A graph of the unit weight plotted versus level can be seen in Appendix C.

Natural water content - w_N

The natural water content, w_N , is obtained from standard tests in laboratory, and is plotted versus level in Figure 3.3. The graph indicates a homogeneous layer of clay, apart from the highlighted area, which implies that there is a section with higher water content.

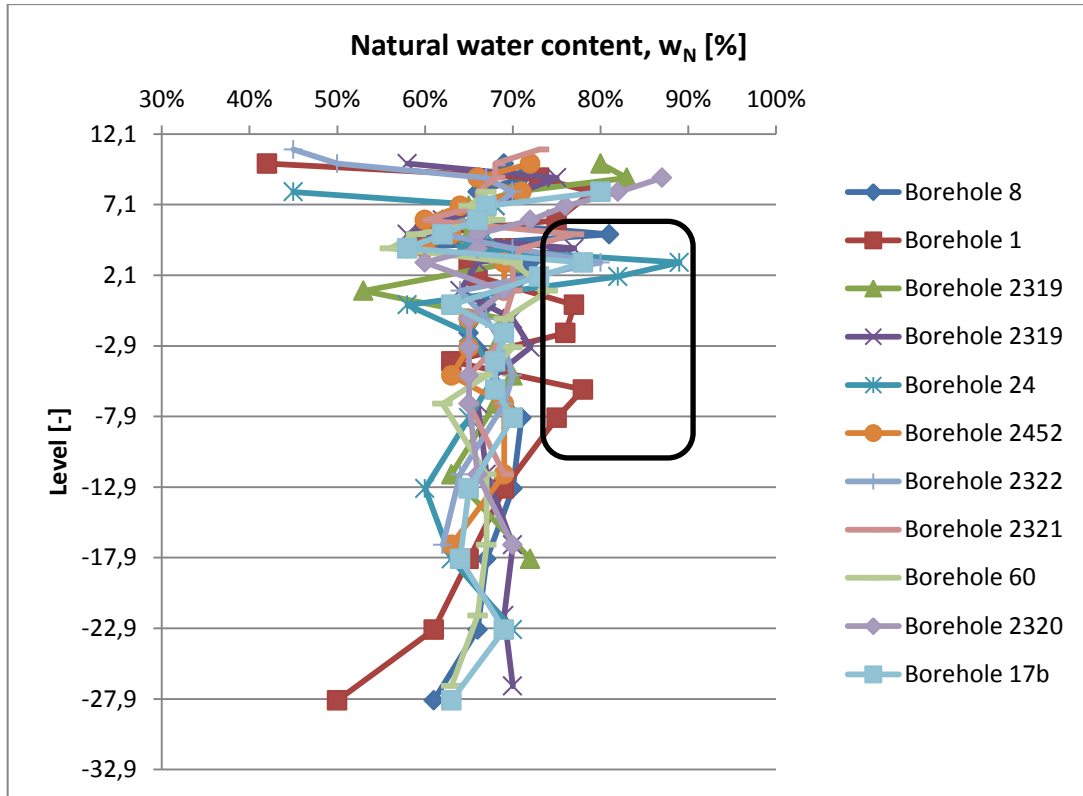


Figure 3.3 Natural water content plotted versus level.

Initial void ratio - e_0

If the soil is assumed to be fully saturated, the initial void ratio can be calculated according to equation 3.1 (Wood, 1990). The specific gravity, G_s , is assumed to 2.71.

$$e = w_N * G_s \quad (3.1)$$

Liquid limit - w_L

The liquid limit is relatively constant with depth at approximately 70%. A graph of the liquid limit plotted versus level can be seen in Appendix C.

Corrected undrained shear strength - c_u

The shear strength, τ_{fu} , is evaluated from data obtained through field vane tests for samples from 8 boreholes and at multiple levels. As vane tests are not as much subject to sample disturbance, they are likely to be more accurate than cone tests, therefore only data from vane tests have been used, even though cone tests were available. The undrained shear strength is overestimated if the liquid limit, w_L , is high. To consider this, equations 3.2 and 3.3, has been used to obtain the corrected undrained shear strength, c_u (Helenelund, 1977).

$$\mu = \left(\frac{0.43}{w_L} \right)^{0.45} \quad (3.2)$$

$$c_u = \mu * \tau_{fu} \quad (3.3)$$

Corrected undrained shear strength is plotted versus level in Figure 3.4 and an approximation is described by equation 3.4.

$$c_u = (22 + 1.07 * z) \text{ kPa} \quad (3.4)$$

where:

z = meters of depth starting at level 3.5.

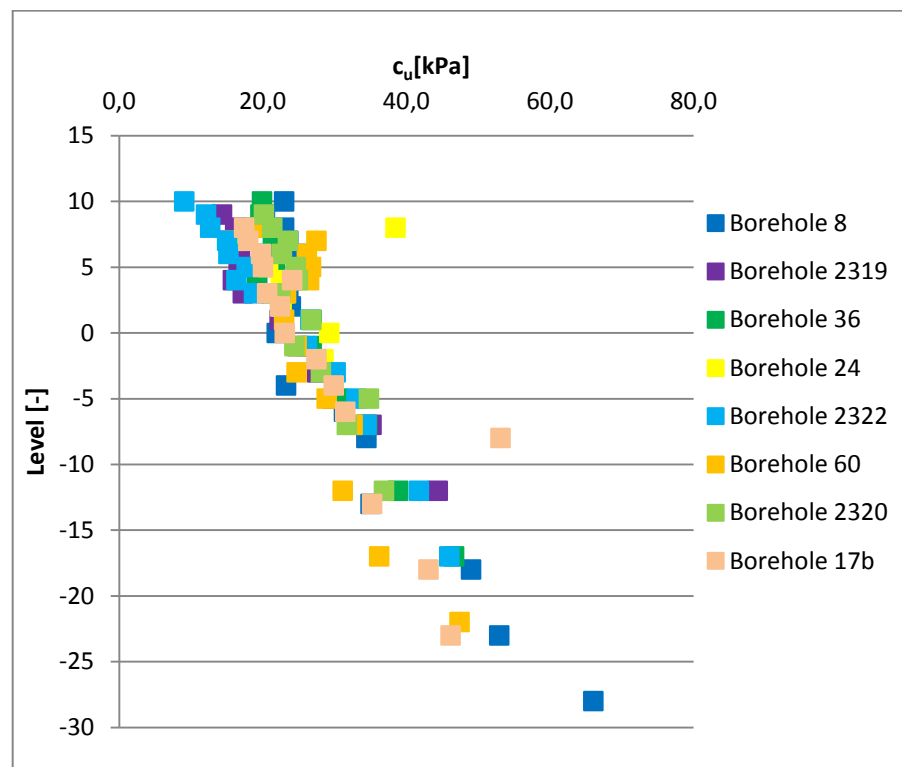


Figure 3.4 Undrained shear strength plotted versus level.

Vertical and horizontal permeability - k_y and k_x

The behaviour over time for the consolidation process can be decided with the consolidation coefficient C_v , presented in equation 3.5.

$$C_v = \frac{k}{\gamma_w * m_v} \quad (3.5)$$

where:

k = permeability

m_v = coefficient of volume compressibility

γ_w = Unit weight water

C_v and m_v are evaluated from the oedometer tests. The vertical permeability, k_y , is evaluated from equation 3.5 and is presented for different depths in Figure 3.5. No data are available for the horizontal permeability, k_x . Due to previous buildings in the area which probably have caused an anisotropic stress state and fabric, k_x is assumed according to equation 3.6.

$$k_x = 1.5 * k_y \quad (3.6)$$

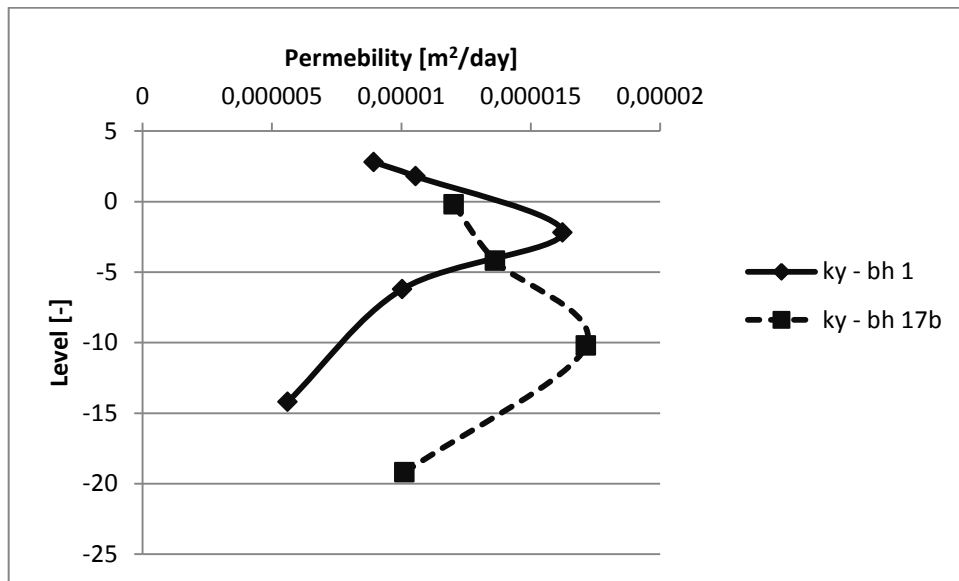


Figure 3.5 Vertical permeability k_y plotted versus depth.

Compression, swelling and creep indices

The compression index, swelling index and creep index are evaluated from oedometer tests.

The inclination of the virgin compression line equals the compression index C_c , see Figure 3.6, and thus, C_c can be described by equation 3.6. C_c is decisive for the consolidation settlements (Craig and Knappet, 2012).

$$C_c \text{ or } C_s = \frac{e_0 - e}{\log\left(\frac{\sigma'_1}{\sigma'_0}\right)} \quad (3.7)$$

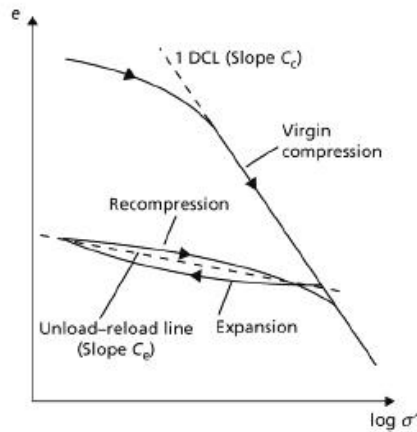


Figure 3.6 Principal skis of a stepwise oedometer test curve with compression and swelling indices (Craig and Knappet, 2012).

In Figure 3.7, the compression indices for the two evaluated boreholes are plotted versus level. Both compression index curves seem to follow a similar pattern.

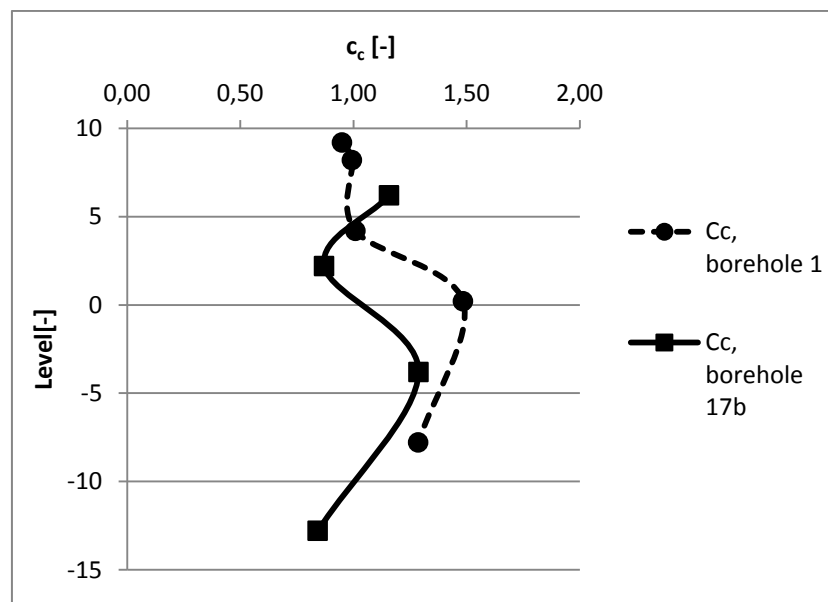


Figure 3.7 Compression index plotted versus level.

The swelling index C_s (also known as expansion index), is evaluated by approximating a straight line between the unloading and reloading curves, see Figure 3.6, which makes it decisive for the swelling of the soil as well as the elastic settlements. It can, like C_c , be described by equation 3.6. In Figure 3.8, the swelling indices for the two evaluated boreholes are plotted versus level. The two curves diverge at the deepest samples. Ideally the swelling index is determined at the stress level where any unloading due to excavation process are expected to take place. Unfortunately this is not often done and hence (just like in this case) the values relate to the unloading at the end of the test.

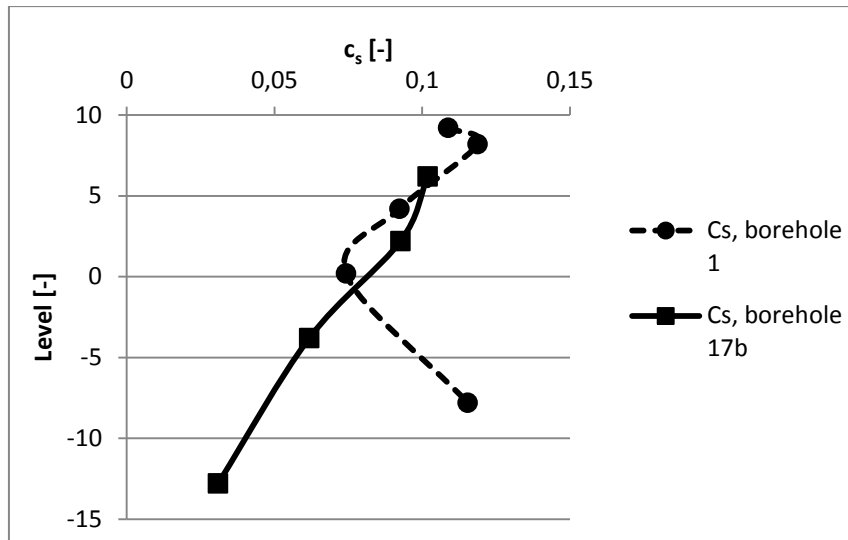


Figure 3.8 Swelling index plotted versus level

Creep index

The rate of secondary compression, or creep index C_{α} , is evaluated as the inclination of the final part of the semi-logarithmic graph in figure Figure 3.9.

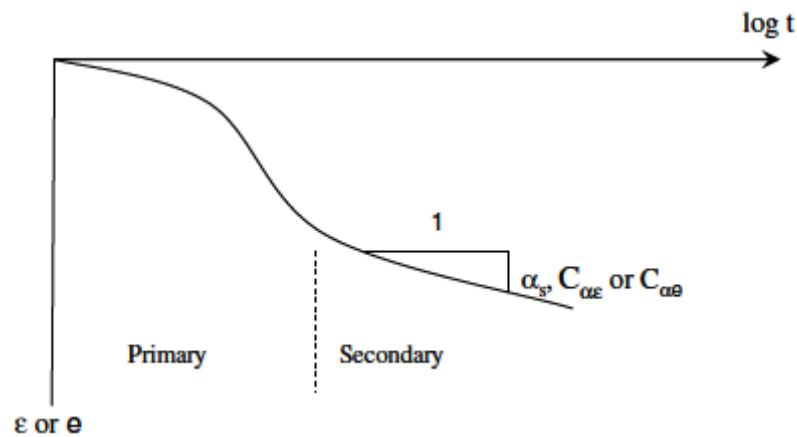


Figure 3.9 Oedometer test plotted as logarithmic time versus strain/void ratio (Olsson, 2010).

In Figure 3.10 the creep index for the two evaluated boreholes are plotted versus level. Both creep index curves seem to have similar patterns, but with the data from borehole 17b reaching higher values.

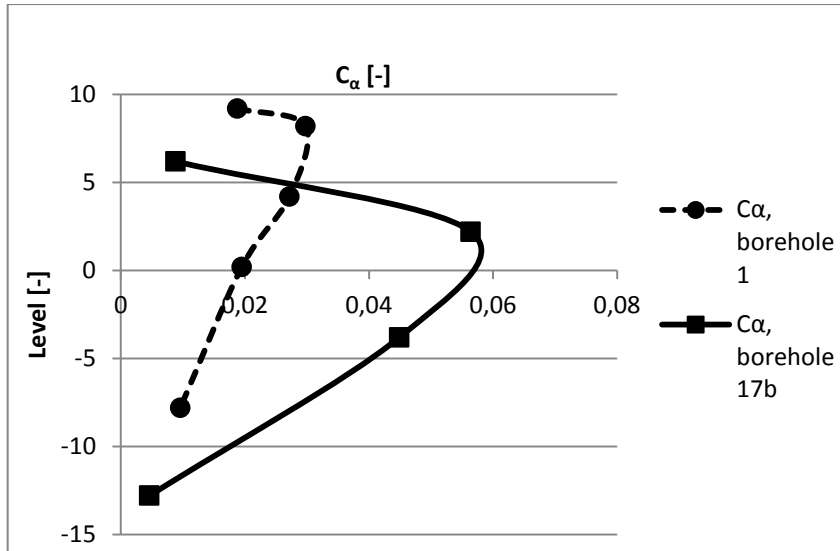


Figure 3.10 Creep index plotted versus level

Stress analysis

The preconsolidation pressure, σ'_c , is obtained from the oedometer test according to Casagrande's method. A tangent is drawn at the point where the radius of the curve is smallest. A horizontal line is drawn from the same point and thereafter a bisector of the angle between the two lines. The "straight part" of the oedometer curve is extended upwards. Where the extended line intersects with the bisector corresponds empirically to the preconsolidation pressure, see Figure 3.11. (Larsson, 2008).

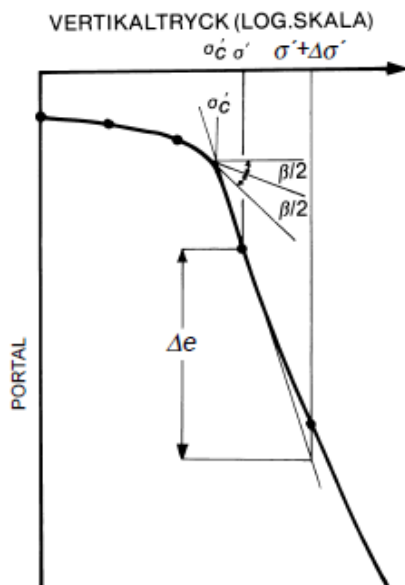


Figure 3.11 Principal steps of how to use Casagrande's method to obtain preconsolidation pressure from an oedometer test (Larsson, 2008).

Stress analyses of both in situ conditions and current conditions, caused by the existing building, are presented in Figure 3.12. The threshold limit for creep is also

shown in the graph. Tests performed on Swedish clays show that the secondary compression is rather low until the compression corresponds with an effective vertical stress according to equation 3.8 (Larsson, 1986).

$$\sigma'_{creep} = 0.8 * \sigma'_c \quad (3.8)$$

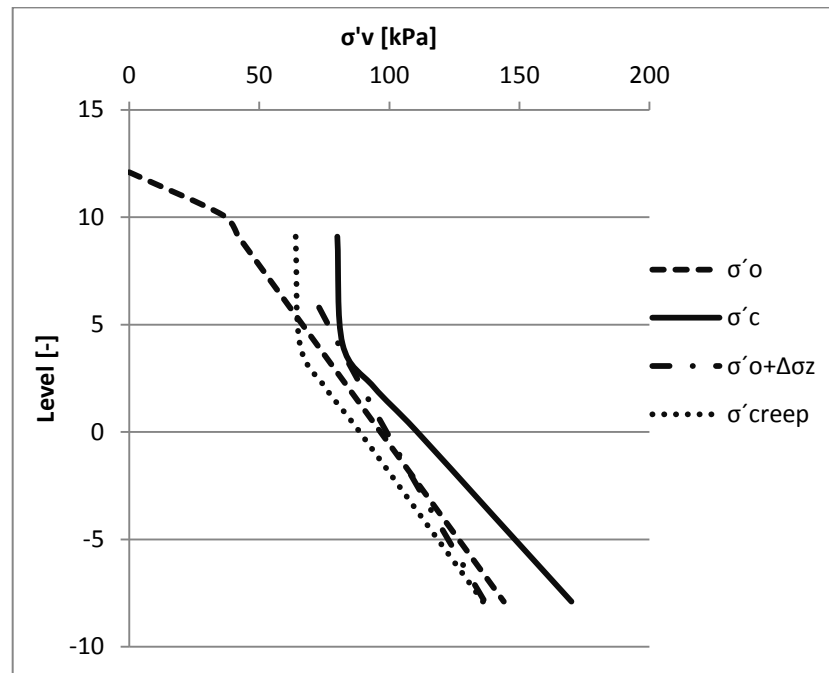


Figure 3.12 In situ, preconsolidation and creep stresses plotted versus level. The change in stress from the construction is also plotted

Since no triaxial tests from the site are available, the values for parameters ν , ϕ' , ψ and c' have all been assumed. The assumed values of these properties are presented in Table 3.1.

ν = Poisson's ratio

ϕ' = Friction angle

ψ = Dilatancy angle

c' = Cohesion

Table 3.1 Assumed values for soil parameters due to lack of triaxial tests.

ν	ϕ'	ψ	c'
0.15	30°	0	1

Earth pressure coefficients - K_0^{NC} and K_0^{OC} at rest

For normally consolidated soils, the value of K_0^{NC} can be obtained by using the friction angle, ϕ' , according to equation 3.9, proposed by Jaky in 1944 (Craig and Knappet, 2012).

$$K_0^{NC} = 1 - \sin \phi' \quad (3.9)$$

For overconsolidated soils, K_0^{OC} depends on the stress history of the clay, which can be taken into consideration with equation 3.10, proposed by Mayne and Kulhawy in 1982 (Craig and Knappet, 2012).

$$K_0^{OC} = (1 - \sin \phi') * (OCR)^{\sin \phi'} \quad (3.10)$$

3.3 Foundation of Nordstan

Due to the local building rules, the height of the building complex was restricted to 28 m. Thus, to have more capacity, it was beneficial to place the foundation of the building as deep as possible into the ground to gain extra area from floors below ground. The optimum depth was decided to be two basement floors, requiring a maximum depth of excavation of about 8 m. All buildings in the complex have a common roof and also share a common basement with a total area of 58 700 m² (Svensson, 1993).

Buildings 1-3 are founded on individual footings with spliced timber piles with a length of 30 m (Hansbo, Hoffman and Mosesson, 1973). The piles are concentrated in groups below the columns of the building above. The weight of these buildings is not compensated by the excavated soil. The foundations of buildings 4-9 is carried out with a combination of the compensation principle, the use of underlying water pressure and friction piles. This is further explained below (Svensson, 1993).

The level of the raft for the different sections are presented in Figure 3.13 (ök = upper edge, uk = lower edge). The foundation level differs among the sections between +5.90 and +7.30. Buildings 6 and 9 both contain a bank vault, where the foundation level has been lowered to +4.50 m and +5.60 m respectively. The ground level is situated at about 12.1 m (Svensson, 1993).

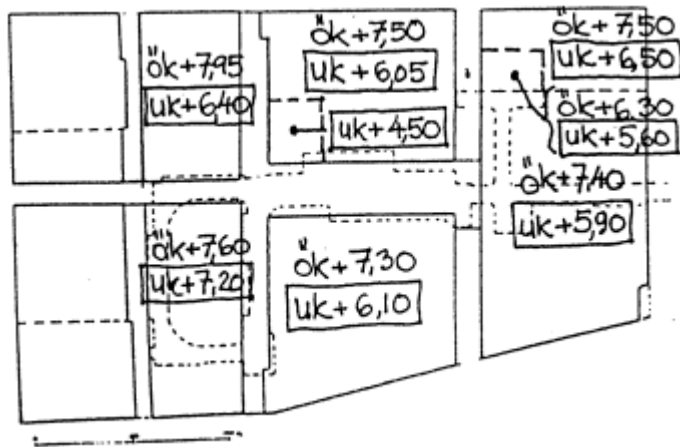


Figure 3.13 Rough sketch of raft levels for the buildings of Nordstan shopping centre (Svensson, 1993).

Below lighter areas, basement parts which consists of streets or have courtyards above, the groundwater has to maintain a level between +8.90 and +9.60. This is to prevent great loads from hydraulic uplift.

As mentioned above, the foundation principle for building 6, Nordstaden 8:27, is a combination of the compensation principle, the use of underlying water pressure and the utilisation of friction piles. The building is positioned so deep that full compensation is obtained. To compensate for the relatively heavy weight from a bank vault and the higher parts of the building, the south-east corner of the ground plate consists of caissons. Compared to the rest of the building the foundation level is lower there, which results in a higher degree of compensation and a higher water pressure acting on the raft. The excavation level is +5.8 under areas without caissons, and +4.25 under areas with them.

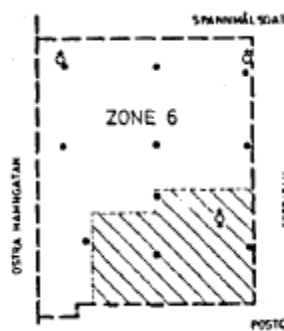


Figure 3.14 Drawing of building 6. The location of the caissons is seen in the down right corner (Hansbo, Hoffman and Mosesson, 1973).

The raft is made of waterproof concrete. The dimensions of the plate are obtained from Figure 3.15. The major part of the ground plate, i.e. the part which does not include the caissons, has a height of 1150 mm of concrete. The total height of the caissons is approximately 3000 mm.

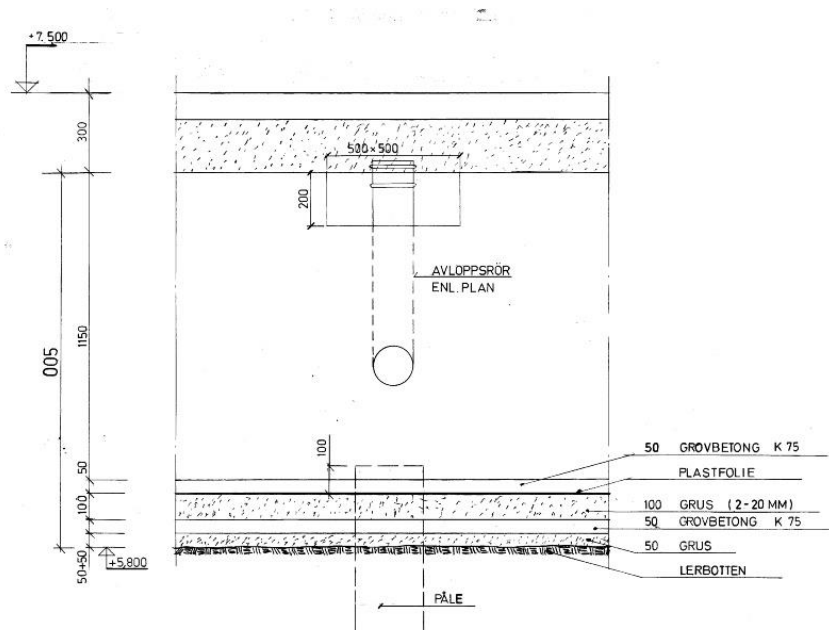


Figure 3.15 Details of the raft including underlying material (concrete K75, plastic foil, gravel (2 – 20 mm), concrete K75, gravel, clay). All dimensions are given in [mm].

Since the groundwater level is located above the foundation level, the loads from the building is partly carried by water pressure, acting on the raft from below. In order to maintain a high groundwater pressure below heavier parts and reduce it below lighter parts, groundwater conditions are regulated. Beneath the raft there is a 10 cm thick permeable layer of gravel. Wooden sheet piles create watertight sections and separate the ground beneath the object, and even parts within the object itself. Because of this the level of the groundwater table varies between different areas. Each encircled area has a regulated water level, controlled by pumps, which automatically handles refill and overflow when needed. There are four different watertight sections beneath building 6. Their positions are presented in Figure 3.16.

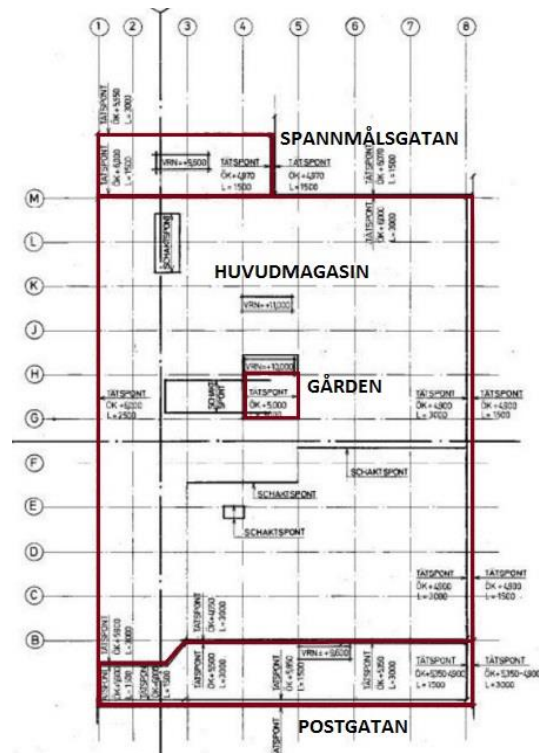


Figure 3.16 Water reservoirs below building 6. The borders of the four different reservoirs are marked with thicker red lines and adjacent names.

As can be seen in Table 3.2, there is a difference between the level set as a limit in the design and the measured water level in the main reservoir. This is due to problems in maintaining the set level. The owners could not tell for how long the level has been this low².

² Torbjörn Petterson, technical manager at Vasakronan, interviewed 14-02-20

Table 3.2 Reservoir levels for building 6

Reservoir	Date	Set water level	Measured water level	Water level according to construction drawing
Gården (Yard)	1974, 1975		+9.08 - +9.5	+10
	2003-08-18	+9.47	+9.47	
	2003-10-20	+9.47	+9.47	
	2012-02-xx		+9.73	
Huvudmagasin (Main reservoir)	1974, 1975		+10.06 - +10.3	+11
	2003-08-18	+9.92	+9.86	
	2003-10-20	+9.92	+9.80	
	2012-02-xx		+9.86	
Postgatan	1974, 1975		+9.41 - +9.57	+9.6
	2003-08-18	+9.40	+9.56	
	2003-10-20	+9.40	+9.38	
	2012-02-xx		+9.44	
Spannmålskatan	1974, 1975		+8.78 - +9.39	+9.6
	2003-08-18		+9.47	
	2003-10-20		+9.47	
	2012-02-xx		+9.73	

The piles are made of timber and have a length of 20 m. The tip diameter is about 0.125 m with an increase of 0.8 cm per m. The pile spacing varies between 1.5-2.4 m, depending on the weight of the building above. Due to the theory of contact pressure for a rigid raft on cohesive soil, discussed in section 2.1.1, the pile spacing is smaller at the edges, since the pressure is higher there.

3.4 Principles behind the foundation method of building 6

Below information is presented on how the design was performed before construction. As can be seen when evaluating the design demands below, see equations 3.11-3.14, the raft alone should be sufficient to carry the building. As stated by Hansbo (1973), the main reason for using friction piles under the raft was mainly to eliminate the risk of differential settlements. Many of the former buildings at the site were founded on timber piles. The unknown amount of remaining piles in the soil could act as reinforcement of the soil, creating great variations in modulus of the subsoil. For the same reason, there were difficulties to estimate the heave of soil during the excavation phase. Thus, a mat of friction piles under a raft was deemed as an appropriate solution. With this foundation method, the disturbance effects caused by installation of the piles as well as heave of the soil during excavation could both be ignored (Hansbo, Hoffman and Mosesson, 1973).

The design demands which the foundation were based on are presented below:

$$1. \quad q_{newbuilding} < q_{excavatedsoil} \quad (3.11)$$

$$2. \quad q_{newbuilding} < q_{ground} + q_{water} + \frac{q_{piles}}{3} \quad (3.12)$$

$$3. \quad q_{newbuilding} < q_{ground} + \frac{q_{piles}}{2} \quad (3.13)$$

$$4. \quad q_{newbuilding} < q_{water} + \frac{q_{piles}}{2} \quad (3.14)$$

where:

$q_{newbuilding}$ = load from the new building

q_{water} = uplifting water pressure

$q_{excavatedsoil}$ = weight of excavated soil

q_{ground} = bearing capacity for the ground

q_{piles} = bearing capacity of the piles/area per pile

Since the bearing capacity of the piles is divided by the area covered by each pile to obtain q_{piles} , the pile spacing was designed to obtain the safety factor of 2.

According to Hansbo, this was the first time foundation design was based on interactivity between friction piles and pressure against the raft. The safety factor used against failure according to conventional methods at the time was set to three. In this case, which can be seen in demands 3 and 4 above, a safety factor of two was used. Thus, the foundation of Nordstan can be seen as an introduction to the creep pile principle, implementing a better utilisation of the piles³.

3.4.1 Bearing capacity of the soil

During the design of the foundation the bearing capacity of the soil was calculated with equation 3.15, according to Svensk Byggnorm 67 (Statens planverk, 1968).

$$\sigma_m = 1.7 * \left(1 + 0.2 * \frac{D}{B}\right) * \left(1 + 0.2 * \frac{B}{L}\right) * \tau_{fu} + 0.1 * \gamma_{soil} * D \quad (3.15)$$

if $D/B \leq 2.5$

where:

D = depth of raft below closest adjacent surface

B = width of raft

L = length of raft

τ_{fu} = undrained shear strength of the soil

γ_{soil} = unit weight of the soil

³ Sven Hansbo, Professor Emeritus, interviewed 14-02-24

D was chosen as zero. τ_{fu} was set to its minimum value of 2.5 MP/m². (2.5 MP/m² was the minimum shear strength from the parameter evaluation made in 1966, where correction factor of shear strength was not considered). The bearing capacity was calculated to 5.1 MP/m² (approximately 51 kPa).



Figure 3.17 Definitions of D and B for equation 3.15 (Statens planverk, 1968).

3.4.2 Bearing capacity of the piles

During the design of the foundation the bearing capacity of the piles was calculated with equations 3.16 – 3.20, according to Pålnormer sbn-n 23:6. The equation only takes the shaft resistance into consideration and is based on Figure 3.18. It should be noted that values in the figure does not consider the building in the case study, but the principle however is accurate.

$$R = R_1 + R_2 \quad (3.16)$$

$$R_1 = \frac{u_2 + u_3}{2} * L_{pile1} * \tau_{fu} \quad (3.17)$$

$$R_2 = \int_0^{L_{pile2}} u * \tau_{fu} dh_p \quad (3.18)$$

$$u = u_3 - \frac{h_p}{L} * (u_3 - u_1) \quad (3.19)$$

$$\tau_{fu} = 0.18 * h_p \quad (3.20)$$

where:

R = bearing capacity of pile

R_i = bearing capacity of pile part i

d_i = diameter at pile part i

u_{pile} = expression for circumference of lower pile part in Figure 3.18

u_i = circumference at pile part i

L_{pilei} = length of pile part i

τ_{fu} = undrained shear strength of the soil

h_p = depth from +3.5 in Figure 3.18. (written as h in the figure)

The shear strength is constant with a value of 2.5 MP/m² (approximately 25 kPa) down to the level of 3.5 m. From that level it is increasing with 0.18 MP per m (approximately 1.8 kPa/m). The pile is divided into two sections according to Figure 3.18

Bearing capacity of the piles was calculated to 45.9 MP.

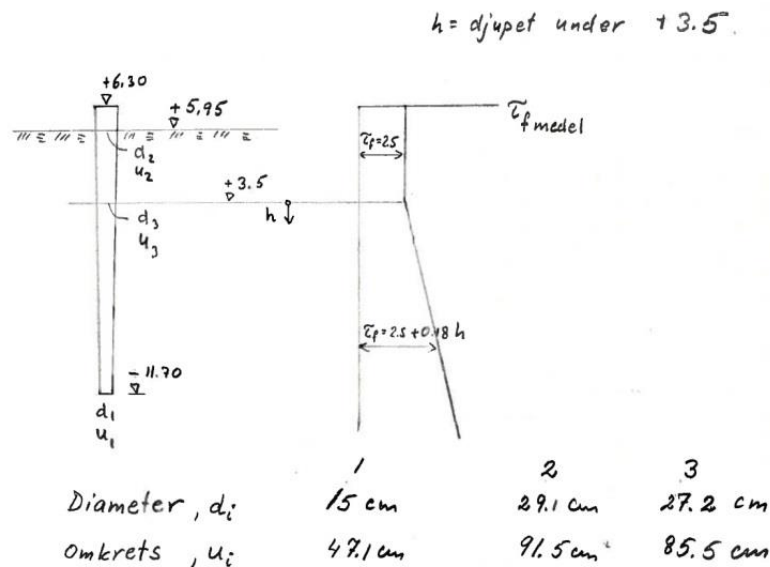


Figure 3.18 Principal sketches of how calculations of pile bearing capacity was made during design.

3.4.3 Settlements readings

Settlement readings for the building have been performed on continuous basis, since 1978, and are presented in Appendix F. The maximum settlement measured is about 15 mm and the maximum heave about 10 mm. The settlements are quite evenly distributed.

Due to water leakage, the water supply was shut down during a major part of 2007. During this period, the settlements increased rapidly. When the water levels were restored the building heaved to its previous position. The lowest level of the water during this period was not recorded.

3.5 Loads acting on the foundation

The applied loads from the building have been assessed, using the construction drawings in Appendix A. In the construction drawings, the loads for each floor are specified. The loads transferred down through the building are divided into dead-weight load and working load. For settlements, it is the long-term loads that needs to be considered. The working load is transformed into permanent load based on the ongoing activity on each floor. The permanent load addition from department stores

can be approximated as 60% of their working load, whereas 30 % percent of the office load is considered as permanent load⁴. When the building was erected, the three lower floors were used both as department stores and offices, in this thesis, they are considered as department stores. The rest of the floors were used as offices, which they also are considered to be in this thesis.

The facade consists of lightweight material (Gustafsson et al., n.d.). Therefore, the load contribution from the facade is considered to be negligible. The load contribution from pillars is approximated as 10 kN per floor. This is considered to be included in the dead weight of each floor. The snow load is neglected due to the long-term perspective⁴. The loads are summarized for each pillar, and is presented in Appendix B.

The weight of the raft is calculated with the input parameters in Table 3.3.

Table 3.3 Unit weight of materials at raft foundation.

Material	Unit weight [kN/m³]
Saturated macadam (Larsson, 2008)	21
Unsaturated macadam (Larsson, 2008)	18
Concrete ⁴	25

Characteristic loads are used as input for PLAXIS. Therefore, no partial factors have been applied on the loads. The total long term load of the building, including the weight from both pillars and raft, is calculated to 96 kPa. The weight of the excavated soil is approximated to 104.8 kN/m/m. The water pressure acting on the raft is approximated to 43 kPa.

⁴ Hans Lindewald, Structural Engineer at ELU, interviewed 14-03-17

4 Numerical analyses. Modelling in PLAXIS 2D

This chapter contains information about the finite element computer software PLAXIS 2D.

4.1 Introduction to PLAXIS 2D

PLAXIS 2D is developed for analysis of deformation and stability problems for different types of geotechnical situations in two dimensions. A geometry model is created in the x-y plane of the global coordinate system, with the z-axis as the out of plane direction, see Figure 4.1. Despite the fact that it is a two dimensional application, stresses are based on the 3D Cartesian coordinate system, according to Figure 4.1. According to the sign convention, compressive stresses are negative (PLAXIS, 2014b).

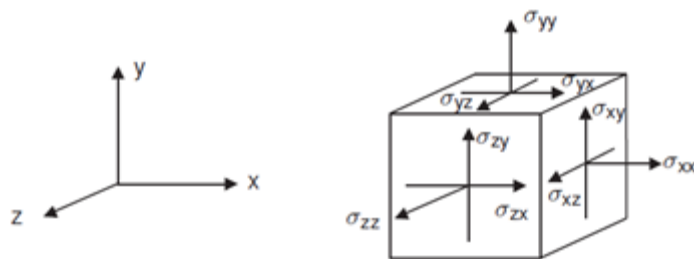


Figure 4.1 Definition of coordinate systems in PLAXIS 2D (PLAXIS, 2014b).

Real scenarios can be modeled with a plane strain or an axisymmetric model, see Figure 4.2. The plane strain model is suitable to implement with a relatively uniform cross-section, loading scheme and a great extent in the z-direction. Normal stresses in the z-direction are fully considered but the displacements and strains are assumed to be zero. The axisymmetric model is suitable when modelling circular structures with a relative uniform radial cross section and loading scheme around the central axis. The stress state and deformations are considered to be equal in any direction (PLAXIS, 2014b).

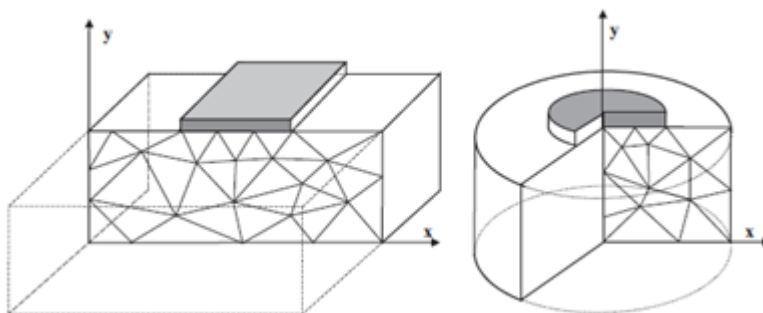


Figure 4.2 Comparison between plane strain and axisymmetric models in PLAXIS 2D (PLAXIS, 2014b).

15- and 6-node triangular elements are available for modelling volume clusters. Material properties are assigned to each volume cluster. In order to perform

calculations on the created model, the geometry needs to be divided into finite elements. The finite elements are the above described triangular elements as well as other special elements for e.g. plates, which together create a mesh. PLAXIS has the ability to automatically create a mesh. However, the automatically created mesh may not be accurate enough to perform an acceptable numerical analysis. To prevent this, the mesh can be manually refined, both as a whole and in areas with large stress and strain concentrations or gradients.

4.2 Soil models

A brief description of the models used for the case study, as well as methods for evaluation of the input parameters, is given below.

4.2.1 Linear elastic (simplification of top layers)

This is a relatively simple model which has a linear elastic behavior. According to the model the soil will never reach failure.

4.2.2 Soft Soil (SS)

The Soft Soil model is suitable for near-normally consolidated clays, clayey silts and peat. These are materials which have a high degree of compressibility (PLAXIS, 2014a). When using the Soft Soil model the stiffness depends on the stress level. The compression behaviour is logarithmic and the model makes a distinction between primary loading and unloading-reloading. Pre-consolidation stress is taken into account and the failure behavior is modelled according to the Mohr-Coulomb criterion (PLAXIS, 2014a).

The logarithmic behaviour during isotropic compression is formulated as:

$$\varepsilon_v - \varepsilon_{0v} = -\lambda^* \cdot \ln\left(\frac{p'}{p_0}\right) \quad (4.1)$$

where p' is the mean effective stress and ε_v is the volumetric strain. λ^* is the modified compression index which determines the compression during primary loading (virgin compression). During isotropic unloading-reloading the relation is formulated as:

$$\varepsilon_v^e - \varepsilon_{0v}^e = -\kappa^* \cdot \ln\left(\frac{p'}{p_0}\right) \quad (4.2)$$

where κ^* is the modified swelling index which determines the compression during this phase. The strain denotations, ε , have the superscript e is because the response from the soil in this phase is assumed to be elastic.

Soft Soil model parameter evaluation

The modified compression and swelling indices, λ^* and κ^* , are evaluated from triaxial tests. The modified compression and swelling indices can be obtained from a plot of the logarithmic mean effective stress, p' , as a function of the volumetric strain, ε_v . The first as the slope of the primary loading line and the latter as the slope of the unloading-reloading line, see Figure 4.3.

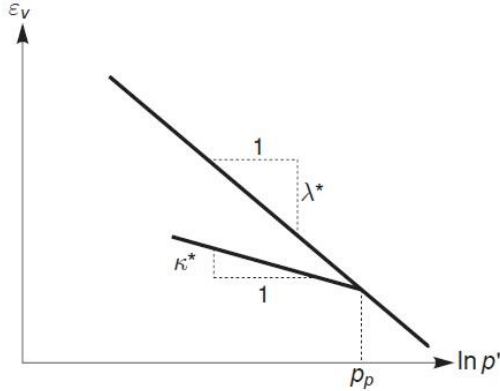


Figure 4.3 Definitions of indices λ^* and κ^* (PLAXIS, 2014a).

These parameters can also be obtained from a one-dimensional oedometer test since there is a relationship between λ^*/κ^* , and the parameters for one dimensional compression and recompression C_c/C_s (PLAXIS, 2014a). In PLAXIS either could be used as input value. Since only oedometer tests were available for this project parameters C_c and C_s were evaluated and then transformed by using relationships described below.

Modified compression index, λ^*

The modified compression index λ^* is obtained from the relationship with the compression index, C_c , in equation 4.3 (PLAXIS, 2014a).

$$\lambda^* = \frac{C_c}{2.3*(1+e)} \quad (4.3)$$

Modified swelling index, κ^*

The modified swelling index, κ^* , is obtained from the relationship with the swelling index, C_s , in equation 4.4 (PLAXIS, 2014a).

$$\kappa^* = 2 * \frac{C_s}{2.3*(1+e)} \quad (4.4)$$

4.2.3 Soft Soil Creep (SSC)

While the Soft Soil model is a suitable tool for modeling clays, it does not consider the secondary compression (creep). The parameters and principles of the both models

coincide well with each other apart from the modified creep index, μ^* , which takes the time aspect into consideration (PLAXIS, 2014a).

Similar to the Soft Soil model, the Soft Soil Creep model distinguish between primary loading and unloading/reloading. The difference is that for the Soft Soil Creep model, the limit between the two loading states is not only determined by the maximum stress state that has been reached in the past, but also by the time aspect (PLAXIS, 2014a).

The Soft Soil Creep model assumes a reference time, τ , of 1 day, which cannot be altered. This is to be used in conjunction with a preconsolidation pressure corresponding to 24 hours load step. For other load/strain rates, the input value of *OCR* or *POP* needs to be scaled accordingly (Leoni, Karstunen and Vermeer, 2008).

Creep is formulated using the concept of constant volumetric creep strain rate, which is inversely proportional to OCR^* . OCR^* is the OCR defined by mapping the normal consolidation surface and current stress state surface to preconsolidation pressure, p' , see Figure 4.4 (Leoni, Karstunen and Vermeer, 2008).

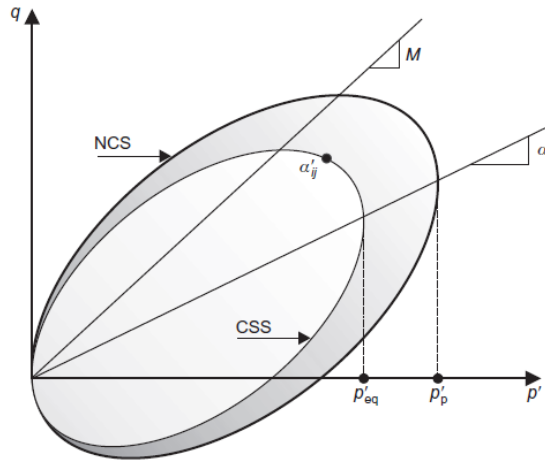


Figure 4.4 Anisotropic creep model in triaxial stress space. NCS = Normal Consolidation Surface. CSS = Current State Surface (Leoni, Karstunen and Vermeer, 2008).

The modified creep index, μ^* , equals to the creep rate after one day. In combination with λ^* and κ^* , the change of creep rate in time can be defined according to equation 4.5.

$$\varepsilon_v^c = \frac{\mu^*}{\tau} * \left(\frac{1}{OCR^*} \right)^{\frac{\lambda^* - \kappa^*}{\mu^*}} \quad (4.5)$$

Evaluation of creep index parameter, μ^*

The modified swelling index, μ^* , is obtained from the relationship with the swelling index, C_α , in equation 4.6 (PLAXIS, 2014a).

$$\mu^* = \frac{C_\alpha}{2.3 \cdot (1+e)} \quad (4.6)$$

When applying a load step, both consolidation and creep will occur simultaneously. For a proper parameter evaluation of the creep parameter, μ^* , when plotting the strain versus the natural logarithm of time, the time period needs to be long enough for the inclination of settlement curve to be straight, i.e. after full consolidation. This makes the consolidation settlement contribution from μ^* minor compared to the contribution of creep (Waterman and Broere, 2005).

4.3 Structural elements

The structural elements that are used in this thesis are presented below.

4.3.1 Plate element

Plate elements are structural objects used to model slender structures. They are often suitable to use when simulating the influence of walls or plates. In the plane strain model the plate extends in the out-of-plane direction.

The plates in the plane strain model have two translational degrees of freedom (u_x , u_y) and one rotational degree of freedom (ϕ_z). The plate elements are based on Mindlin's beam theory which allows for deflections due to bending as well as shearing. The plate element can also change length when axial force is applied. When a prescribed maximum bending moment or axial force is exceeded the element becomes plastic (PLAXIS, 2014b).

In order to allow for a proper modeling of soil-structure interaction, an interface can be applied to a structural element (PLAXIS, 2014b).

Plate element parameters

The general properties are:

d_{eq} : Equivalent thickness of the plate. Automatically calculated from stiffness parameters EA and EI , see *Stiffness properties*. [m]

w_{plate} : Weight of the plate material per unit of length per unit of width in the out-of-plane direction [kN/m/m]

The stiffness properties are:

EI : The flexural rigidity, or bending stiffness, for a rectangular cross section is calculated according to equation 4.8.

$$EI = \frac{b * h}{12} \quad (4.8)$$

EA : The normal stiffness, for a rectangular cross section is calculated according to equation 4.9.

$$EA = E * h * b \quad (4.9)$$

For equations 4.8 and 4.9 b and h are chosen according to Figure 4.5.

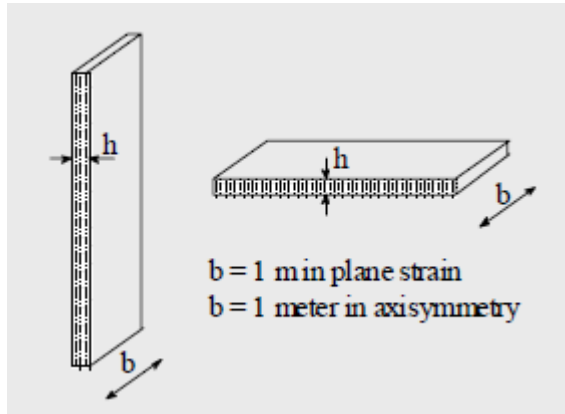


Figure 4.5 Definitions for b and h in equations 4.8 and 4.9 (Waterman, 2006).

d_{eq} : The element thickness d_{eq} (h in Figure 4.5) is calculated according to equation 4.10.

$$d_{eq} = \sqrt{12 * \frac{EI}{EA}} \quad (4.10)$$

ν : Poisson's ratio

4.3.2 Embedded pile row element

It is of course difficult to model piles realistically in a two-dimensional plane strain model, since the stress state and deformation pattern is fully three-dimensional. In PLAXIS 2D there is a feature called embedded pile row element which is a simplified approach to deal with out-of-plane directed pile rows in a two-dimensional plane strain model (PLAXIS, 2014b). Earlier analyses comparing 3D and 2D models indicate that this element is able to represent the pile behaviour in a 2D model better than node-to-node anchors or plates (PLAXIS, 2012).

The pile is represented by a beam element which is superimposed on the mesh rather than being in it, which a plate element would be. The mesh is thus continuous and the soil can “flow through” the embedded pile row. The beam is connected with the

underlying soil element by an out-of-plane interface, as can be seen in Figure 4.6 (PLAXIS, 2014b). Since there are special interface elements included in the embedded pile row feature, there is no need to create additional interface elements for the piles.

The embedded pile row element have three different connection options: Free, Hinged and Rigid. If it shares a geometry point with a structure and both elements are active, the node created at the connection is by default rigid. If however the structural element is not active the point has a hinged connection to the soil. When there is an interface between the plate and the soil the embedded pile row can be connected to either the structure or the soil (PLAXIS, 2014b).

The line elements which compose the embedded pile rows have two translational degrees of freedom (u_x , u_y) and one rotational degree of freedom (ϕ_z). The elements are based on Mindlin's beam theory which allows for deflections due to bending as well as shearing. The elements can also change length when axial force is applied (PLAXIS, 2014b).

To consider skin resistance, line-to-line interface elements along the shaft and perpendicular to the model plane, are used as connection between the pile and the surrounding soil. These consists of springs and a slider in the longitudinal direction and springs also in the transverse direction (PLAXIS, 2014b), see Figure 4.6. There is also the option of involving a point-to-point interface at the pile base to consider the base resistance.

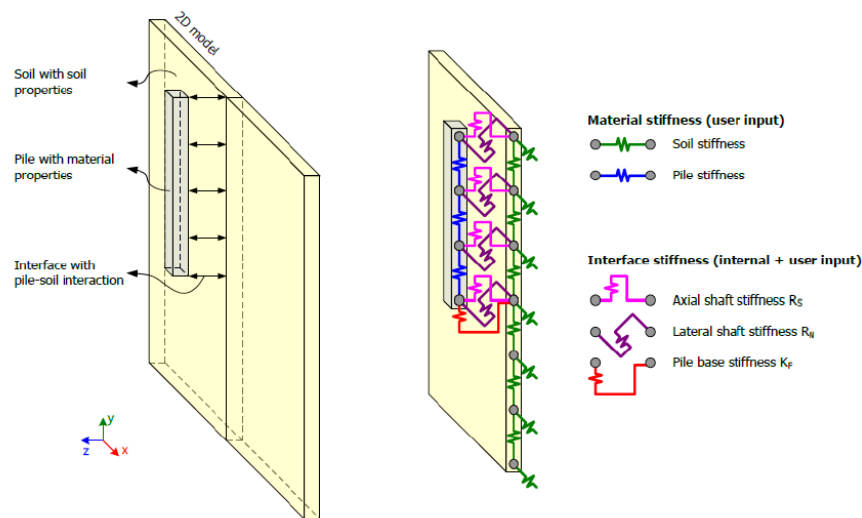


Figure 4.6 Embedded pile row interaction with soil (PLAXIS, 2014b).

The embedded pile row element is supposed to combine features of earlier modelling methods, where node-to-node anchors and plates have been used (Sluis et al., 2013), such as:

- Soil-structure interaction due to line-to-line interfaces and a continuous mesh (the soil can “flow through” the element);
- Axial stiffness can be applied;

- Bending stiffness can be applied;
- Structural forces in piles can be obtained;
- Unrealistic shear planes are not introduced.

Embedded pile row element parameters

The embedded pile row feature differs somewhat to most finite element methods since the bearing capacity (skin friction) is considered to be an input parameter rather than the result of calculation. The input value of this is preferably based on representative data from pile load testing. It is advised to compare the behaviour from a calibration with the results from the pile load test. The group action of the pile row must be taken into account when defining the pile bearing capacity (PLAXIS, 2014b).

The single pile material properties:

E : Young's modulus. [kN/m²]
 γ_{pile} : Unit weight of pile material. [kN/m³]

The geometric properties of the embedded pile row:

Pile type: *Predefined* or *User defined* can be chosen

Predefined pile type: *Massive circular pile*, *Circular tube* or *Massive square pile* can be chosen.

d_{pile} : For *Massive circular pile*, the pile diameter is defined and determines the size of the elastic zone where soil behaviour is excluded. [m]

User-defined piles are defined by the pile cross section area, A , and moment of inertia, I .

$L_{spacing}$: Pile spacing perpendicular to the model plane. [m]

The interaction properties of the embedded pile row:

In order to describe the behaviour of the special interface element, an elastic-plastic model is used. The elastic behaviour accounts for the difference in average soil displacements and the displacements of piles in the out-of-plane direction and depends on the pile diameter in relation to $L_{spacing}$. The plastic behaviour is regarded

by skin resistance T_{max} [kN/m], defined at the pile top and bottom, $T_{top,max}$ and $T_{bot,max}$, and *Base resistance* [kN]. These values are automatically recalculated per unit of width in the out-of-plane direction (PLAXIS, 2014b).

For the interface to remain elastic the shear force t.s must be lower than T_{max} . When it is exceeded the behaviour is plastic. The pile bearing capacities are automatically recalculated per unit of width in the out-of-plane direction by using the $L_{spacing}$ input (PLAXIS, 2014b).

4.4 Loads in PLAXIS 2D

A point load are created in a similar manner as geometry points and given the input value in force per unit of width [kN/m] in the direction perpendicular to the model plane. In the 2D plane strain model the point load thus is a line load. Also in the axisymmetric model the point load is a line load, in this case on a circle section, if not located at $x = 0$, where it is a real point load and the input value is given in the unit of force [kN] (PLAXIS, 2014b).

Distributed loads are created in a similar manner as geometry lines. Like the point load, the distributed load extends in the out-of-plane direction and thus has the input value of force per area [kN/m²]. In the input window for distributed loads the input values for the two geometry points at each end of the load line can be applied. The load can be uniform if the same value is given to the two points. If there is a difference between the input values the load is linear along the line (PLAXIS, 2014b).

Characteristic values of the loads are used as input for PLAXIS.

5 Verification of soil parameters and soil models

This chapter contains information about how evaluated parameters have been adjusted to give an accurate representation of the soil in the PLAXIS 2D model.

5.1 Soil tests performed in PLAXIS 2D

An important aspect of creating models using numerical software is to be able to validate that the model is acting as anticipated. In order to verify that the soil model created in PLAXIS is able to express the actual behaviour of the in situ soil, it is possible to simulate different kinds of soil tests in PLAXIS. Soil test results from real laboratory tests can be compared with the results from simulated tests in PLAXIS and thus show if the model corresponds to the real case in a realistic way. Based on the comparison, the input parameters could be calibrated to find the optimal input values.

For this thesis the stepwise oedometer tests carried out in 1966, used to evaluate the soil parameters, have been simulated using an axisymmetric model as described below. To compare the shear strength, triaxial test simulations have also been carried out.

The oedometer tests from 1966 were not fully performed according to the recommended practice, with the time for each loading step set to one day. Several load steps have been applied for shorter periods. This has been taken into account in the soil test simulations by using the same length of time steps, as in the oedometer tests from 1966.

As is described in section 6.1, the clay below the excavation bottom is in this thesis divided into three different layers. Soil tests simulations, both oedometer and triaxial, with the Soft Soil model have been performed for each of the three layers. The Soft Soil Creep model has only been evaluated with an oedometer simulation and only for Clay 1. The Soft Soil Creep simulation is made as a comparison with the Soft Soil model. Therefore, the curve of the Soft Soil Creep has not been modified.

5.1.1 Axisymmetric model, Stepwise oedometer test

A stepwise oedometer test is simulated in PLAXIS as an axisymmetric scale model with a closed consolidation boundary and dimensions according to Figure 5.1. When performing the soil test simulations by scale modelling rather than the Soil Test feature in PLAXIS 2D, the possibility to set time is given. This should be the preferred way to model, especially for Soft Soil Creep which is time dependent.

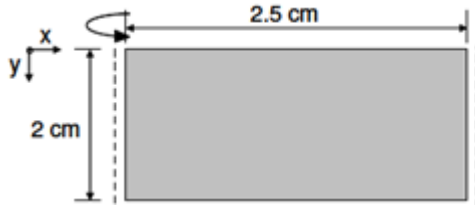


Figure 5.1 Principal sketch of the axisymmetric model in PLAXIS for a stepwise oedometer test. Dashed line means closed boundary (Olsson, 2010).

In both the Soft Soil model and the Soft Soil Creep model, the stiffness is stress dependent. This means that since the top layer of the soil profile is subjected to zero vertical stress, the stiffness in the top of the soil profile will be very small. This causes large deformations to occur in the beginning, when the soil is loaded. To prevent this from happening in a soil test simulation, an initial stress can be applied to the soil specimen. This is done by applying a layer of elastic soil on top of the test sample with a corresponding overburden effective stress to the real test sample (Olsson, 2010).

The test is simulated by calculation phases where a distributed load is increased according to the test documentation from 1966. Consolidation for each phase is calculated and the time is set to the corresponding value from 1966, for each load step.

5.1.2 Triaxial soil test

The triaxial soil test in the Soil Test application is used to simulate shear strength at failure. Since no triaxial tests have been done for the site the input values have to be calculated. The horizontal pressure σ'_3 is calculated according to equation 5.1.

$$\sigma'_3 = K_0^{OC} * \sigma'_1 \quad (5.1)$$

The test is performed in undrained conditions.

5.2 Evaluating results

Since settlements are the focus of this thesis, the most important parameters to match with the soil test simulations are λ^* , κ^* and the OCR , which all have a big influence on the predicted deformation of the soil.

Due to the lack of triaxial tests, the parameters in

Table 5.1 are assumed and will be constant during all soil test simulations.

Table 5.1 Assumed values for the soil models.

$v [-]$	$K_0^{NC} [-]$	$c' [kPa]$	$\phi' [^\circ]$
0.15	0.5	1	30

5.2.1 Stepwise oedometer simulations

If the curve from the simulated oedometer test does not fit sufficiently well, when compared to the curve from the laboratory test, the parameters are adjusted until the fit is estimated to represent the behaviour of the soil in a realistic way. Presented below in Figure 5.2, Figure 5.4 and Figure 5.5 are the oedometer curves from 1966, plotted together with the soil test simulations, which have been adjusted until as a sufficiently good fit is reached. In Figure 5.3, the strain is plotted versus time for the load step 160-320 kPa, which is the load step that μ^* is being evaluated from. The curves in the strain versus time graph have not been modified to match better. The input parameters are presented in Table 5.2, Table 5.3 and Table 5.4.

Since λ^* , κ^* and OCR are the most important parameters to match, the whole curve does not need to have a good fit. Thus, the inclinations of the curves as well as where the preconsolidation pressure is reached is where focus of the comparison should be.

The inclination of the different curves, prior to reaching the preconsolidation pressure, does not fit well. However, the input value for the κ^* value is evaluated from the unloading-reloading curve, of which the fit is good.

Clay Layer 1

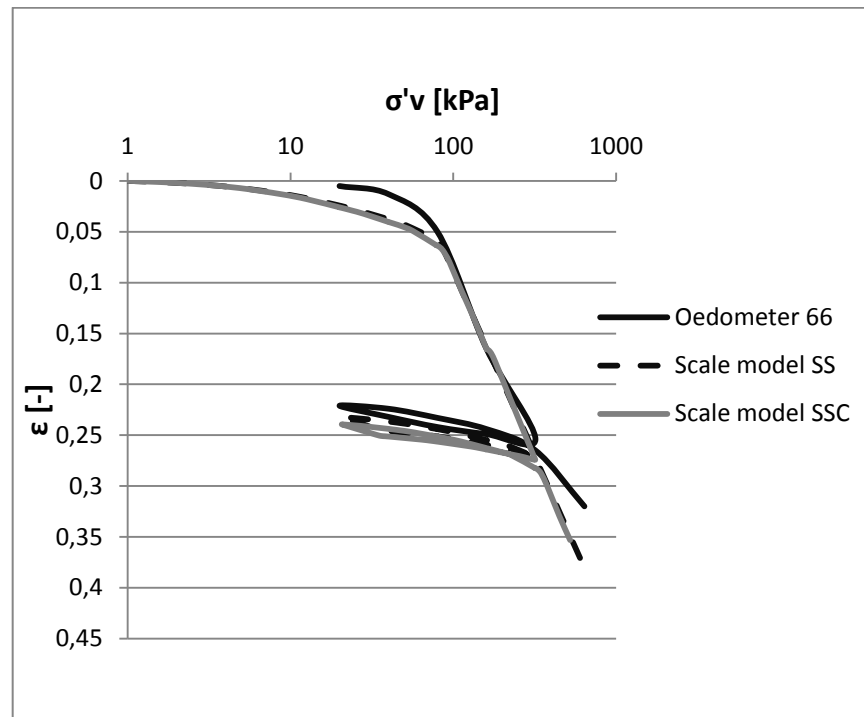


Figure 5.2 Oedometer test from 1966 compared to simulated oedometer tests in PLAXIS for Soft Soil model and Soft Soil Creep model. The oedometer tests represents clay layer 1.

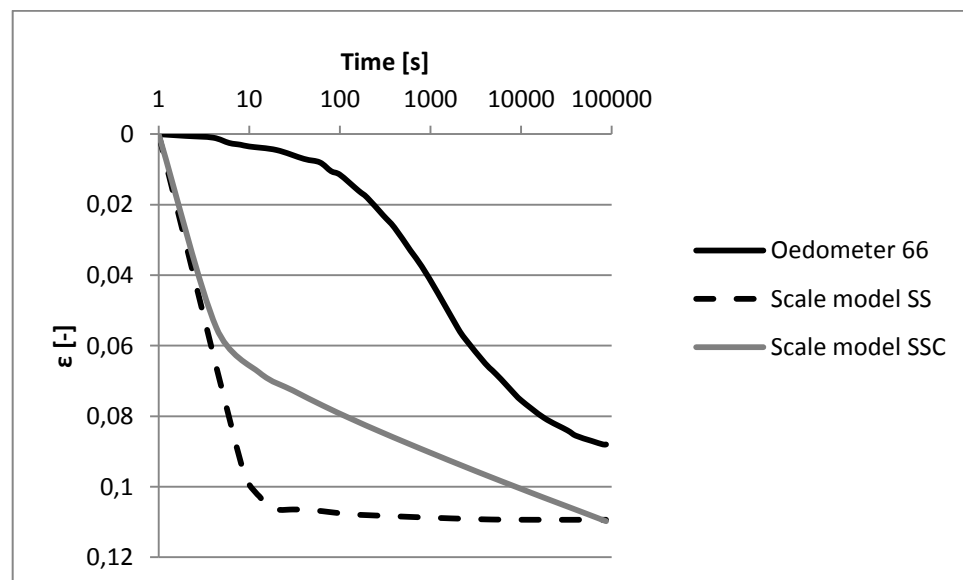


Figure 5.3 Strain plotted versus time for the load step 160-320 kPa. The oedometer test from 1966 is compared to soil test simulations in PLAXIS for Soft Soil model and Soft Soil Creep model.

Table 5.2 Input parameters for clay layer 1

λ^* [-]	κ^* [-]	K_0^{OC} [-]	OCR [-]	e_0 [-]	σ'_c [kPa]	k_y [m/day]	k_x [m/day]
0.153	0.02797	0.547	1.14	1.87	82	1.62E-5	2.44E-6

Clay layer 2

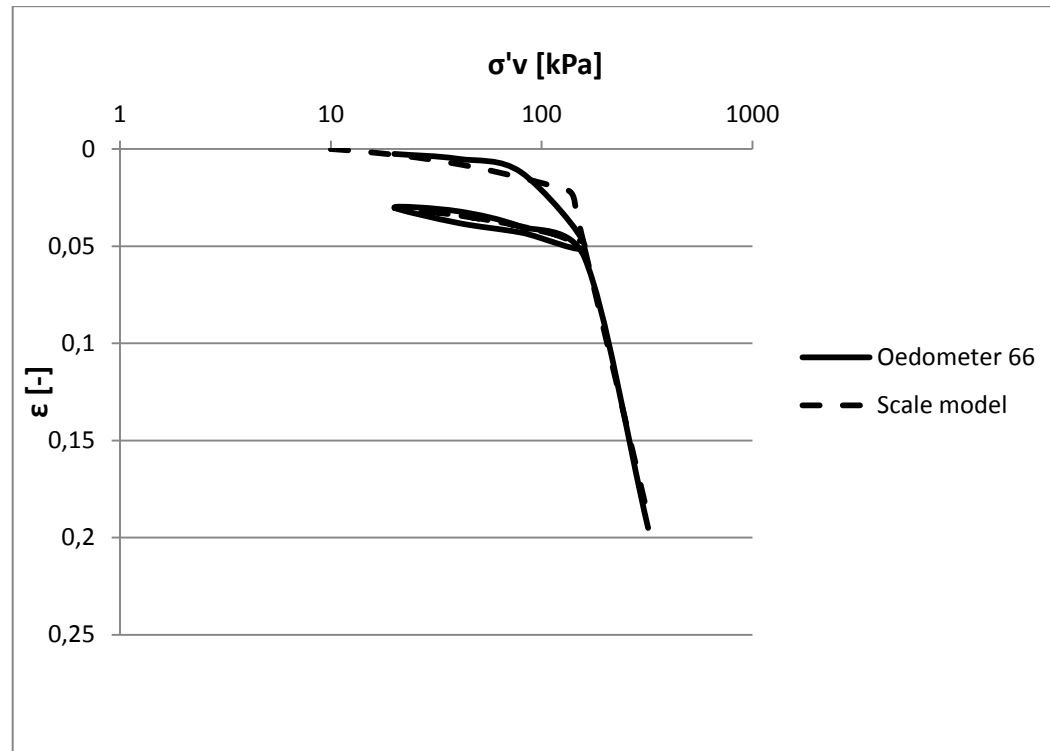


Figure 5.4 Oedometer test from 1966 compared to simulated oedometer tests in PLAXIS for Soft Soil model. The oedometer tests represents clay layer 2.

Table 5.3 Input parameters for clay layer 2

λ^* [-]	κ^* [-]	K_0^{OC} [-]	OCR [-]	e_0 [-]	σ'_c [kPa]	k_y [m/day]	k_x [m/day]
0.198	0.0189	0.54	1.167	1.84	140	1.71E-5	2.57E-5

Clay layer 3

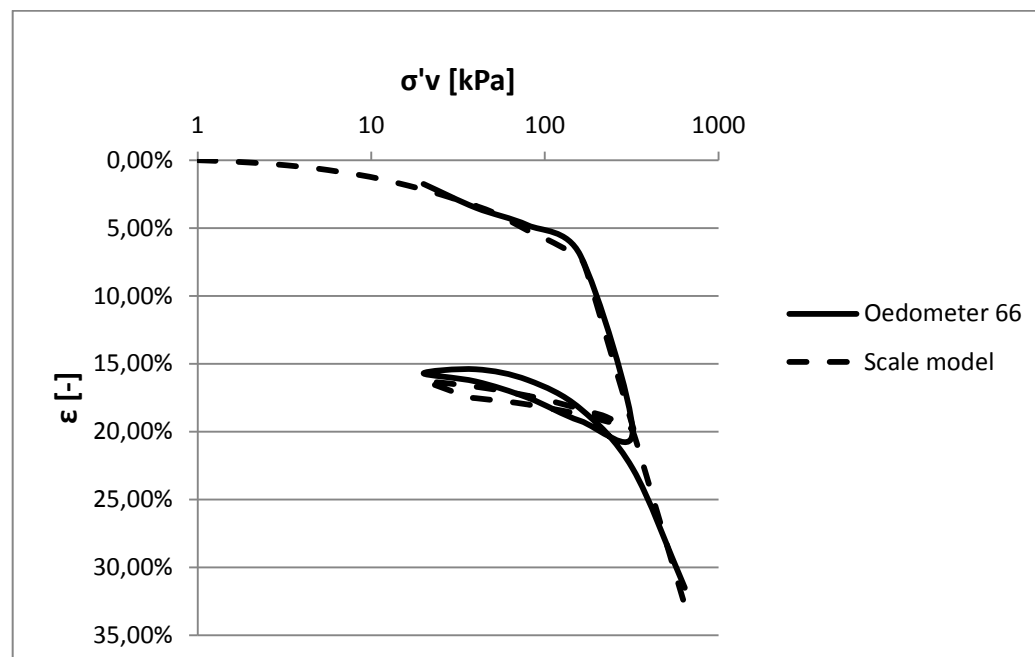


Figure 5.5 Oedometer test from 1966 compared to simulated oedometer tests in PLAXIS for Soft Soil model. The oedometer tests represents clay layer 3.

Table 5.4 Input parameters for clay layer 3

λ^* [-]	κ^* [-]	K_0^{OC} [-]	OCR [-]	e_0 [-]	σ'_c [kPa]	k_y [m/day]	k_x [m/day]
0.185	0.025	0.543	1.18	2.03	170	5.6E-6	8.46E-6

5.2.2 Triaxial test simulations

The input data and the borehole used for each soil layer is the same as in the oedometer simulations presented above.

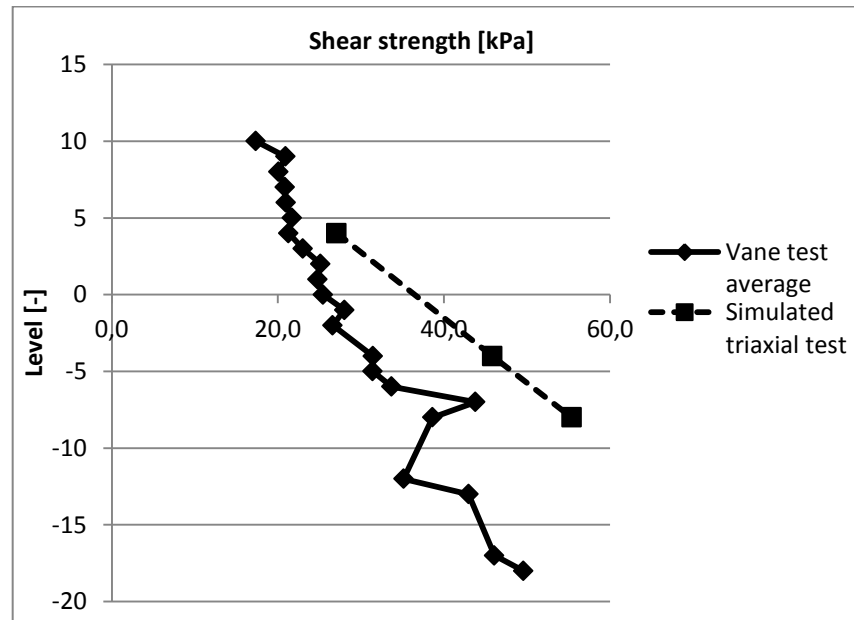


Figure 5.6 Shear strength obtained from vane tests from 1966 compared with shear strength from a triaxial test simulation performed in PLAXIS

As mentioned above, triaxial tests are simulated in order to investigate the evaluated shear strength of the soil. The results differ from the measured values from 1966, which can be seen in Figure 5.6. The curves do not have a good fit relative each other and the inclinations are different, but these differences can partly be explained by different modes of failure, as vane tests does not correspond to undrained failure in triaxial compression. Unfortunately there is no real triaxial test to compare it with, and hence it is pointless to attempt to calibrate parameters for a better fit.

6 Modelling

This chapter contains information about how the modelling for the case study was performed.

The case study of Nordstaden 8:27 is modelled using the plane strain model. Thus, a whole cross section can be investigated. According to Prakoso and Kulhawy (2001) this type of model can somewhat overestimate settlements, but can still provide reasonable results and the possibility to analyse large piled rafts with relatively low computing time.

Initially, loads and dimensions from multiple cross sections were to be investigated to compensate for the simplifications when designing a 3D-problem in 2D. However, due to a tight time frame and the difficulty of modelling the caissons in 2D, only one cross-section is modelled. Also, the caissons make the bottom plate stiffer, which is beneficial in terms of settlements. The cross-section is chosen over the short side of the building at line K, see Figure 3.16, in order to make the plane strain conditions better utilised.

The settlement analyses are performed after the additional loading with all prior displacements being reduced to zero. This is done since it has been deemed that the settlements of interest are the ones resulting from the construction of additional floors.

6.1 Geometry and simplifications

The geometry model, which can be seen in Figure 6.1 and Figure 6.2, is based on construction drawings for Nordstaden 8:27 and the soil parameter evaluations. In the geometry input the elevation on the y-axis has been given the same values as in the local coordinate system of Gothenburg. The ground level is located at $y = 12.1$, the excavation bottom is located at $y = 5.8$. Coordinates for the embedded pile row elements are obtained from construction drawings, where piles closest to line K have been regarded. Point loads are located at gridlines 1-8 in the construction drawings. For construction drawings see Appendix A.

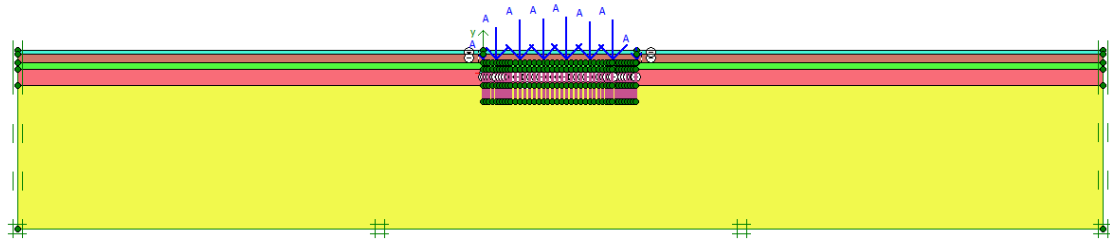


Figure 6.1 Overview of the model geometry. Coordinates for corners (clockwise from the top left corner): $(-240, 12.1)$, $(320, 12.1)$, $(320, -80)$ and $(-240, -80)$.

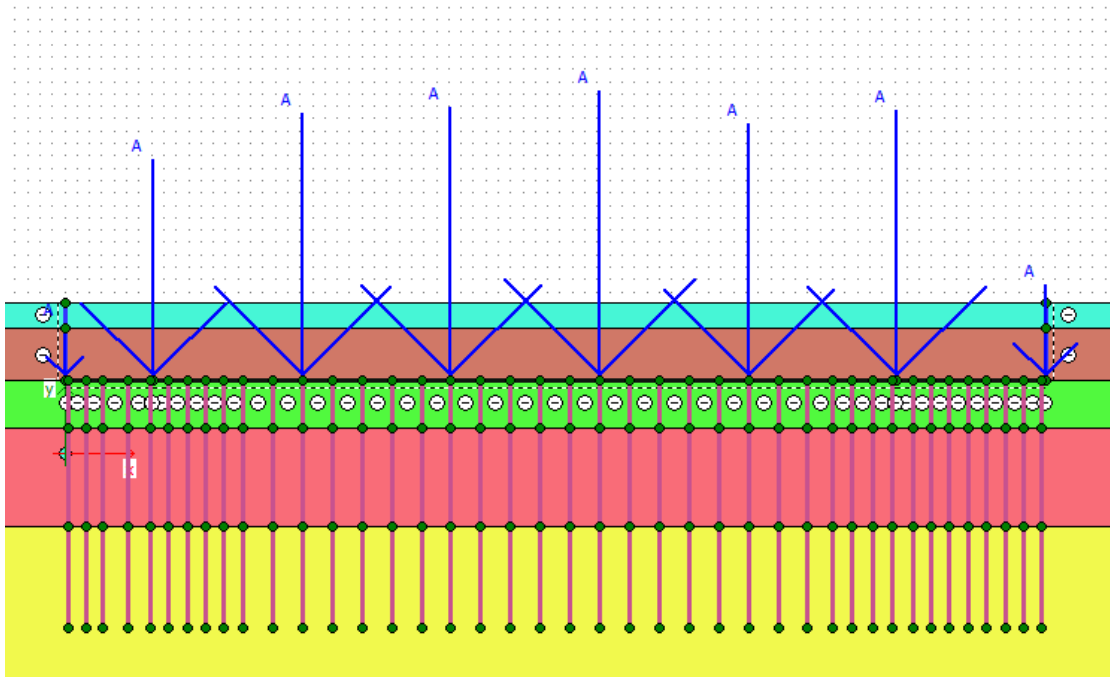


Figure 6.2 Zoom in of the geometry for the construction. The excavation and plate are located between x -coordinates 0 and 79.2.

The groundwater head is placed at +10.1. The assumption is made that the water pressure acting on the raft is set to the same level. No consideration is made regarding the difference in groundwater pressure below the raft.

The shape of the compression index curves as well as the creep index curves indicate that the properties of the soil change with depth. This can also be seen in the permeability-level graph. Based on this, a sectioning of three layers is suitable, see Table 6.1. Furthermore, the natural water content diverges at approximately the same levels as the indices, indicating that the soil properties have altered there. For the swelling index, no such pattern is found. The unloading-reloading curve of borehole 17b - 25 m, has an odd shape, which indicates that this might be due to sample disturbance.

Appropriate borehole and depth is used for each layer, see Table 6.1. Based on the compression index curves, it would be appropriate to use borehole 17b at a depth of 25 m for soil layer three. However, due to the potential sample disturbance at that depth discussed above, the input data would be to dubious to use. Therefore, borehole 1 at a depth of 20 is better to use.

Table 6.1 Levels for the layers modelled as Linear Elastic (LE) and Soft Soil and sample used for the corresponding input parameters for the Soft Soil layers.

	Start level, y	End level, y	Borehole and depth
LE layer 1 (fill)	+12.1	+10.1	-
LE layer 2	+10.1	+5.8	-
Clay layer 1	+5.8	+2	Borehole 1, 8m
Clay layer 2	+2	-6	Borehole 17b, 16m
Clay layer 3	-6	-90	Borehole 1, 20 m

The stress-void ratio curves, evaluated from the soil tests, in Figure 6.3, show two distinct trends. This might imply that there would be sufficient with two layers for the model. However, only the compression indices for the chosen two deeper layers are similar. The rest of the parameters differ too much to model it as one layer.

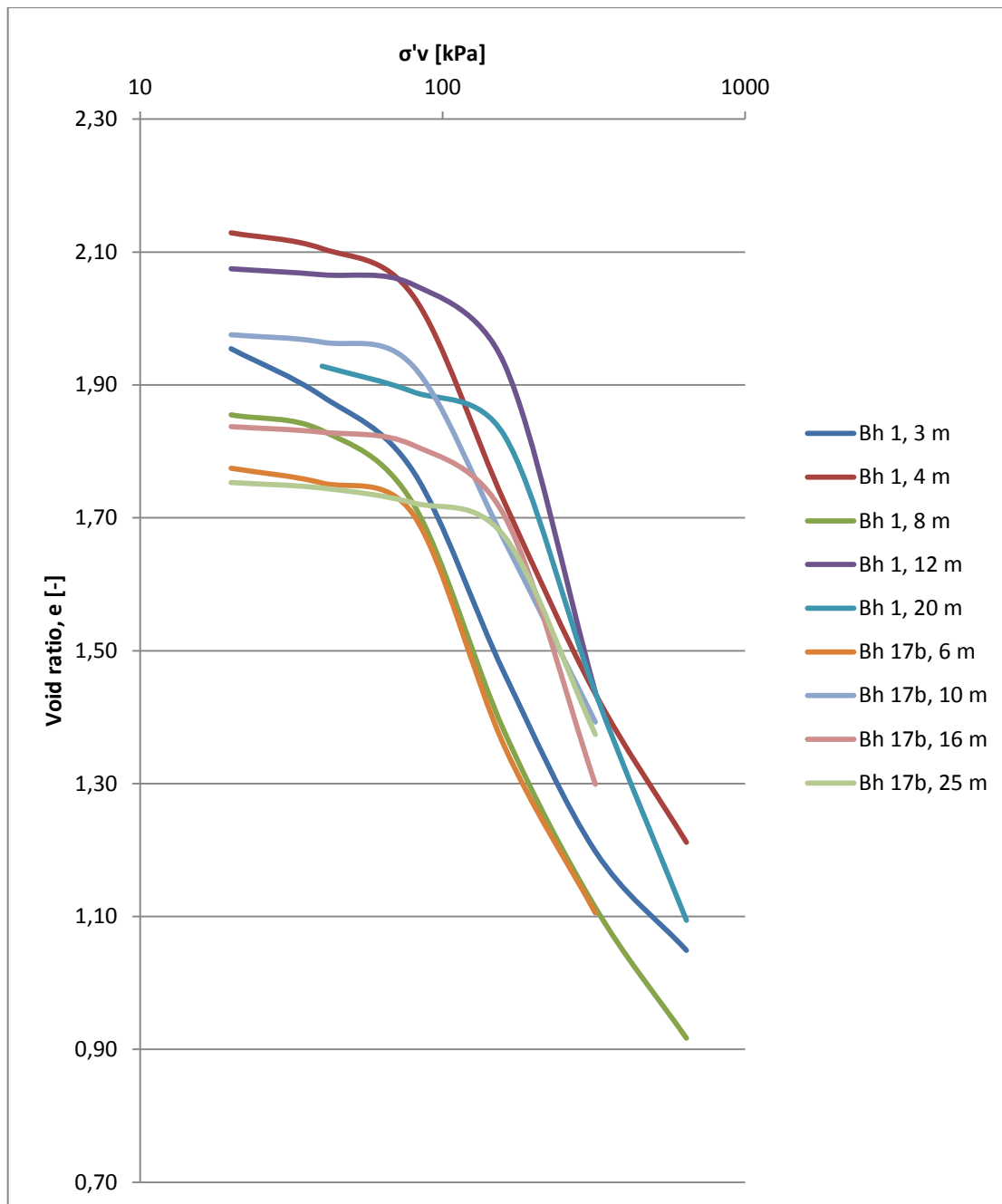


Figure 6.3 Vertical stress plotted versus void ratio for oedometer tests from holes 1 and 17b.

The building is surrounded by streets and other large buildings which in reality of course affect the foundation and ground conditions. This has not been considered in the analyses of this thesis. The model expands to a relatively large distance in the x-direction, on both sides of the building, to prevent influence from the fixed boundary.

6.2 Soil Model

To represent the settlement behaviour of the soft clay in Gothenburg the Soft Soil model has been chosen to model the clay below excavation level. The top layer, which represents the fill, has been modelled as linear-elastic with a thickness of 2 m

and a unit weight of 18kN/m^3 . The clay layer down to the excavation depth has also been modelled as linear-elastic, but with a unit weight of 16 kN/m^3 . The choice of modelling these as linear elastic is to simplify the excavation process for the model. Since settlements under the foundation are the focus of the investigation, the two upper soil layers only need to contribute with unit weight and permeability.

The model Soft Soil Creep is included in the investigations as, a comparison to the Soft Soil model, to see if the behaviour over time can be considered in a reasonable manner.

6.3 Structural elements

If not stated otherwise, the input parameters are based on construction drawings.

6.3.1 Embedded pile row element

The piles are modelled by using the embedded pile row element in PLAXIS 2D. Construction drawings are used to obtain the pile spacing for each strip.

The strength class of the timber is assumed to be K12, which has a Young's modulus E of 2200 MPa (Carling et al, 1992).

In reality the timber piles have a conical shape, which cannot be modelled by the embedded pile row element in PLAXIS. Therefore a diameter has been approximated. The diameter is assumed to be 0.205 m, which is the diameter at half the pile length.

The weight, real density, r_u , of the timber piles was calculated to 12 kN/m^3 , according to equation 6.1.

$$r_u = r_{ou} \left(1 + \frac{u}{100}\right) \quad (6.1)$$

where:

r_{ou} = dry density, approximated as 400 kg/m^3 (Carling et al, 1992).

u = moisture content. Since the piles are located below the groundwater level the moisture content is considered to be at its maximum, which equals to 200 % (Carling et al, 1992).

When calculating the skin resistance, T_{max} , for pile top and bottom, equation 6.2 is used. The equation is based on the bearing capacity of a pile without considering the circumference of the pile. Toe resistance is neglected.

$$T_{max} = \alpha * c_u \quad (6.2)$$

where:

α = adhesion factor 1.2 for timber piles

c_u = undrained shear strength at the top respectively bottom of the pile, according to equation 3.4.

Table 6.2 Input parameters for the embedded pile row element.

Parameter	Size	unit
E	2.2E6	kN/m ²
γ_{pile}	12	kN/m ³
Predefined pile type	Massive circular	-
Diameter	0.205	m
$L_{spacing}$	1.5	m
$T_{top,max} (c_u = 22 \text{ kPa})$	26.40	kN/m
$T_{bot,max} (c_u = 40.9 \text{ kPa})$	49.1	kN/m

The connection between pile and raft is chosen as Rigid.

6.3.2 Plate element

The building is simulated by the use of plate elements. The ground plate has been given input values for normal stiffness and flexural rigidity. Only the concrete part contributes to the stiffness of the plate, which is why 1150 mm is used as height when performing the stiffness calculations. It has also been given a weight input value to simulate the load from the raft itself together with the layers of concrete and macadam located between the raft and the clay. An interface is applied to the bottom of the raft and as well as the sides of the walls.

The plate elements which represent the walls have been given the same values as the raft but with a weight value of zero, since they are considered light and only are used in the model to prevent the excavation from collapse.

Young's modulus and Poisson's ratio for the concrete C25/30 are obtained from "Boverkets handbok om betongkonstruktioner" (Boverket, 2004) presented below:

$$E_{ck} = 31 \text{ GPa}$$

$$\nu_{concrete} = 0.1-0.2$$

For long-term loads⁵, Young's modulus is approximated as $0.5 * E_{ck}$.

The input parameters for slab and walls are presented in Table 6.3.

Table 6.3 Input parameters for the plate elements.

	Slab	Walls	[unit]
EA_I	17.83E9	17.83E9	kN/m
EI	1.964E9	1.964E9	kNm ² /m
w	39.80	0	kN/m/m
$\nu_{concrete}$	0.2	0.2	-

6.4 Loads

To consider the loads from the building, load elements and properties assigned to structural elements have been used when modelling. Each structural element is assigned with its corresponding weight.

The remaining load from the structure above the plate is modelled by point load elements, where the pillars are placed. The loads from the pillars are entered as point loads in PLAXIS, but since the model is in 2D, the input unit is kN/m. Thus an approximation is made. A point load is divided by the in plane width between two pillars, in order to get an average load per meter. The distribution of the loads between the pillars is based on the theory of continuous beams with uniformly distributed loads, according to Appendix D.

6.4.1 Load scenarios

In order to simulate different scenarios describing how many floors are added to the building, five loading scenarios, 10 kPa–50 kPa, have been chosen, with the assumption that each new floor increases the load with 10 kPa. Since the original weight of the building is fully compensated by the excavation of soil ($104.8 - 96 = 8.8$ kPa), the net increment of each load step is 8.8 kPa less than stated.

10 kPa: +10 kPa in total stress = +1.2 kPa in effective stress

20 kPa: +20 kPa in total stress = +11.2 kPa in effective stress

30 kPa: +30 kPa in total stress = +21.2 kPa in effective stress

40 kPa: +40 kPa in total stress = +31.2 kPa in effective stress

50 kPa: +50 kPa in total stress = +41.2 kPa in effective stress

This increment is equally distributed to the point loads by multiplying each point load with a corresponding factor, see Appendix C.

⁵ Hans Lindewald, Structural Engineer at ELU, interviewed 14-03-17

6.5 Mesh optimization

A medium coarseness of the grid has been chosen. A finer mesh was tested but the differences were deemed to be negligible.

6.6 Phases

The different phases are presented below:

1. Initial phase

Represents the ground conditions before the construction of the building begins. A phreatic level of $y = 10.1$ is chosen.

2. Piles

The embedded pile row elements are activated. Undrained behaviour is ignored and displacement are reset to zero.

3. Construction (drained)

The excavation and construction are simulated as an instantaneous event by deactivating the soil clusters and activating the plate elements and loads. No time aspect is given to the construction to prevent the sides of the excavation from collapsing. Undrained behaviour is ignored and replacements are reset to zero.

4. Construction of x number of additional floors (undrained)

Every point load is increased by a factor which corresponds to the total load increment, depending on which loading scenario that is being tested. No time aspect of the construction is taken into consideration.

5. Consolidation

A consolidation analysis for the first 10 years is performed.

6. Consolidation

A consolidation analysis for the first 40 years is performed.

7. Consolidation (90%)

A consolidation analysis until 90% of the excess pore water pressure has dissipated is performed.

To create the current conditions in the model, the time span until today was simulated in drained conditions. This assumption is based on the settlement readings, which indicates that there is close to none consolidation occurring today. Also, it is difficult to model the conditions of today in a realistic way. Since the building is more than fully compensated, a simulation in PLAXIS will cause the soil to heave. The settlement readings indicates that some parts do heave, but there has also been settlement occurring. The assumption of using drained scenario results in a state where there are no excess pore water pressures in the ground at the time additional loads are applied.

A model with undrained conditions, for phase 3 ("3. Construction"), with a following consolidation phase until today, 40 years, will also be simulated. This is done both to compare the current settlement readings with the results from the PLAXIS model as well as to analyse what effects the assumption of a drained scenario in phase 3 has.

A model will also be made without the installation of piles. This is done to be able to evaluate the effects of the embedded pile row element.

6.7 Validation analysis

A hand calculation of the stress distribution with depth is made for a scenario with equal amount of load, but with the load uniformly distributed and without piles. This same scenario is modelled in PLAXIS as a comparison. This is done to control if the effective stresses in PLAXIS correspond to the hand calculations, when modelling an excavation.

6.8 Sensitivity analysis

In order to investigate how much influence different parameters have, parametric sensitivity analyses are performed. Depending on which parameter is tested different behaviours are compared with the default model. For parameters κ^* , λ^* and OCR comparisons regarding settlements versus depth and settlements versus time are made. The influence of permeability parameters k_y and k_x have also been evaluated by these comparisons as well as comparisons of p_{excess} at different levels. The parametric analyses of the embedded pile row element regard the $L_{spacing}$ and pile diameter, d_{pile} .

The methods of how the parameters are changed are different. For κ^* , λ^* , k_y and k_x (depends on k_y) the standard deviation of the measured values from 1966 are added and subtracted from the reference value. The lower value for OCR was set to 1.0 (normally consolidated clay) and the higher value to 1.3. The clay in Gothenburg usually has an OCR around 1.25⁶. The values used for the parametric analyses are presented in Table 6.4-Table 6.7. Only one parameter is changed per comparison, but for all the soil layers at the same time. For example Clay layers 1-3 are all given their respective high value of κ^* when that parameter is analysed.

All sensitivity analyses regard the default model as reference and are observed after a 40 year consolidation, if nothing other is stated.

Table 6.4 Input parameters for Clay 1 for parametric sensitivity analyses

Clay 1	Reference	High	Low
κ^* [-]	0.028	0.033	0.023
λ^* [-]	0.153	0.181	0.125
OCR [-]	1.14	1.3	1
k_y [m/day]	1.62E-05	1.83E-05	1.41E-05
k_x [m/day]	2.43E-05	2.75E-05	2.11E-05

⁶ Lars Hall, Geotechnical engineer at ELU, interviewed 14-03-04

Table 6.5: Input parameters for Clay 2 for parametric sensitivity analyses

Clay 2	Reference	High	Low
κ^* [-]	0.019	0.024	0.014
λ^* [-]	0.198	0.225	0.170
OCR [-]	1.167	1.3	1
k_y [m/day]	1.71E-05	1.93E-05	1.50E-05
k_x [m/day]	2.57E-05	2.89E-05	2.25E-05

Table 6.6: Input parameters for Clay 3 for parametric sensitivity analyses

Clay 3	Reference	High	Low
κ^* [-]	0.025	0.030	0.020
λ^* [-]	0.153	0.213	0.157
OCR [-]	1.18	1.3	1
k_y [m/day]	5.61E-06	7.74E-06	3.47E-06
k_x [m/day]	8.41E-06	1.16E-05	5.2E-06

Table 6.7: Input parameters for embedded pile row element for parametric sensitivity analyses

Embedded pile row element	Reference	High	Low
$L_{spacing}$ [m]	1.5	1.9	-
d_{pile} [m]	0.205	0.285	0.125

7 Results

Results from the PLAXIS 2D modelling and the hand calculations are presented in this chapter. Due to the extension of the result chapter, presented in several graphs, discussion regarding the results has been included in this chapter rather than in a separate one. This is done in order to make it easier for the reader to comprehend the discussion.

7.1 Results from PLAXIS analyses

The presented results from the PLAXIS 2D calculations describe the behaviour of the ground and foundation in form of excess pore water behaviour, pile interaction and settlements. Relevant loading scenarios and modelling approaches are presented for each specific comparison. Results from the parametric studies are also presented.

To be able to make comparisons between different models, phases and load scenarios, a default scenario is chosen. This scenario is labelled as “Piled raft” and has been chosen according to the following criteria:

- The foundation is a piled raft.
- The additional load is 20 kPa.
- The timespan until today, the first 40 years, has been modelled as a drained scenario.
- Soft Soil is used as soil model.

These criteria apply for “Piled raft” if nothing else is stated. This is also chosen as “Reference” for the parametric studies.

Note that when it is stated that the data is obtained after a consolidation of 40 years, this refers to the consolidation after the additional load of 10-50 kPa has been applied. This should not be confused with the different modelling approaches where the piled raft either has a drained scenario or a 40 year long consolidation (labelled as “Piled raft B”) before the additional load is applied. The scenario “Raft only” has the same criteria as “Piled raft” but with the exception that it considers a raft without piles.

Different load scenarios are presented according to definitions given in section 6.4.1.

Comparisons of the PLAXIS models Soft Soil and Soft Soil Creep are presented as SS and SSC, respectively.

Combinations of different aspects occur. For example “SSC – 50 kPa” labels a scenario where the soil model used is Soft Soil Creep and the additional loading is 50 kPa.

7.1.1 Excess pore water pressure

Below the results from excess pore water pressure analyses are presented. Negative values for p_{excess} correspond to compression since compressive stress has a negative sign in PLAXIS 2D.

Figure 7.1 displays the distribution of excess pore water pressure, p_{excess} , for “Piled raft”, immediately after the additional load of 20 kPa. A zone of relatively high p_{excess} can be seen at the foot of the piles in Figure 7.1. This is probably the result of a pile group effect. The piles stiffen the soil below the raft which makes the soil act like a stiff block. The loads are transferred to the bottom where as a result the largest excess pore water pressures are located.

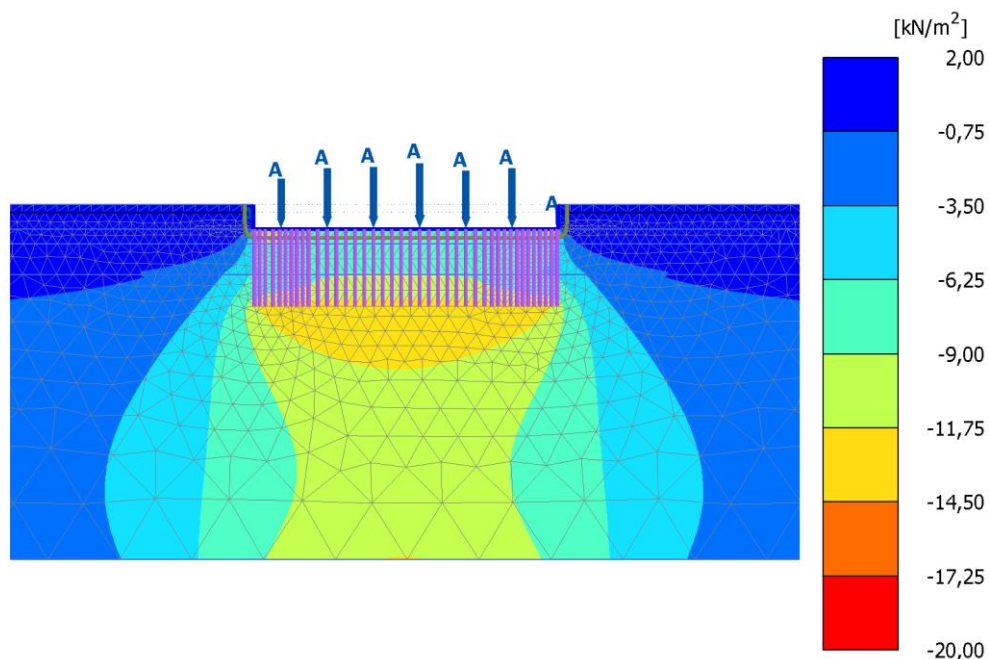


Figure 7.1: Excess pore water pressure distribution for “Piled raft”, immediately after the additional loading of 20 kPa.

In Figure 7.2, a comparison between four different phases, after an additional loading of 20 kPa, can be seen. The phases are:

- “Construction”: Data obtained immediately after the additional loading (there has not yet been any consolidation).
- “Consol 10 y”: Data obtained after the soil has consolidated for 10 years (after the additional loading).
- “Consol 40 y”: Data obtained after the soil has consolidated for 40 years (after the additional loading).

- “Consol 90%”: Data obtained after 90% of p_{excess} has dissipated (after the additional loading).

The data is obtained from a vertical cross-section below the middle of the piled raft and show that p_{excess} near the raft increases during the first consolidation period of 10 years. This could be due to the Mandel Cryer effect (Gibson, Gobert and Schiffman, 1990) since the model is made in 2D, using fully coupled consolidation theory.

In the phase “Construction”, immediately after the additional load of 20 kPa, p_{excess} seems to increase with depth at the lower levels, in spite of the fact that the bottom is an open boundary. This is probably only a momentarily behaviour since the consolidation not yet has begun.

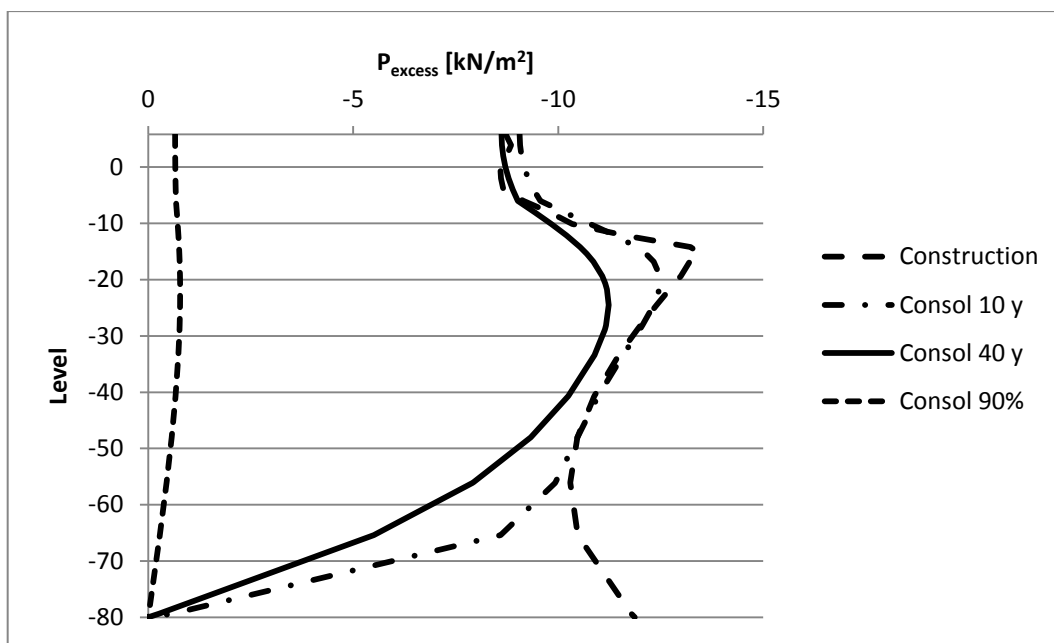


Figure 7.2: Excess pore water pressure plotted at different levels at the middle of the piled raft for different phases, after an additional loading of 20 kPa.

The effect of the piles can be seen in Figure 7.3, where p_{excess} is plotted versus level and “Piled raft” is compared with “Raft only”. p_{excess} values at the top levels are higher for “Raft only” since there are no piles to transfer the loads deeper.

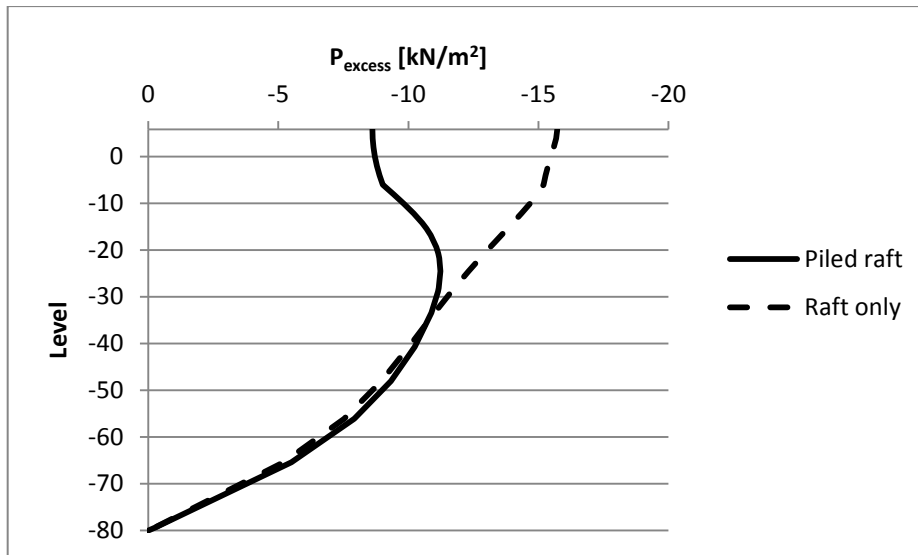


Figure 7.3: Excess pore water pressure at different levels after 40 years consolidation at the middle of the raft for different models. An additional load of 20 kPa has been applied.

In “Piled raft B”, where the first 40 years before the additional construction are modelled as an undrained rather than a drained scenario, there are still some excess pore water pressures which have not dissipated. In Figure 7.4 it can be seen that the highest value is approximately 5 kPa. Note that this has a positive sign and therefore the ground heaves rather than settles. Thus, the difference in p_{excess} between “Piled raft B” and the default model is at most 5 kPa. This will reduce predicted overall settlements but since the p_{excess} is unevenly distributed, it will contribute to larger differential settlements.

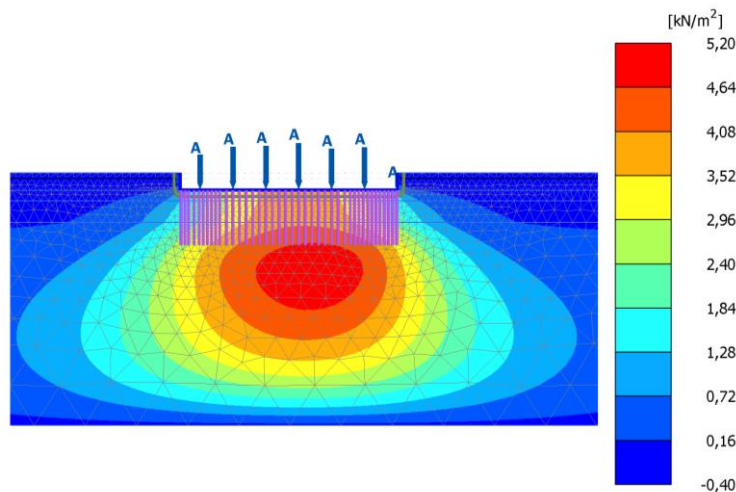


Figure 7.4 Excess pore water pressure distribution for “Piled raft B”, immediately after the additional loading of 20 kPa.

7.1.2 Settlements

Figure 7.5 shows the predicted heave that occurs during the first 40 years of the construction, i.e. up until today. There is almost no difference between the Soft Soil

model and the Soft Soil Creep model, as would be expected since the unloading behaviour is largely elastic.

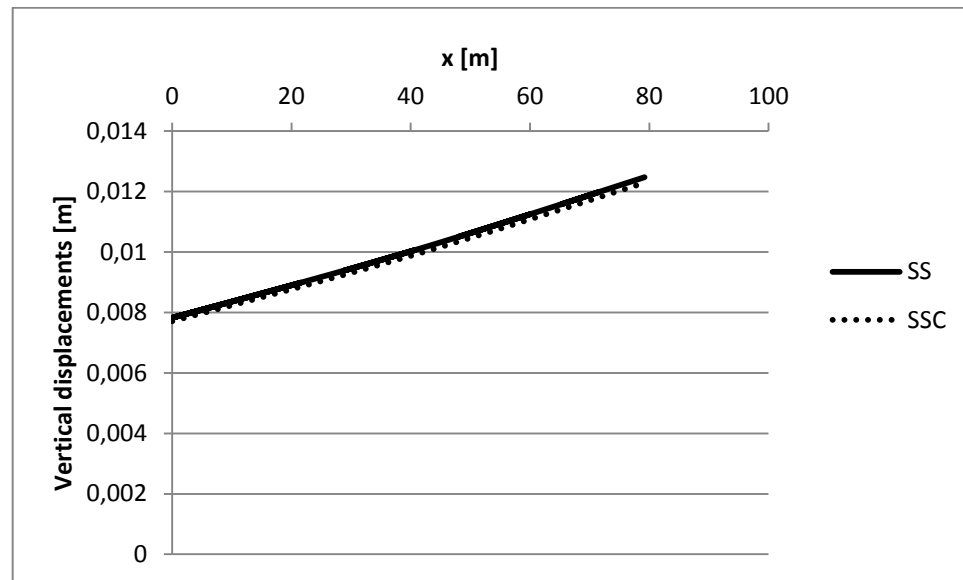


Figure 7.5 Heave that have occurred until today for both the Soft Soil model (SS) and the Soft Soil Creep model (SSC).

Figure 7.6 shows a comparison between settlements over time for the soil under the left edge of the raft and the settlement target closest to the investigated cross-section. Figure 7.7 illustrates a similar comparison for the left edge of the plate. The results seem to differ quite a lot since the model predicts a heave of 10-15 mm. While Point 4 does show a heave, it is smaller than the result from the model. Points 15 and 16 show a settlement. However, considering the size of the model, the deformations can be regarded as being of the same magnitude, which would indicate that the model represents the actual case rather well. The choice of using a drained scenario, before the additional construction, for the default model, means that no remaining p_{excess} exist. Considering the differences between the PLAXIS results and the settlement readings, it seems like a reasonable assumption that p_{excess} in reality is closer to zero than Figure 7.4 indicates, and hence a drained scenario is appropriate to use.

Since the readings did not start until 1978, 4 years after the construction was finished, the settlement readings do not cover the same time span as the model. This would also mean that instantaneous deformations are not measured. However, the difference can hardly be explained by that. The 3D-effects that are not accounted for in the model could be one explanation, i.e. loads in other parts of the building can affect the cross-section investigated in this thesis. For example, the settlement targets in Figure 7.7 are located only a couple of meters from each other, but they show different patterns. Other explanations could be that the loads acting on the foundation are underestimated. Additional factors of uncertainty are the weight of the building or assumption of the activity on each floor and that no consideration has been given to the reconstruction of the building. Since the weight of the excavated soil masses exceeds the applied loads on the building, heave that is predicted by PLAXIS for the first 40 years is reasonable. Also, the fact that the model does not consider the effect of surrounding streets and building could contribute to the difference in vertical displacements.

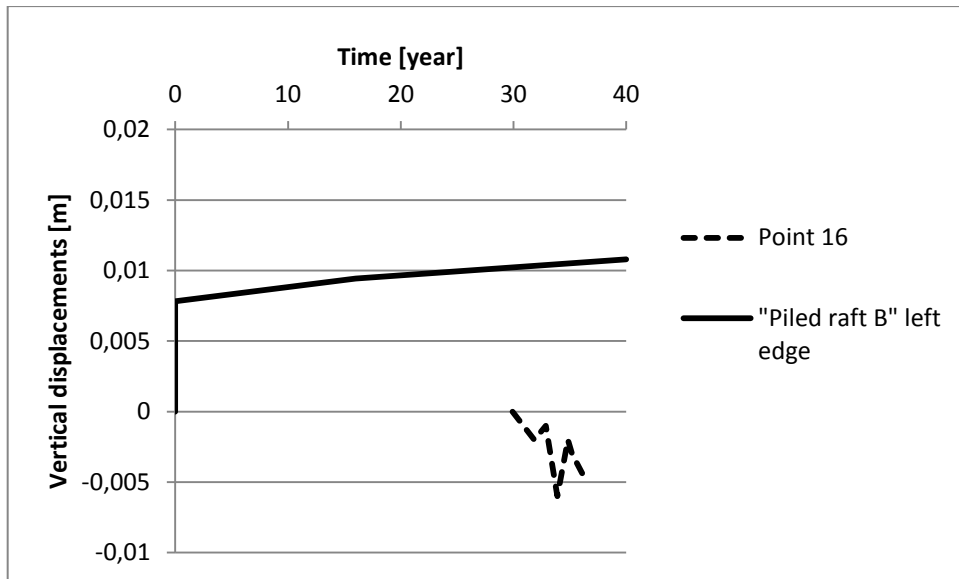


Figure 7.6 Settlement readings over time for point 16, starting in 2003, compared with results from the PLAXIS model, scenario “Piled raft B”. Both are located close to the left edge.

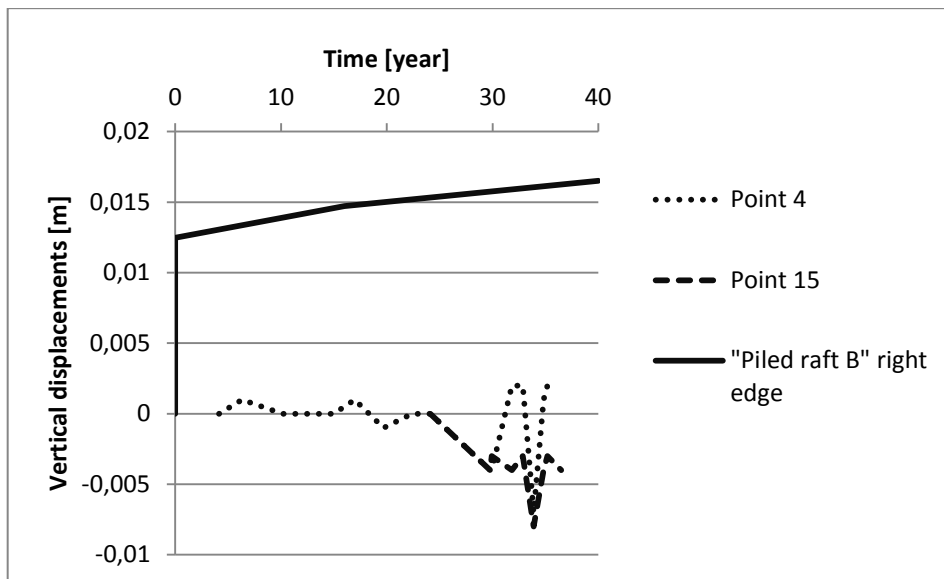


Figure 7.7 Settlement readings over time for point 4 and 15, starting in 1978 and 1998, respectively, compared with results from the PLAXIS model, scenario “Piled raft B”. Both are located close to the right edge.

Figure 7.8 shows the predicted settlements over time for all five loading scenarios. The linear increase with load implies an elastic behaviour, which is reasonable since the piles are transferring loads to stiffer soil.

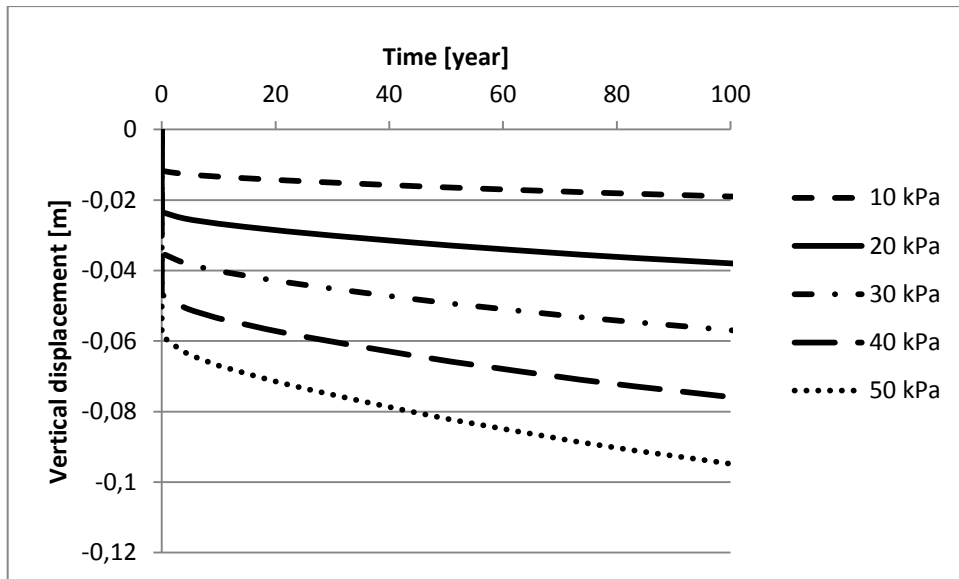


Figure 7.8 Settlements plotted versus time, in the middle of the raft, for all five loading scenarios.

Figure 7.9 and Figure 7.10 show settlements along the raft, from $x=0$ to $x=79,2$, for a piled raft and a raft without piles, respectively, when exposed to the different loading scenarios 10-50 kPa followed after a consolidation of 40 years. It can clearly be seen that the piled raft has smaller settlements than the raft without piles. For both models predicted settlements more or less have linear increment relative each other, which correspond to the relative increment of the loading scenarios. This also suggests elastic behaviour.

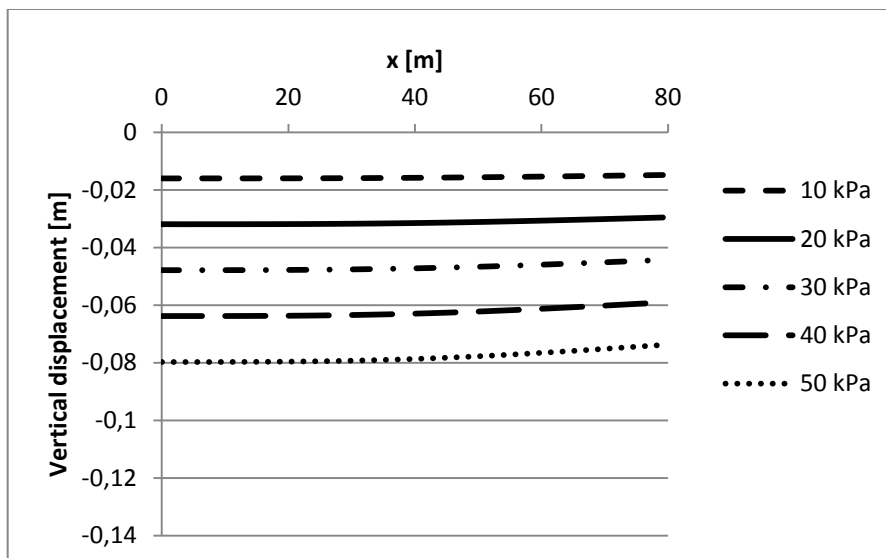


Figure 7.9: Settlements along the piled raft after 40 years of consolidation, following the additional construction.

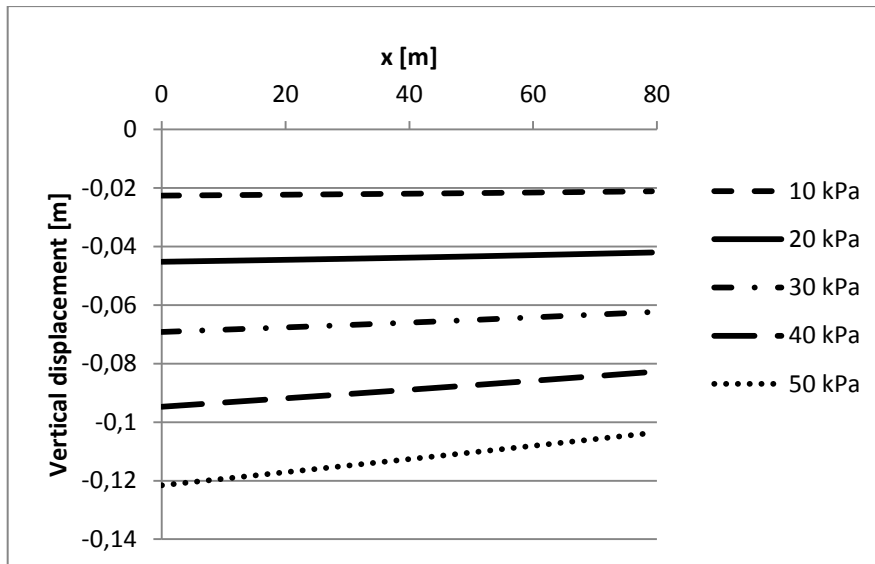


Figure 7.10: Settlements along raft without piles after 40 years of consolidation, following the additional construction.

When analysing the differential settlements, the raft is divided into 7 parts which correspond to the sections between the point loads. Sections 1-7 are located in that order from left to right along the plate. Section 1 is 7.2 m wide and the others are 12 m wide each.

From Figure 7.11 it can be noted that the load affects the size of the differential settlements the more to the right the observation is made. While hardly any difference can be seen for section 1, a difference of approximately 4.5×10^{-5} can be seen for section 7. This however is still regarded as small compared to limit values.

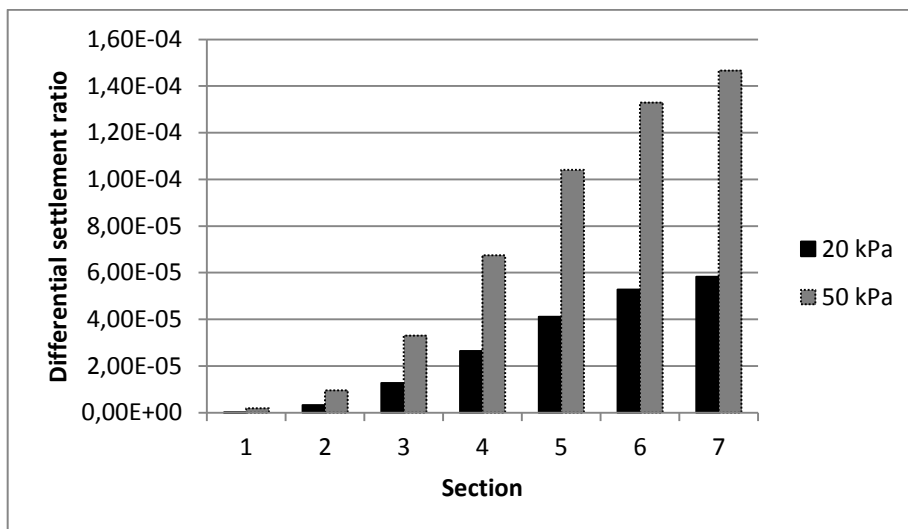


Figure 7.11: Differential settlements after 40 years consolidation, following the additional construction, at different parts of the piled raft during loading scenarios 20 kPa and 50 kPa.

When comparing the predictions by different models, see Figure 7.12, it is observed that, for most sections, the raft without piles has greater differential settlements. However, it can be seen that for sections 6 and 7, the piled raft has greater differential settlements than the raft without piles. This is remarkable since one of the main reasons this foundation method was implemented was to reduce differential settlements. One possible reason for this is overdesign at the right edge. Since the building settles more to the left, it can be assumed that a greater part of the load is applied there. Thus, a smaller load than anticipated is applied to the right. If the foundation is overdesigned at the right edge, it will not settle in the same rate as the rest of the construction. This is under the assumption that the construction is not stiff enough to distribute the loads. It must however be taken into consideration that the models are based on a relatively small part of the building and that it is not certain this would have been the case if the whole building was modelled in 3D. Also note that even the largest differential settlements are far below the limit value.

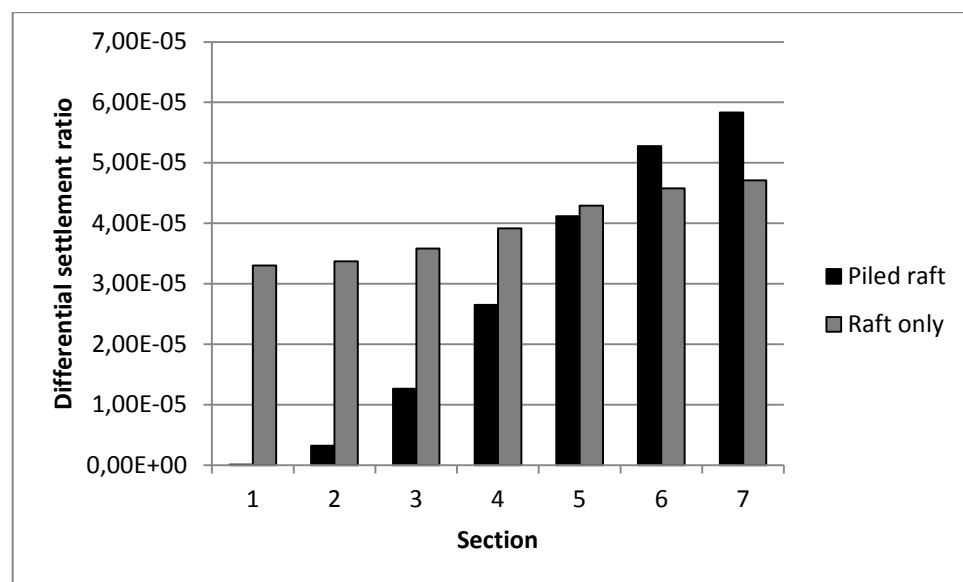


Figure 7.12: Differential settlements after 40 years consolidation, following the additional construction, at different parts of the piled raft for different models.

When analysing the settlements for different levels, a cross-section below the middle of the raft has been chosen.

In Figure 7.13 it can be seen that the increase in settlements with depth corresponds linearly to the increase in loads. This is a similar behaviour to the settlements along the raft, and again underlines the elastic behaviour.

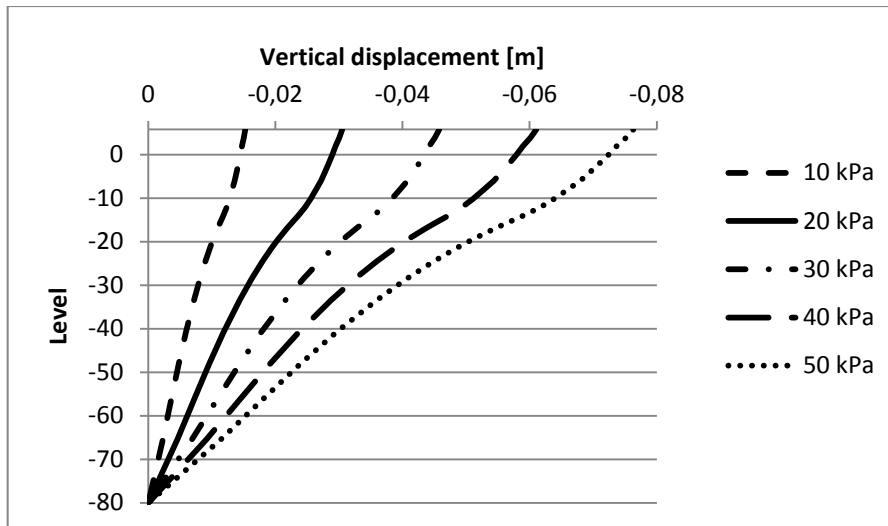


Figure 7.13: Settlements at different levels for different loading scenarios measured at the middle of the raft after 40 years of consolidation, following the additional construction.

In Figure 7.14, where settlements are plotted versus level for two rafts, one piled and one without piles, it is shown that the settlements near the surface are larger for the raft without piles. The settlement curves approach each other at deeper levels. At the level of the pile head, a change in inclination can be observed, which means that the load is transferred there, causing larger settlements. This corresponds well to Figure 7.3, where excess pore water pressure at different levels is plotted for different models. When the loads are transferred to deeper levels, where the soil is more resistant to compression, the total settlements are smaller.

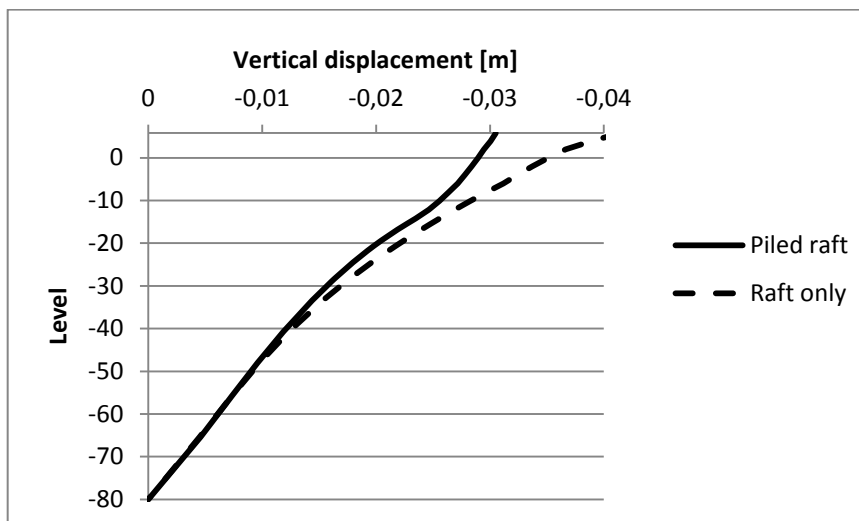


Figure 7.14: Settlements versus level for different models measured below the middle of the raft.

In Figure 7.15 the predicted settlements over time for the middle of the raft, after the additional loading of 20 kPa, are shown. The settlements for the raft without piles are significantly larger.

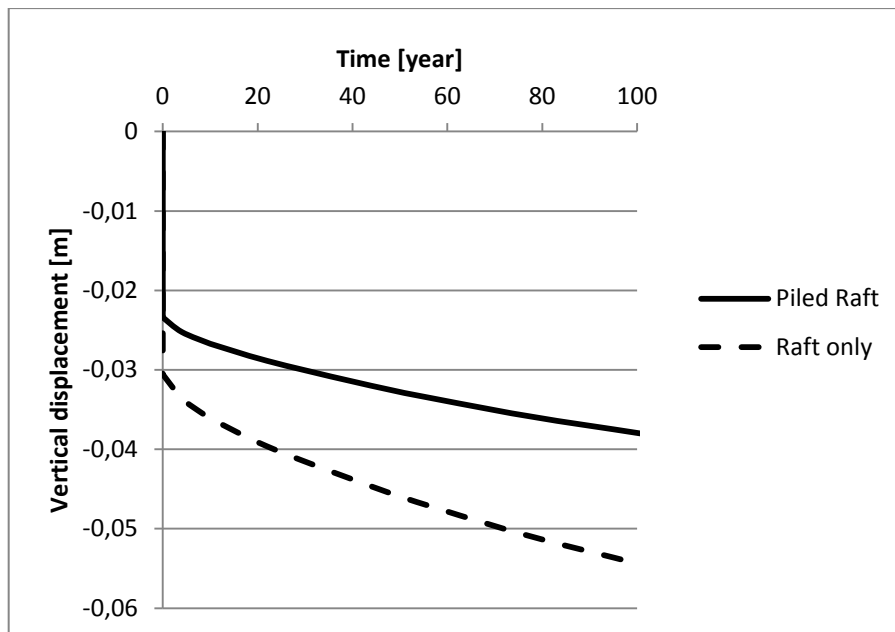


Figure 7.15: Settlements at different times after the additional load of 20 kPa, obtained at the middle of the raft. The timespan observed is 0-100 years, since this is the technical lifespan for buildings.

Soft Soil Creep

Figure 7.16, Figure 7.17 and Figure 7.18 show how settlements by time and level differ for the two material models Soft soil and Soft Soil Creep.

When evaluating μ^* from the oedometer tests, the inclination of the curves might be too steep to get the proper μ^* value. It is important to evaluate the parameter when the primary consolidation has ended and any effects of structure (for sensitive soils) are no longer present (i.e. pure creep at high stress levels). If consolidation is still occurring, it might overestimate μ^* and thus contribute to that larger settlements being predicted, than will actually happen. Looking at the inclination of the curves in Appendix C, it is hard to tell if consolidation is still occurring. However, the settlement over time for the Soft Soil Creep model indicates that it occur very little creep during the first 100 years. Also, when applying the Soft Soil Creep model on the time span up until today, the difference in heave is negligible. This is logical for low loads, since if studying the stress analysis graph, see Figure 7.35, the stress level should be below the creep limit when the piles are transferring some of the applied loads to a greater depth. However, it is a bit more remarkable that there is no significant creep during the first 100 years when applying a load of 50 kPa. The results above point at elastic response of the soil.

In Figure 7.17 “SSC – control” is plotted. It is a point located at the surface at a relatively large distance from the raft, and is not exposed to any load elements. As can be seen the deformation will with time be larger than the ones predicted below the raft. This is caused by an error in the formulation of the Soft Soil Creep model. Due to heave at the excavation, the soil located there behaves more elastically than the soil not located at the excavation. This indicates that the Soft Soil Creep model overestimates the time dependent settlements and hence the model does not consider the creep deformations in a realistic way.

With a new corrected Soft Soil Creep model and with better soil tests, it might be possible to get a more realistic creep prediction. The simulated soil test where the strain versus time is plotted has a very bad fit compared to the original oedometer test. Even though no effort has been put into making the curves fit better, this also indicates that the creep parameter needs to be re-evaluated. However, it could also be very tricky conditions at the investigated site, with the old remnants in the ground in mind.

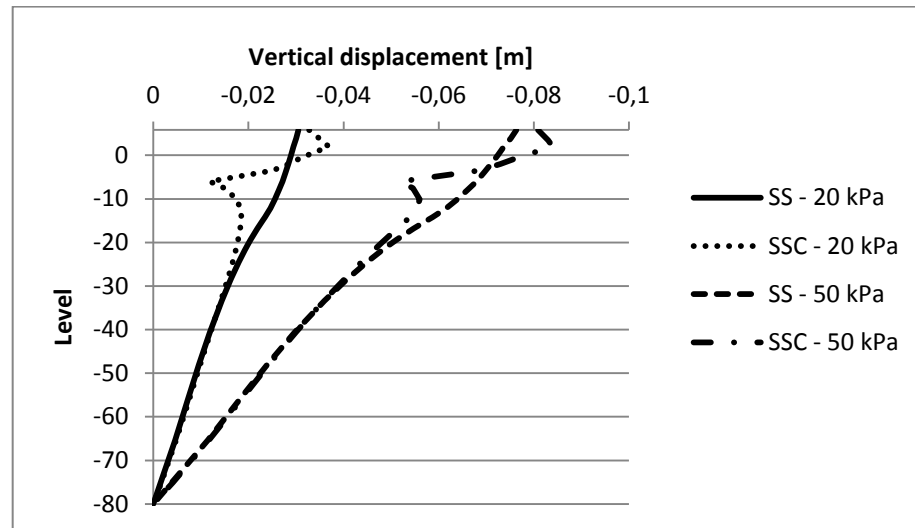


Figure 7.16 Settlement versus level, in a cross-section below the middle of the raft, for the models Soft soil (SS) and Soft Soil Creep (SSC), after a consolidation of 40 years for loading scenarios 20 kPa and 50 kPa

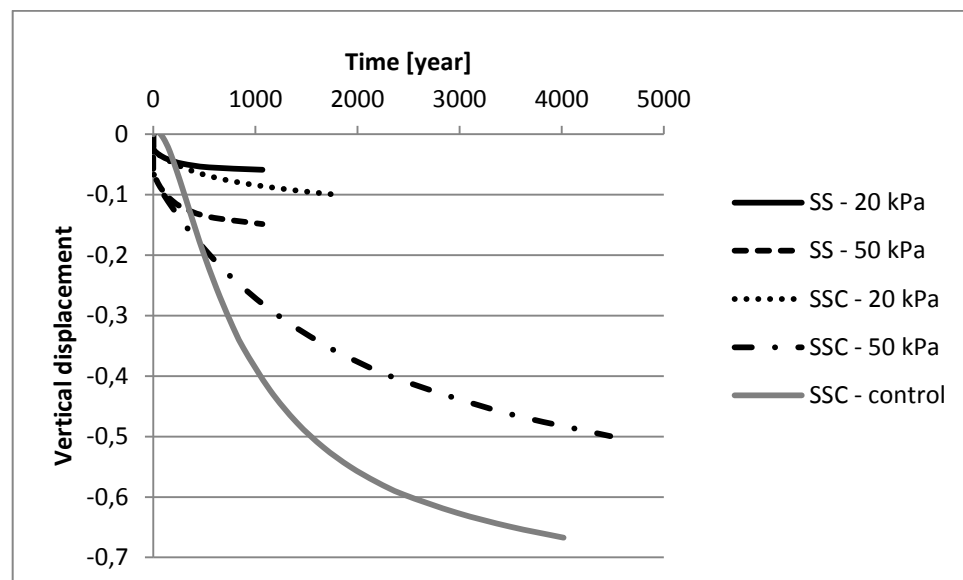


Figure 7.17 Settlement versus time, in a point directly below the middle of the raft, for models Soft Soil (SS) and Soft Soil Creep (SSC) during loading scenarios 20 kPa and 50 kPa. The last result is when 90 % of p_{excess} has dissipated. "SSC – control" represents a node at a far distance from the building.

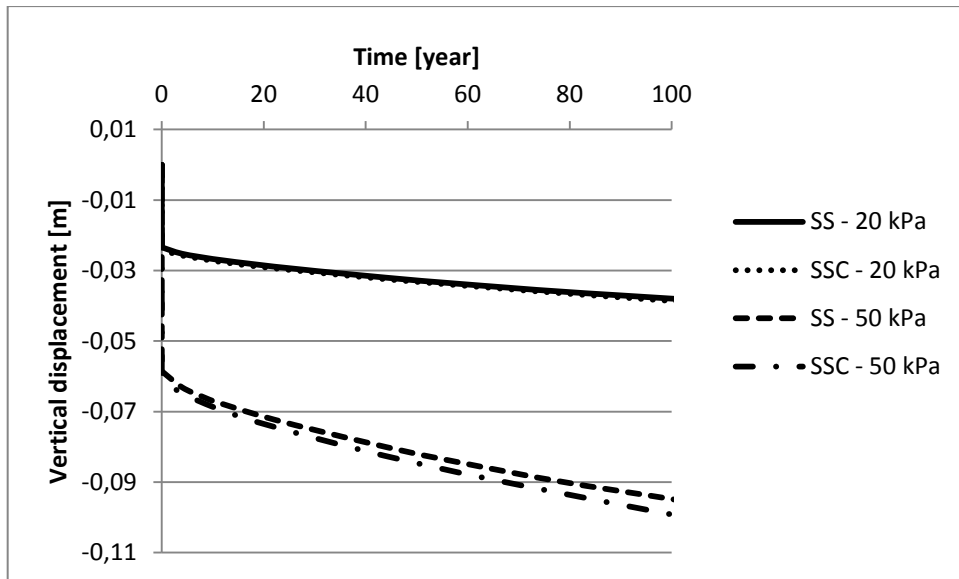


Figure 7.18 Enlarged version of Figure 7.17 showing the settlement during the first 100 years.

7.1.3 Pile interaction

In Figure 7.19 the ratio of load carried by piles, α_{rp} , is plotted for different load scenarios. The ratio is increasing with both an increasing load and over time.

The results regarding how big part of the load that is carried by piles seems reasonable, when the different scenarios are compared to each other. The piles carry a greater part of the loads when the loads are larger. The same thing can be seen when observing one load scenario over time. The reason for this is that the neutral plane rises when loads are larger or is transferred from excess pore water pressure to piles during consolidation.

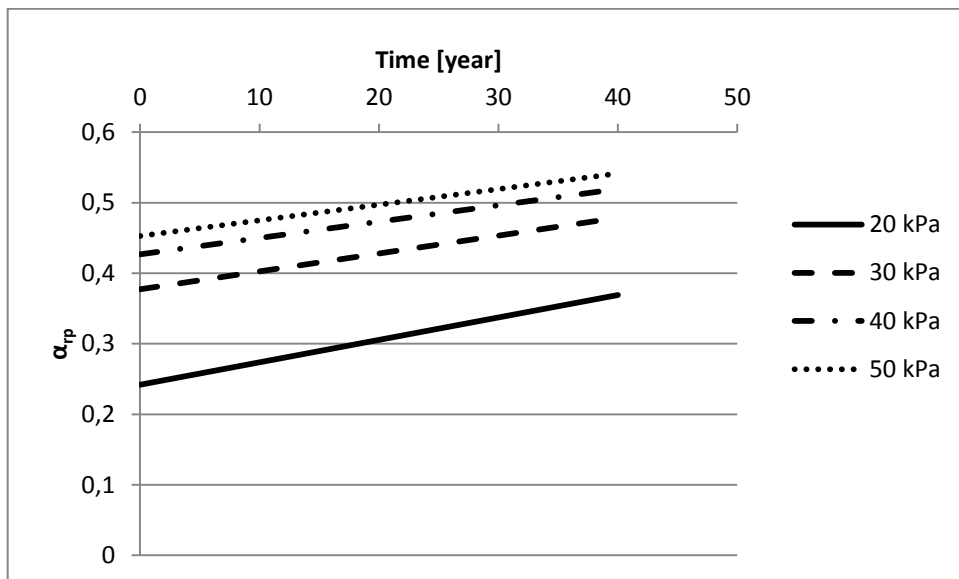


Figure 7.19 Ratio of load carried by piles, for different load steps

Axial force developed in each pile along the raft, immediately after an additional load of 20 kPa, is presented in Figure 7.20. Axial loads are larger for the piles positioned at the edges of the plate.

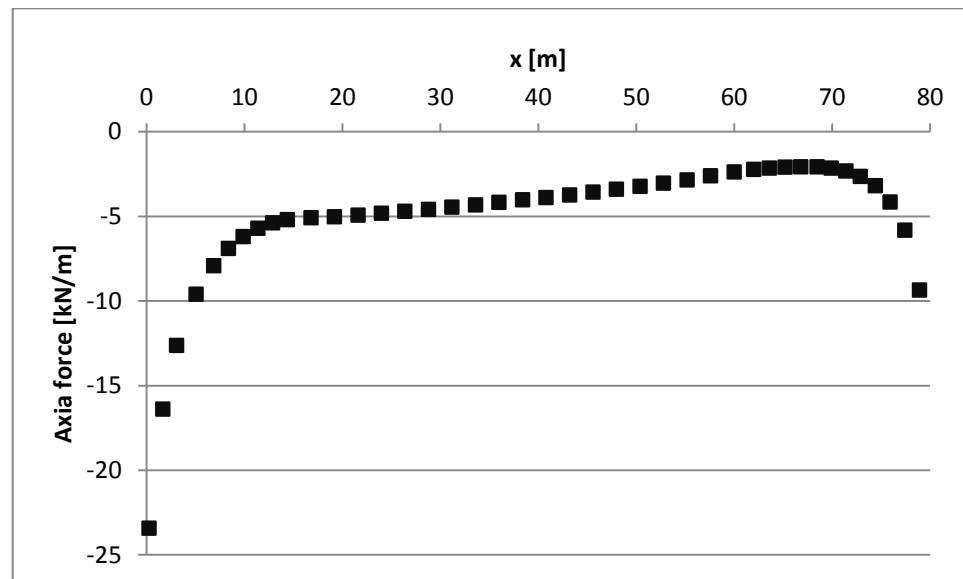


Figure 7.20 Axial force for each pile along the raft immediately after an additional load of 20 kPa.

In Figure 7.21, axial forces versus level is plotted for a pile in the middle of the raft, for loading scenarios 20 and 30 kPa, as well as a pile located at the left edge of the raft, for loading scenario 20 kPa. For the middle pile with an additional load of 20 kPa, the peak value is located around the middle of the pile. For the other two piles presented, the peak value is found at the top of the piles. This should indicate the level where the neutral plane is located and that full friction has not been developed for the middle pile. The pile at the left edge, where the axial force is larger, has its peak value at the top, which should mean full friction is developed. For the loading scenario of 30 kPa full friction is developed also for the middle pile. This is according to the theory that the neutral layer gets closer to the raft with increased loading. Despite of where the neutral plane is located, the largest loads are transferred down to the pile toe. As discussed for Figure 7.1, this is the effect of pile group behaviour, which stiffens the whole soil body under the raft down to the pile toe.

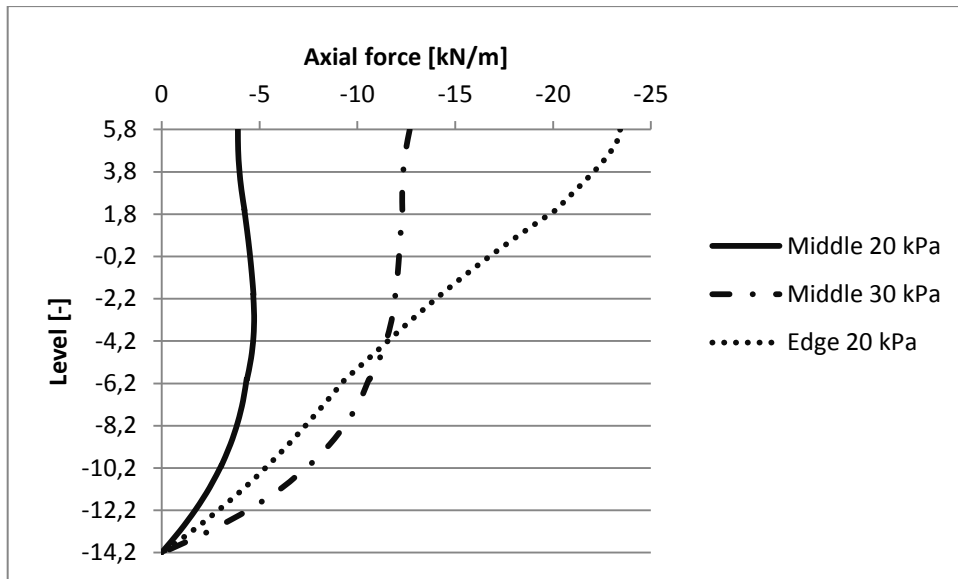


Figure 7.21 Axial force with depth for one pile at the middle of the raft and one pile at the left edge of the raft. For the former, results from two loading scenarios, 20 kPa and 30 kPa, are plotted.

7.2 Sensitivity analyses results

Below are results from the sensitivity analyses presented in form of graphs. Each parameter is presented in a separate section.

κ^*

In

Figure 7.22 the predicted vertical displacement is plotted versus level for different κ^* -values. It can be seen that the swelling index κ^* has approximately as much influence when increased as decreased, with a difference of 5 mm. This applies more or less for the entire depth. When plotting the deformations versus time a similar linear behaviour is observed.

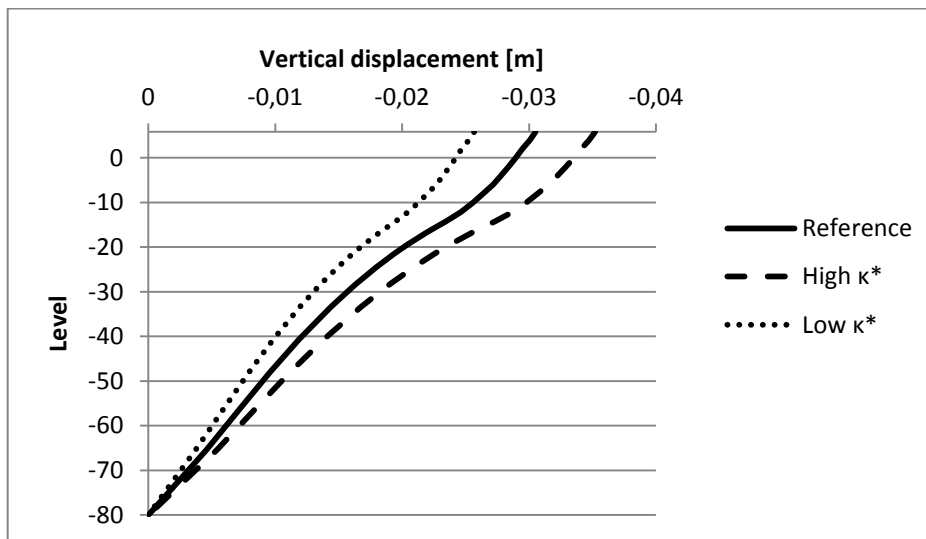


Figure 7.22: Settlement versus level for the swelling index sensitivity analysis.

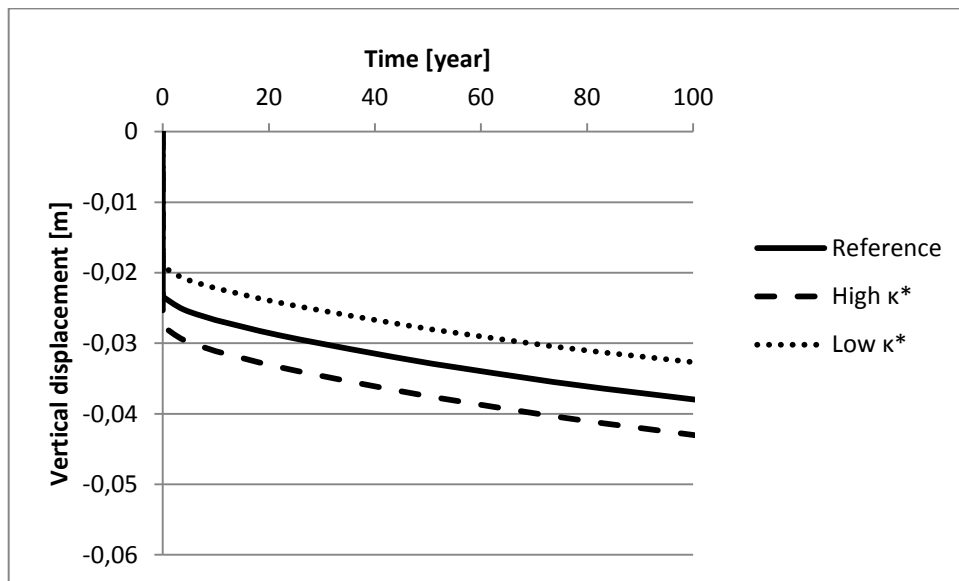


Figure 7.23: Settlement versus time for the swelling index sensitivity analysis.

λ^*

In figure Figure 7.24 vertical displacement is plotted versus level. As can be seen, the compression index λ^* has little influence on the settlements, since all three lines overlay each other. Similar observations are made when observing settlements versus time in Figure 7.25. This indicates that the pre-consolidation pressure is not reached even when two additional floors are constructed and is a further indication that the deformations are predicted to be elastic.

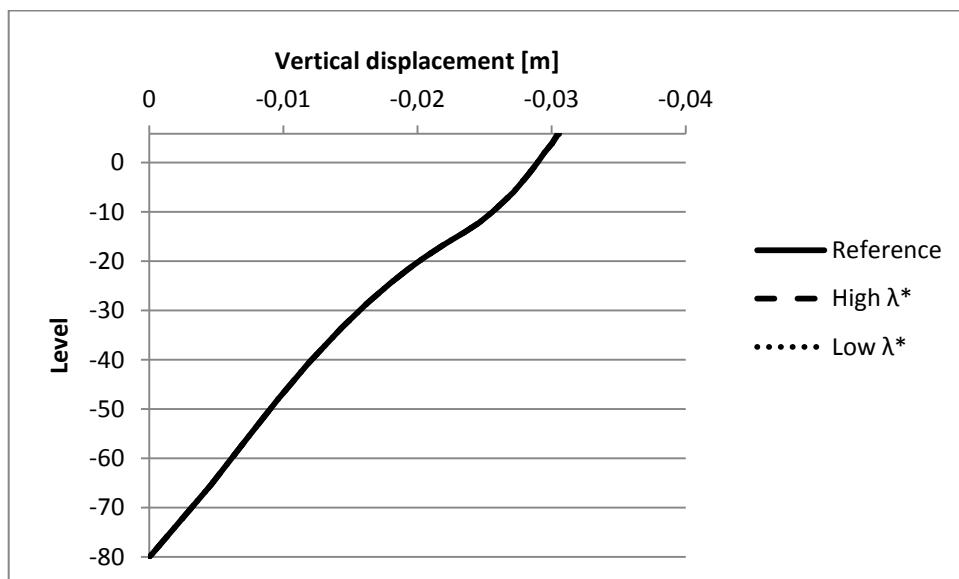


Figure 7.24: Settlement versus level for the compression index sensitivity analysis.

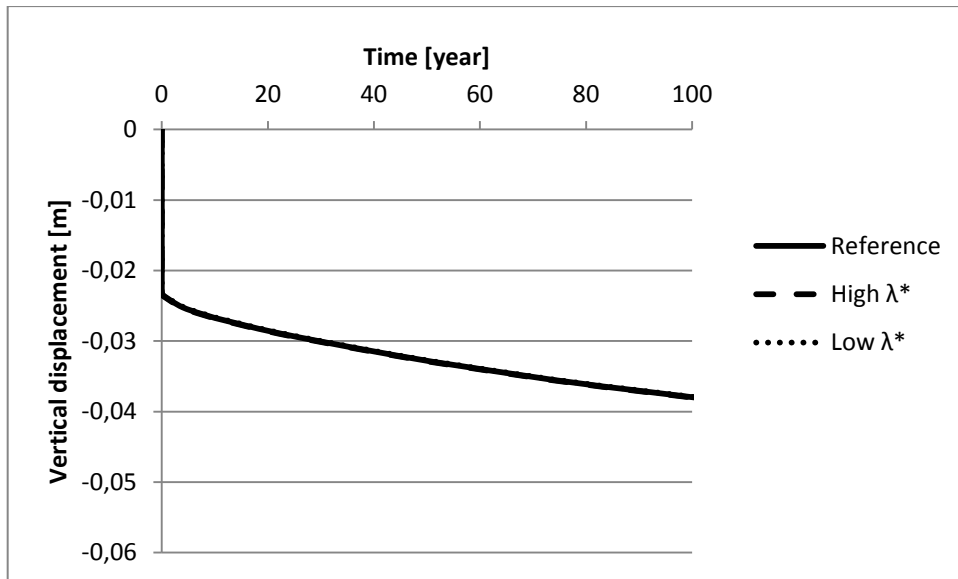


Figure 7.25: Settlement versus time for the compression index sensitivity analysis.

OCR

In Figure 7.26 and Figure 7.27 it can be seen that an increase in the value of the over consolidation ratio has no significant effect on the settlements. When the soil however, is set to be normal consolidated a difference is relatively large (approximately 9 mm at the top).

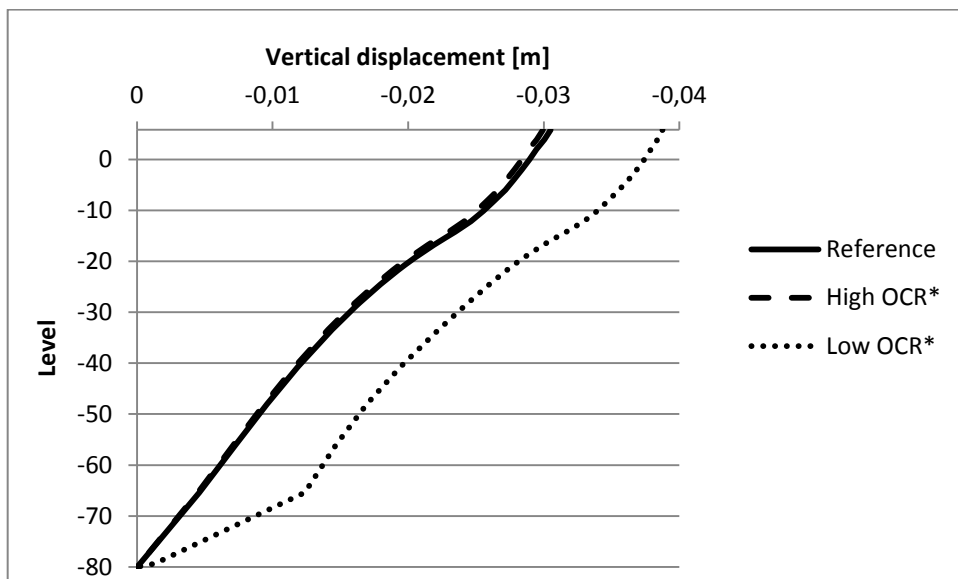


Figure 7.26: Settlement versus level for the over consolidation ratio sensitivity analysis.

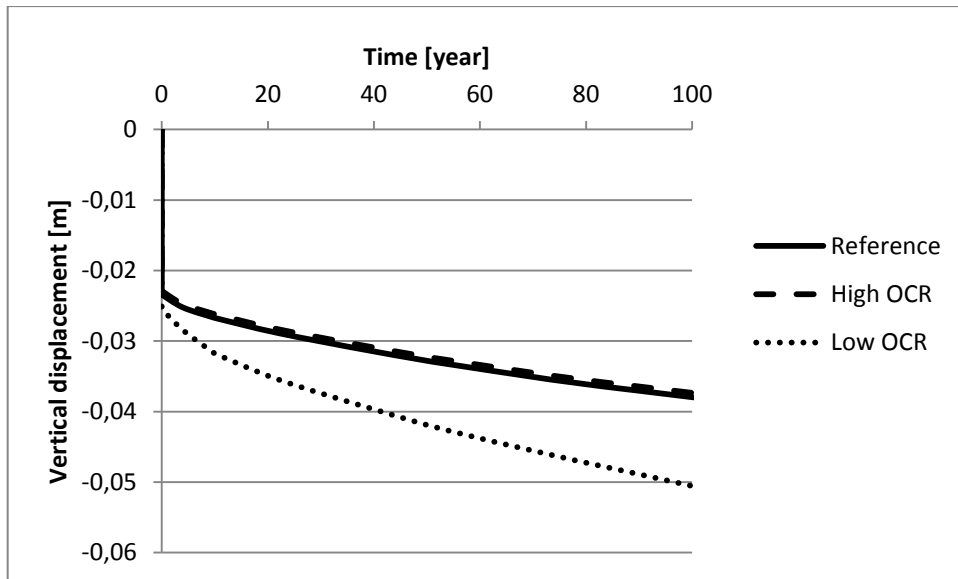


Figure 7.27: Settlement versus time for the over consolidation ratio sensitivity analysis.

In summary the stiffness parameters, κ^* has some effect while λ^* hardly has any at all. This indicates that the preconsolidation pressure is not reached when two floors are added, and the deformations are mainly elastic. This is further proved when the *OCR* is compared and only a lowering of this has a significant change of the results. Evaluated *OCR* values are relatively low compared to what is usually evaluated from clay in the Gothenburg region. This means that the *OCR* values are more likely underestimated than overestimated. Since higher *OCR* gives approximately the same results as the default model, the *OCR* should not have great influence on the uncertainty of the modelling.

The graph of the hand calculated stress analysis, for a raft without piles when two floors are added, see Figure 7.35, shows that the current stress touches the σ'_c line. However, since the piles in the default model are transferring a part of the load to greater depth, the preconsolidation pressure is not reached.

k_y and k_x

In Figure 7.28 and Figure 7.29 the influence of the permeability parameter, k , on vertical displacement versus level can be seen. The influence on the settlements seems to be relatively small and increase or decrease about as much for a higher or lower permeability respectively.

The influence on p_{excess} in Figure 7.30 and Figure 7.31 is more interesting. While the lower permeability does not seem to change much from the results of the reference model, the higher value affects the results more since a greater part of the excess pore water pressure has dissipated after 40 years. The small effect regarding settlements could be an indication that deformations are mainly elastic in the model.

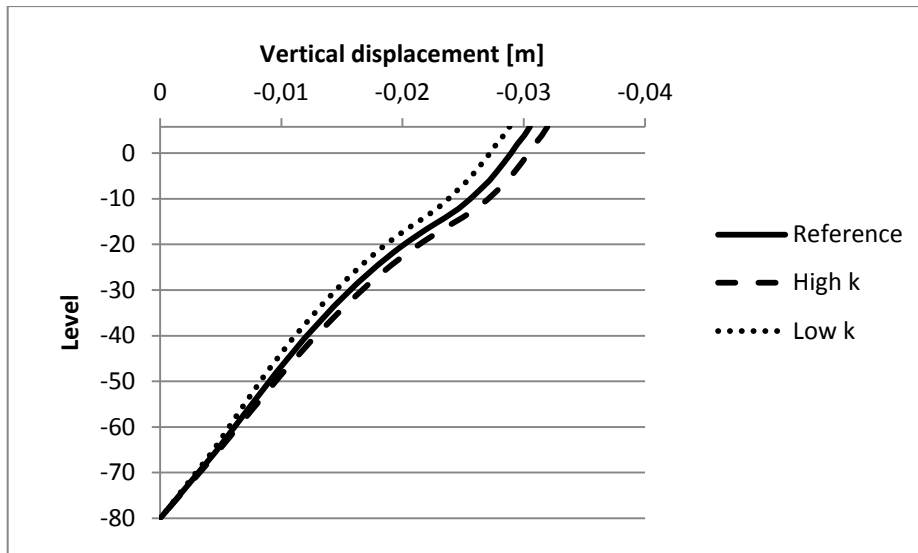


Figure 7.28 Settlement versus level for the permeability sensitivity analysis.

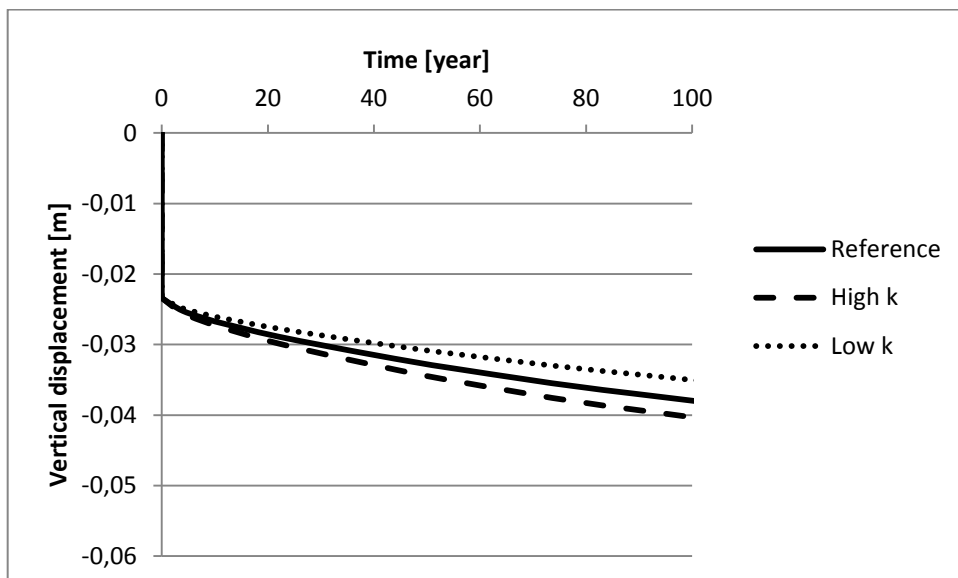


Figure 7.29 Settlement versus time for the permeability sensitivity analysis.

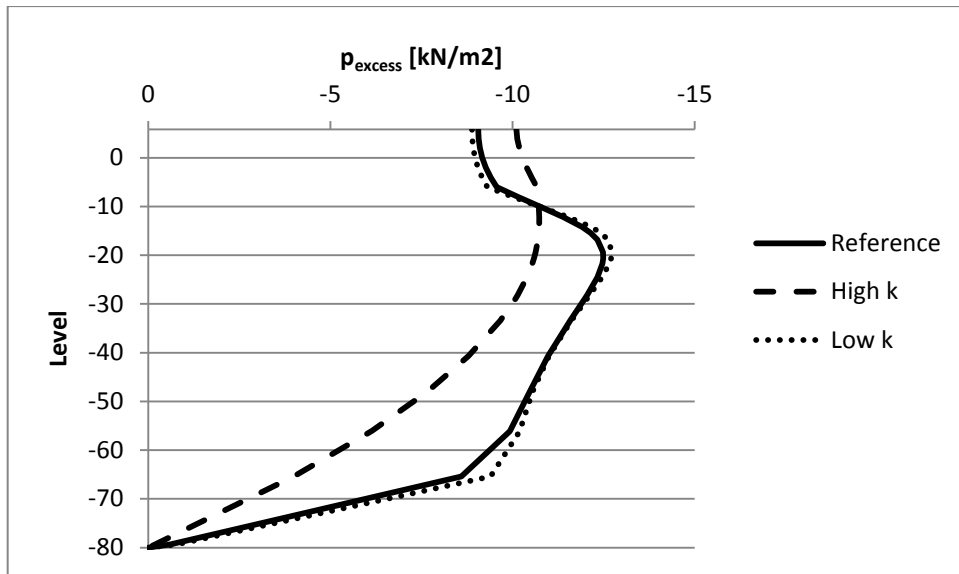


Figure 7.30: Excess pore water pressure versus level for the permeability sensitivity analysis, after 10 years of consolidation.

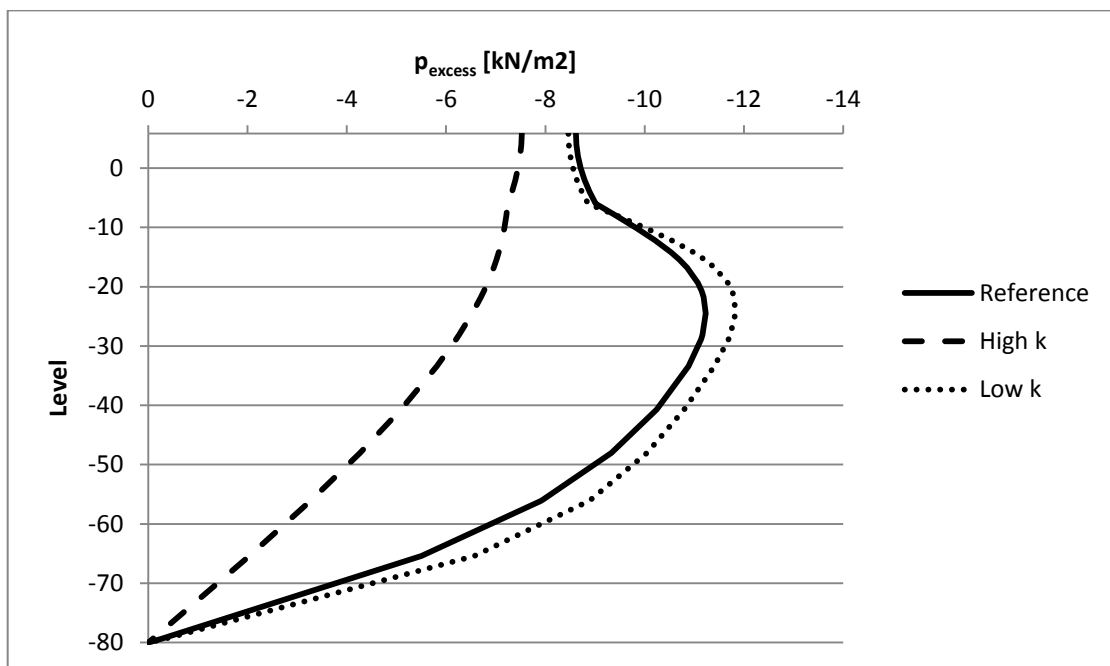


Figure 7.31: Excess pore water pressure versus level for the permeability sensitivity analysis, after 40 years consolidation.

d_{pile}

Since the embedded pile element does not consider conical piles, a sensitivity analysis has been performed in order to investigate which influence this parameter has. In Figure 7.32 some influence can be seen. There are negative values at sections 1 and 2 for piles with the larger diameter. This means that the inclinations of these sections have opposite directions of the one for the other sections. The diameter clearly has more influence on the differential settlements of the leftmost sections while the value for section 7 does not have a noticeable change at all. The increased settlements are

still very small when compared to the limit values. It is hard to tell which diameter gives a more correct result without real pile test to compare with. Such tests should be performed in order to evaluate how to model conical piles with the embedded pile row element.

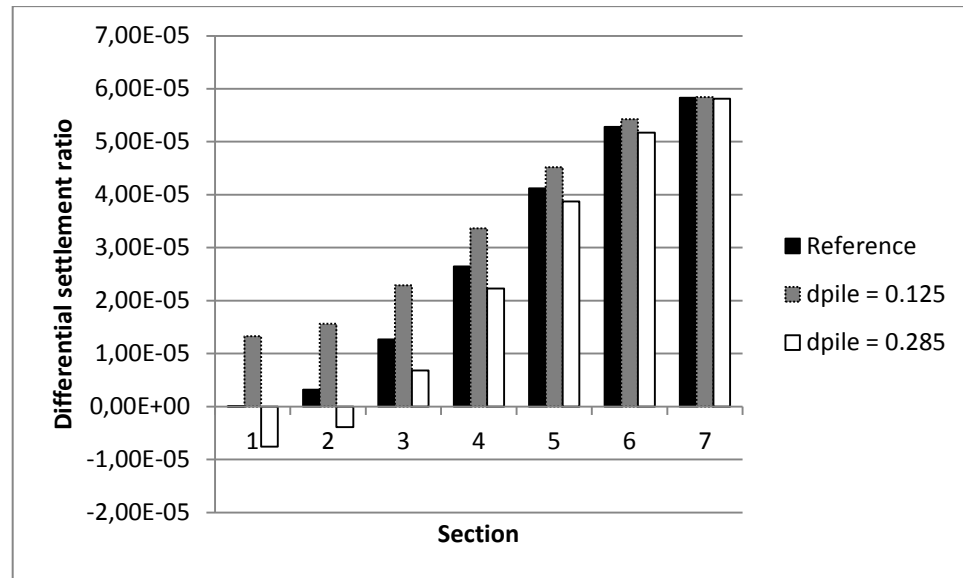


Figure 7.32: Differential settlements for different d_{pile} input values.

$L_{spacing}$

In Figure 7.33 in can be seen that $L_{spacing}$ does not have any significant influence on the differential settlements.

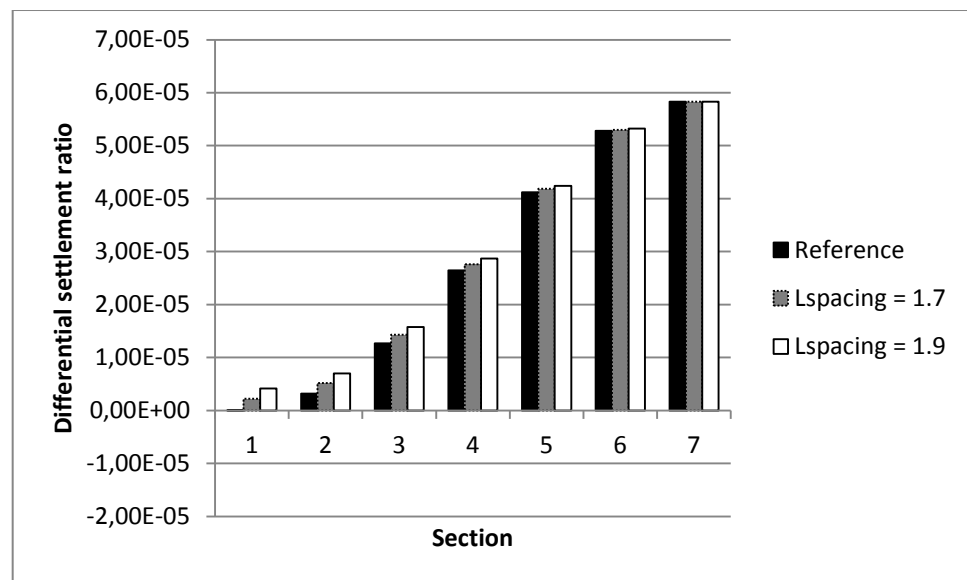


Figure 7.33: Differential settlements for different $L_{spacing}$ input values.

7.3 Hand calculations

7.3.1 Stress distribution

The stress distribution with level, between hand calculations and PLAXIS, are compared in Figure 7.34 below. The comparison is made with distributed load and without the pile elements. The stress distribution is presented for three phases.

1. Initial Hand/PLAXIS. Represents the stress state in the soil before the excavation was made and the original building was constructed.
2. Construction Hand/PLAXIS. Represents the stress state immediately after the original building was constructed.
3. Construction 20 kPa Hand/PLAXIS. Represents the stress state immediately after an additional load of 20 kPa is applied.

The curves for all three phases coincide well with each other. The stress distribution is reasonable since it decreases, due to the excavated soil masses, when the original construction is built. When two floors are added, it increases with approximately 20 kPa.

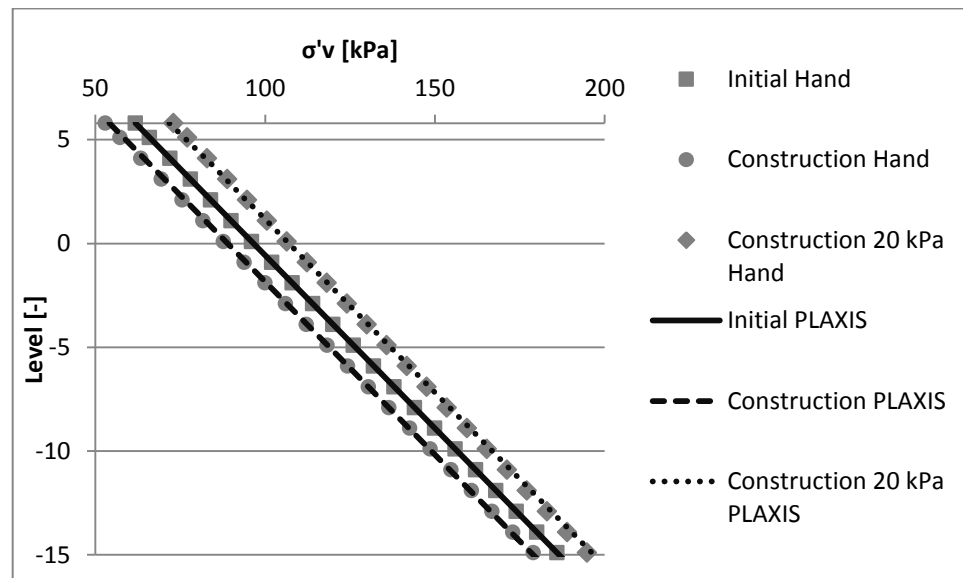


Figure 7.34 Stress distribution comparison between hand calculations and PLAXIS 2D. The comparison is made without piles and with distributed load.

Figure 7.35 and Figure 7.36 presents the stress distribution with level for a raft without piles during load scenarios 20 kPa and 50 kPa, respectively. Each figure includes curves which describes in-situ earth pressure, preconsolidation pressure, σ'_c , creep limit and current stress state, caused by the weight of the building. According to these graphs the preconsolidation pressure should be reached for all loading scenarios above 20 kPa in a model without piles. This is contradictive to the results, which indicate elastic behaviour for all loading scenarios.

For a model with a piled raft of course the loads would be transferred deeper into the ground and the preconsolidation pressure might not be reached.

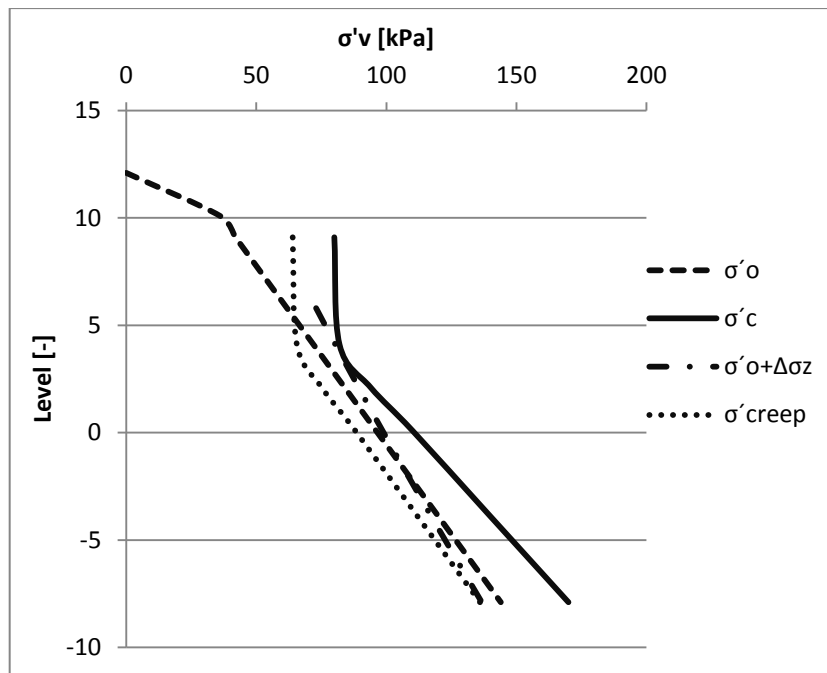


Figure 7.35 Stress analysis with depth for load scenario 20 kPa and a raft without piles.

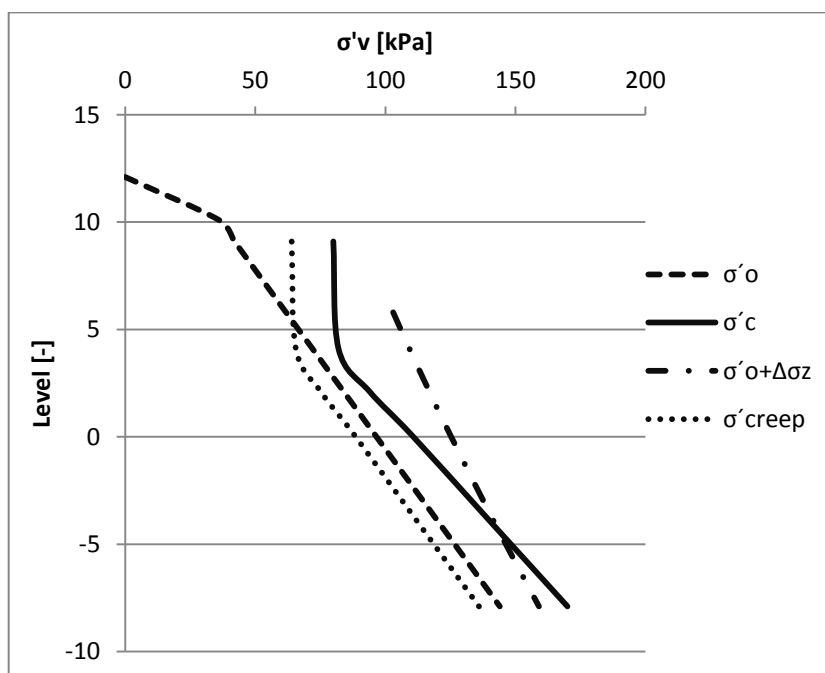


Figure 7.36 Stress analysis with depth for load scenario 50 kPa and a raft without piles.

7.3.2 Design demands

The results below are based on the assumption of a distributed load across the raft. The difference in edge and middle of the plate is due to different pile spacing. The

calculations are made with the same input values, for weight of the excavated soil and for loads of the building, which are used for the PLAXIS modelling.

Table 7.1 presents how the design demands are met, with the assumption made that the water level in the reservoir below the building is kept at its original design level, +11m, see Table 3.2

Table 7.1 Results of design demands with a reservoir level of +11. All values are given in MP/m².

Design demand	Edge	Middle	Demand
1	0.8	0.8	>0
2	16.9	13.5	>9.6 MP/m ²
3	15.3	10.1	>9.6 MP/ m ²
4	15.2	10.0	>9.6 MP/ m ²

Table 7.2 presents how the design demands are met, with the assumption made that the water level in the reservoir below the building is kept at +9.9, which is the obtained level during the last reading, see Table 3.2. Note that design demand 4 is not met.

Table 7.2 Results of design demands with a reservoir level of +9.8. All values are given in MP/m².

Design demand	Edge	Middle	Demand
1	0,8	0.8	>0
2	15.7	12.3	>9.6 MP/ m ²
3	15.3	10.1	>9.6 MP/ m ²
4	14	8.8	>9.6 MP/ m ²

8 Discussion

This chapter contains discussion regarding general aspects of the model and the thesis as a whole.

No consideration has been taken to the group effect of the piles, when calculating the input value for the skin friction. It was difficult to know beforehand how the modelled piles would behave, but since the behavior seems to correspond to a pile group, this needs to be considered in further analysis. Since the behaviour of a pile element is a 3D problem, it is of course difficult to model it in a 2D model. Since there is little literature to find regarding the embedded pile row element, it is difficult to interpret how accurate it is working. Based on our results, the pile elements seem to behave in reasonable way. However, real pile tests needs to be performed in order to validate their function.

When observing the comparisons between results from different loading scenarios it can be seen that total settlements, both by time and depth, seem to correspond to the increase in loads in a linear manner. The differential settlements at the right most sections of the piled raft have a greater increase than the left edge. Since these still are quite small, compared to maximum allowed values, it is likely that total settlements at connections with the surrounding streets will be decisive for whether further construction can be made. Since the surroundings have not been considered in this thesis, only speculation can be made, but of course if the settlements at the connections are too large, it could lead to problems with for example pipes, cables or cracking of joints.

In this specific case, it is hard to predict the stiffness of the ground only from soil tests, since there are old remnants there from old construction, e.g. old timber piles. It is difficult to predict how this would affect the construction of additional floors. A logical reasoning would be that it reduces the settlements since the soil gets stiffer. But irregular stiffness might also cause differential settlements.

There are several uncertainties and simplifications to consider regarding the evaluations and calculations performed. One of the most obvious is of course the choice of modelling in 2D. Since a plane strain model would over- rather than underestimate settlements, there might be more capacity of the foundation than these calculations indicate.

The data which the geological and hydrological conditions are based on are old and the equipment used for obtaining them might not be as good as the ones used today. The lack of triaxial tests has also resulted in the need to assume key parameters. Real triaxial tests should be performed, since they should give a better foundation than using relationships to evaluate results from one-dimensional oedometer tests together with assumptions. The construction drawings are from the 1970's. It might be needed to recalculate the loads since there has been some reconstruction of the building and relocation of former activities.

No parametric study regarding ϕ' has been performed, but the value used when modelling is somewhat lower than average for clay in Gothenburg, which means the calculations are conservative. For further investigation the influence of ϕ' should be considered.

A scenario where the water level in the reservoirs below the building would drastically sink has not been considered. This partly because it is difficult to model

and time is restricted. A simplification of a scenario would be that for each meter the water level is lowered, 10 kPa is added as an applied load on foundation. Thus, by simulating a total addition of five floors, we have also simulated a scenario where the water level drops five meter. For further studies investigations regarding a possible increase in ground water level should also be carried out.

The model does not include the non-hydrostatic over pressure of pore water, 20-30 kPa at 20 meters depth. This is because there has not been very detailed information about this, for example how it increases with depth and at which depth it starts.

An error made during simulation was that only embedded pile row elements with $L_{spacing} = 1.5$ m were used. Some piles in the middle should have been given input value $L_{spacing} = 1.9$ m. This was noticed late in the investigations and because of the time frame there was no time to redo all calculations. However this only affects the spacing in the out of plane direction. The parametric analysis of $L_{spacing}$ show that there was little influence regarding differential settlements. The α_{rp} value would probably have been slightly reduced if the middle piled would have had the larger $L_{spacing}$ value, since fewer piles would increase the contact stress between ground and raft.

According to our calculations, the design values are not fulfilled today. It should be noted that they are made with our evaluation of loads, which could differ from the original, since we have not been able to find the old calculations for building 6.

The analysis does not consider any time aspect for construction phases. This might lead to prediction of larger instant settlements than if the load from construction phases would have been applied over time.

9 Conclusions

Below conclusions drawn from the results and the discussion are presented.

The aim of this project has been to investigate the foundation principle of a piled raft and how well this can be modelled with numerical analysis, using a plane strain model and the embedded pile row element, in the computer software PLAXIS 2D. A case study model has been made of the building Nordstaden 8:27, where geotechnical effects, in terms of settlement caused by additional construction, is investigated.

The model in this case study seems to work in a fairly reasonable manner, considering the magnitude of settlements. This indicates that a plane strain model in PLAXIS 2D can be a good and time effective tool to get a first result, before using a more complicated three-dimensional model.

Using the embedded pile row element to model the behavior of piles seems to give qualitatively reasonable results in our model. However, real pile tests need to be performed in order to validate their behavior.

For further investigations, Nordstaden 8:27 should be modeled in 3D. A piled raft is a very complex foundation method and in 2D there are too many 3D interactions and factors of uncertainty to be able to fully trust the results. Surrounding buildings and streets would also have to be taken into consideration. It might also be needed to make calculations based on newer construction drawings for loads acting on the foundation.

New soil tests, especially triaxial tests and a new evaluation of the permeability, need to be performed. The soil tests used in this thesis are from 1966, which makes it hard to validate their reliability. Due to the lack of a triaxial test, some parameters have been approximated for this case study, which have added an uncertainty factor to the model.

The magnitude of the differential settlements is very low compared to the limit values, for all the modeled loading scenarios. Therefore, differential settlements should not cause any problems. Since Nordstaden 8:27 is connected to the surrounding streets, it is instead the settlements at the edges of the raft that will be decisive for how many floors that can be added. Further studies should investigate how much settlements can be allowed without causing too much cracking in the connection or any damage to the reservoirs or sensitive parts below the building.

10 References

- Alén, C. (2012) *Pile foundations - Short handbook (Educational material in Geotechnics)*, Gothenburg: Chalmers University of Technology.
- Bergdahl, U., Malmberg, B.S. and Ottosson, E. (1993) *Plattgrundläggning*, Solna: AB Svensk Byggtjänst.
- Boverket (2004) *Boverkets handbok om betongkonstruktioner BBK 04*.
- Carling et al, O. (1992) *Dimensionering av träkonstruktioner*, Stockholm: AB Svensk Byggtjänst and Trätek.
- Chai, J.C., Huang, J.Z. and Wu, W.J. (2002) 'Interaction between pile and raft in piled raft foundation', *Advances in Building Technology*, Hong Kong, 603-610.
- Craig, R.F. and Knappet, J.A. (2012) *Craig's soil mechanics*, 8th edition, Abingdon: Spon Press.
- Eriksson, P., Jendeby, L., Olsson, T. and Svensson, T. (2004) *Commission on Pile Research: Report 100 - Cohesion Piles*, Linköping: Swedens Geotechnical Institute (SGI).
- Fellenius, B.H. (2004) 'Unified design of piled foundations with emphasis on settlement analysis', *Geo-Institute Geo-TRANS Conference*, Los Angeles, 253-275.
- Fellenius, B.H. (2006) *Basics of Foundation Design*, Calgary.
- Flemming, W.G.K., Weltman, A.J., Randolph, M.F. and Elson, W.K. (1992) *Piling engineering*, 2nd edition, Glasgow and London: Blackie and Son Ltd.
- Fredriksson, A. and Rosén, R. (1988) 'Kryppålar och bottenplatta - Hållbart alternativ på besvärlig mark', *Byggindustrin*, No 34.
- Fritz, M. (1997) *Nordstan - Från gårdagens vision till dagens affärscentrum*, Gothenburg: Tre Böcker Förlag AB.
- Gibson, R.E., Gobert, A. and Schiffman, R.L. (1990) 'On Cryer's problem with large displacements and variable permeability', *Géotechnique* 40, No. 4, pp. 627-631.
- Giretti, D. (2009) *Modelling of piled raft foundations in sand*, Ferrara: University of Ferrara.
- Gustafsson, L., Gustavsson, T., Lund, R., Lüscher, K., Röine, H., Tauson, S., Söderquist, J. and Waldenström, L. (n.d) *Objekt 6 i Östra Nordstan*, Gothenburg: Artmen ab.
- Hansbo, S. (1989) *Grundläggning av byggnader och maskinfundament*, 2nd edition, Gothenburg: Chalmers University of Technology.
- Hansbo, S., Hoffman, E. and Mosesson, J. (1973) 'Östra Nordstaden, Gothenburg. Experiences concerning a difficult foundation problem and its unorthodox solution', *Proceedings of the eighth international conference on soil mechanics and foundation engineering*, Moscow, 105-110.
- Hansbo, S. and Jendenby, L. (1998) 'A follow-up of two different foundation principles', *Fourth International Conference on Case Histories Geotechnical Engineering*, St. Louis, Missouri, 259-264.

- Hansbo, S. and Källström, R. (1983) 'Creep piles - a cost-effective alternative to conventional friction piles', *Väg- och vattenbyggaren*, No 7-8.
- Helenelund, K.V. (1977) *Methods for reducing undrained shear strength of clay*. SGI report 3., Linköping: Swedish Geotechnical Institute.
- Holm, G. and Olsson, C. (1993) *Pålgrundläggning*, Solna: AB Svensk Byggtjänst.
- Holtz, R.D. (1991) *Foundation Engineering Handbook*, New York: Van Nostrand Reinhold.
- Jedenby, L. (1986b) 'Grundlägg inte på pålar - utan med hjälp av pålar', *Väg- och vattenbyggaren*, No 3, pp. 21-23.
- Jendeby, L. (1986a) *Friction piled foundations in soft clay - A study of load transfer and settlements*, Gothenburg: Chalmers University of Technology.
- Katzenbach, R., Gutberlet, C. and Bachmann, G. (2007) 'Soil-Structure Interaction aspects for ultimate limit state design of complex foundations', First International Symposium on Geotechnical Safety & Risk, Shanghai, 585-596.
- Kulhawy, F.H. and Prakoso, W.A. (2001) 'Contribution to piles raft foundation design', *Journal of geotechnical and geoenvironmental engineering*, January, pp. 17-24.
- Larsson, R. (1986) *Consolidation of soft soils*, Linköping: Swedish Geotechnical Institute (SGI).
- Larsson, R. (2008) *Soil properties*, Linköping: Swedish Geotechnical Institute (SGI).
- Leoni, M., Karstunen, M. and Vermeer, P.A. (2008) 'Anisotropic creep model for soft soils', *Géotechnique* 58, No. 3, pp. 215-226.
- Nguyen, D.D.C., Jo, S.-B. and Kim, D.-S. (2013) 'Design method of piled-raft foundations under vertical load considering interaction effect', *Computers and Geotechnics* 47, pp. 16-27.
- Olsson, M. (2010) *Calculating long-term settlement in soft clays - with special focus on the Gothenburg region*, Linköping: Swedish Geotechnical Institute (SGI).
- PLAXIS (2012) *Embedded pile row: A case study in PLAXIS 2D*, 6 November, [Online], Available: http://kb.plaxis.nl/sites/kb.plaxis.nl/files/kb-publications/CaseStudy_embedded_pile_row_nov2012_0.pdf [16 June 2014].
- PLAXIS (2014a) *Material Models Manual*, [Online], Available: <http://www.plaxis.nl/files/files/2DAnniversaryEdition-3-Material-Models.pdf> [03 Jun 2014].
- PLAXIS (2014b) *Reference Manual*, [Online], Available: <http://www.plaxis.nl/files/files/2DAnniversaryEdition-2-Reference.pdf> [03 Jun 2014].
- PLAXIS (2014c) *Embedded Pile Row in Plaxis 2D*, 16 Jun, [Online], Available: http://kb.plaxis.nl/sites/kb.plaxis.nl/files/kb-publications/CaseStudy_embedded_pile_row_nov2012_0.pdf [16 Jun 2014].
- Poulos, H.G. (2001) *METHODS OF ANALYSIS OF PILED RAFT FOUNDATIONS*, Sydney: Coffey Geosciences Pty. Ltd. & The University of Sydney.

Sluis, J., Besseling, F., Stuurwold, P. and Lengkeek, A. (2013) 'Validation and Application of the Embedded Pile Row-feature in PLAXIS 2D', *Plaxis Bulletin, Issue 34*, pp. 10-13.

Statens planverk (1968) *Svensk Byggnorm 67 (SBN 1967)*, Stockholm.

Svensson, L. (1993) *Östra Nordstan, Göteborg - Grundvattennivåer och sättningar*, Gothenburg: J&W Bygg & Anläggning AB.

Waterman, D. (2006) *Structural elements and excavations*, Chile: Plaxis.

Waterman, D. and Broere, W. (2005) *Practical application of the Soft Soil Creep model - Part III*, Delft: Delft University of Technology / Plaxis BV.

Wood, D.M. (1990) *Soil behaviour and critical state soil mechanics*, Cambridge: Press Syndicate of the University of Cambridge.

Appendices

Appendix A – Construction drawings

Appendix B – Hand calculations

Appendix C- Soil test evaluations

Appendix D – Continuous beams with uniformly distributed loads –
Sectional forces

Appendix E – Settlement limits

Appendix F – Settlement readings

Appendix A – Construction drawings

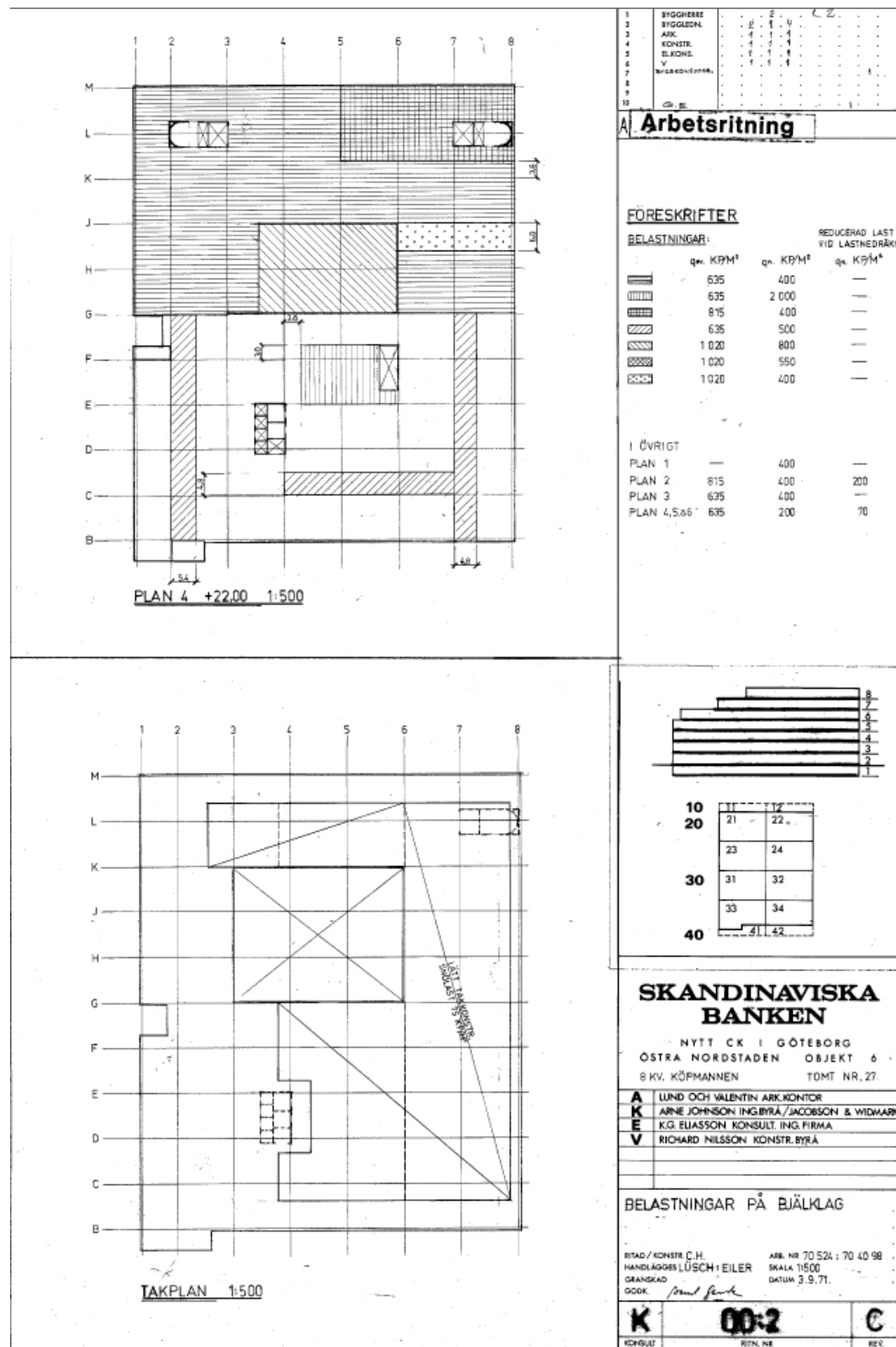


Figure A 1 Loads acting on floor 4 and roof as well as the magnitude of loads.

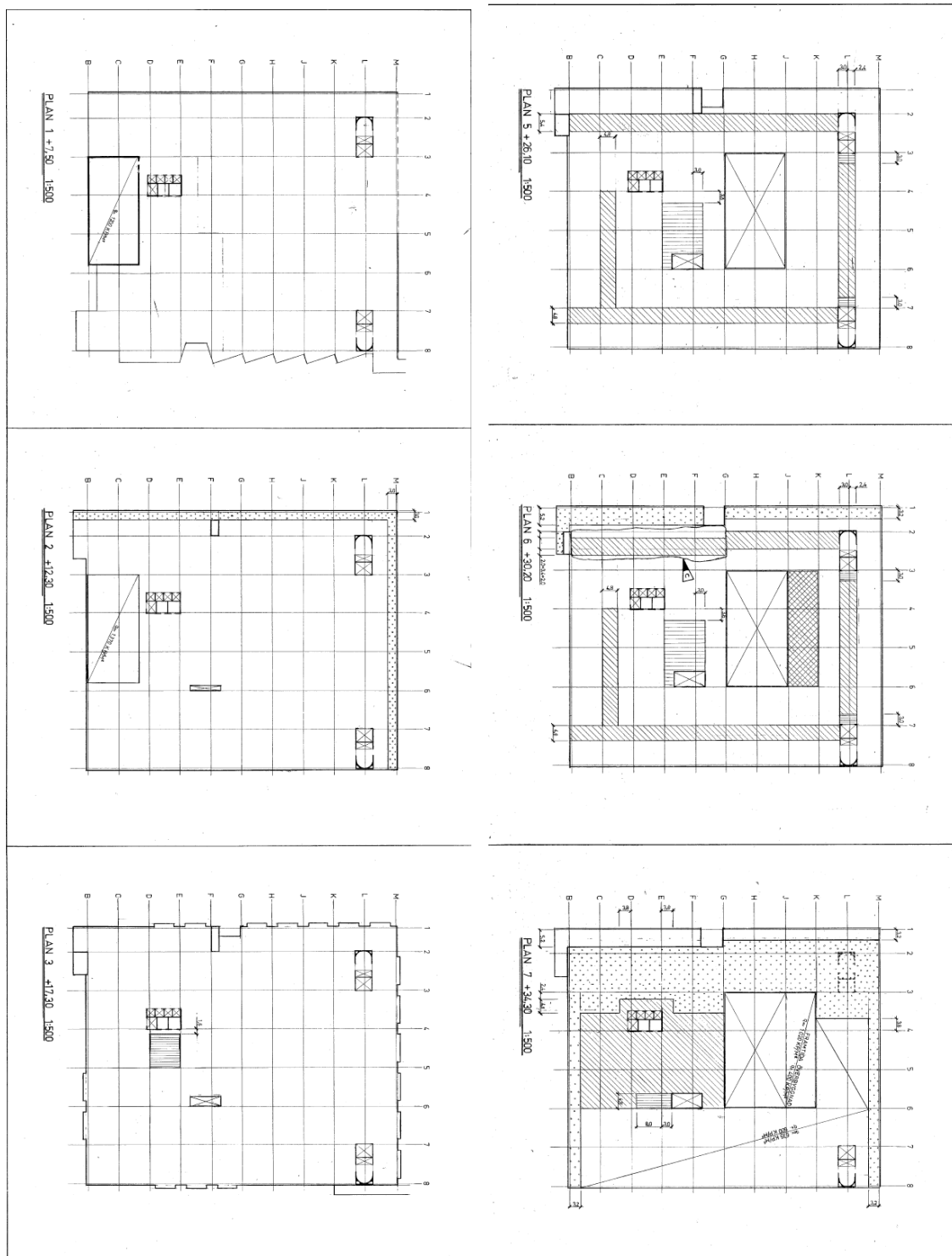


Figure A 2 Loads acting on floor, 1, 2, 3, 5, 6 and 7. Magnitude of the loads can be found in figure A-1.

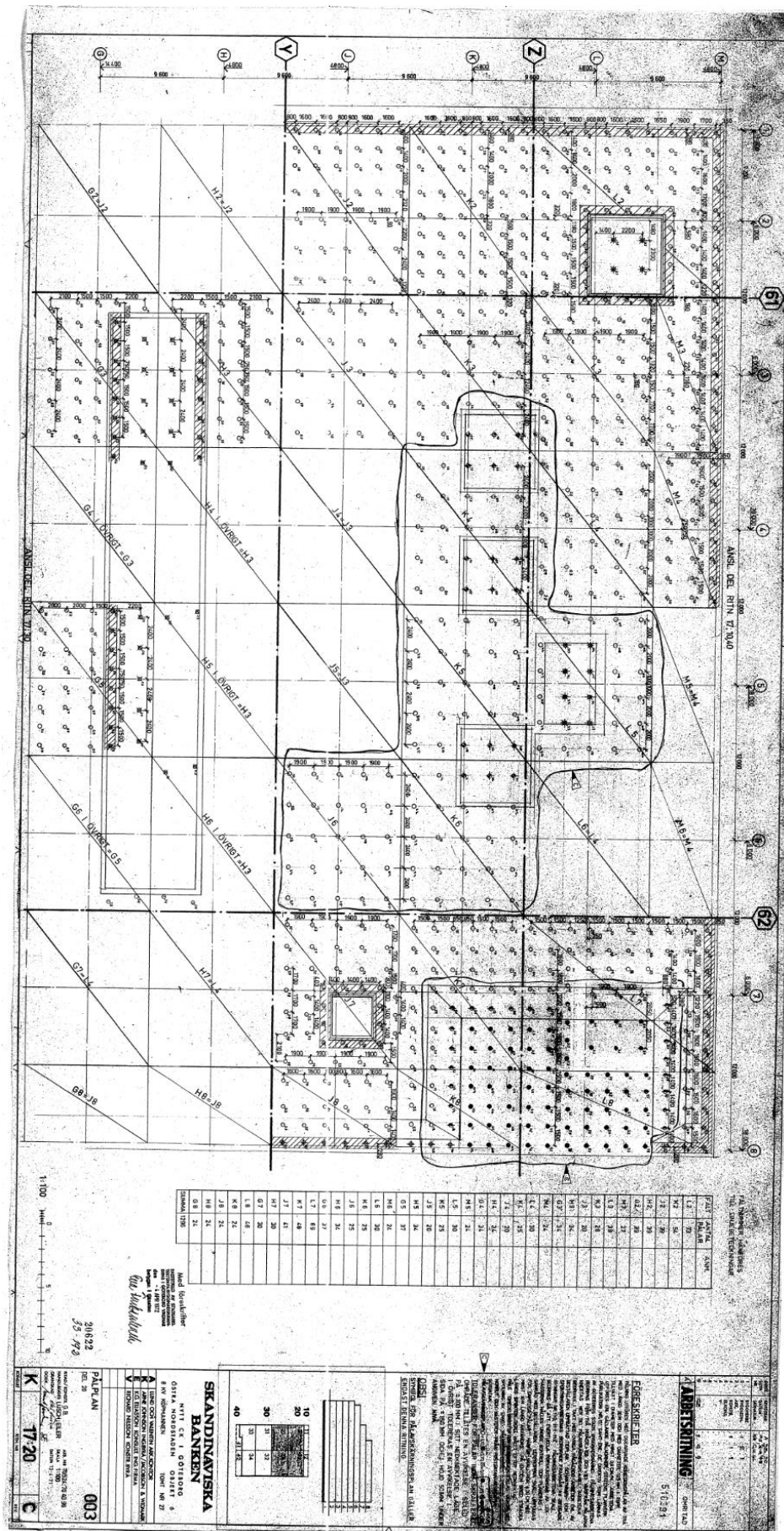


Figure A 3 Construction drawing for location of the piles.

Each colour represents a load, presented in the construction drawings above.

Figure B 1 Calculation of load acting on each pillar, based on construction drawings in figures A1-A3.

Table B 1 Dead weight load + working load acting on the foundation from the pillars. All different load steps are included

Loading scenario	Factor, pillars	Dead weight load+ working load [kN]							
		Pillar	Pillar 2	Pillar 3	Pillar 4	Pillar 5 [k]	Pillar 6	Pillar 7	Pillar 8
Original construction	1,00	1373	5479	6599	6761	7156	6344	6612	2374
10 kPa	1,18	1617	6454	7774	7965	8430	7474	7790	2797
20 kPa	1,36	1862	7430	8949	9169	9704	8604	8967	3220
30 kPa	1,53	2106	8405	10125	10373	10979	9733	10144	3643
40 kPa	1,71	2350	9381	11300	11577	12253	10863	11322	4065
50 kPa	1,89	2595	10357	12475	12781	13527	11993	12499	4488

Table B 2 Summary of ng on the foundation. All different load steps are included.

Loading scenario	Tot Pillars	Area cross-section [m ²]	Load Pillars [kPa]	Load plate	Tot Load [kPa]
Original construction	42699	760,3	56,2	39,8	96,0
10 kPa	50302	760,3	66,2	39,8	106,0
20 kPa	57905	760,3	76,2	39,8	116,0
30 kPa	65508	760,3	86,2	39,8	126,0
40 kPa	73112	760,3	96,2	39,8	136,0
50 kPa	80715	760,3	106,2	39,8	146,0

Appendix C- Soil test evaluations

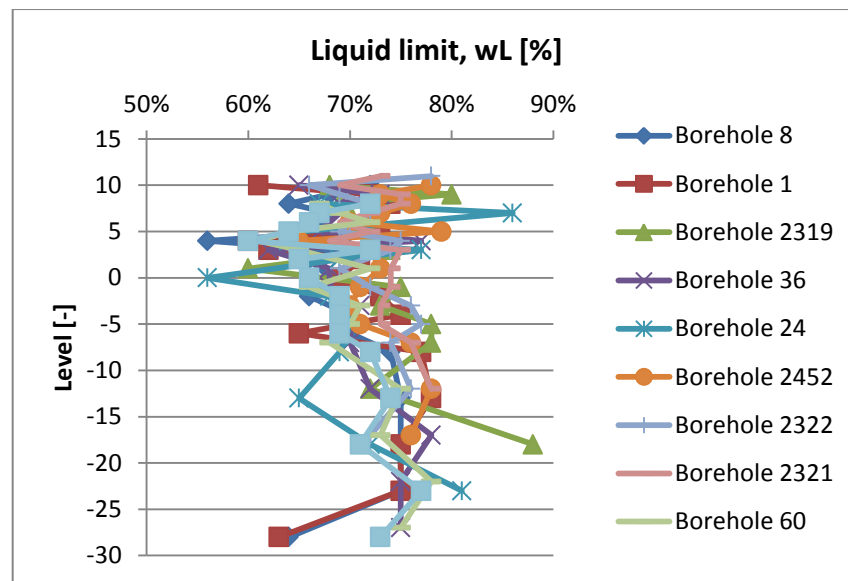


Figure C 1 Liquid limit plotted versus level.

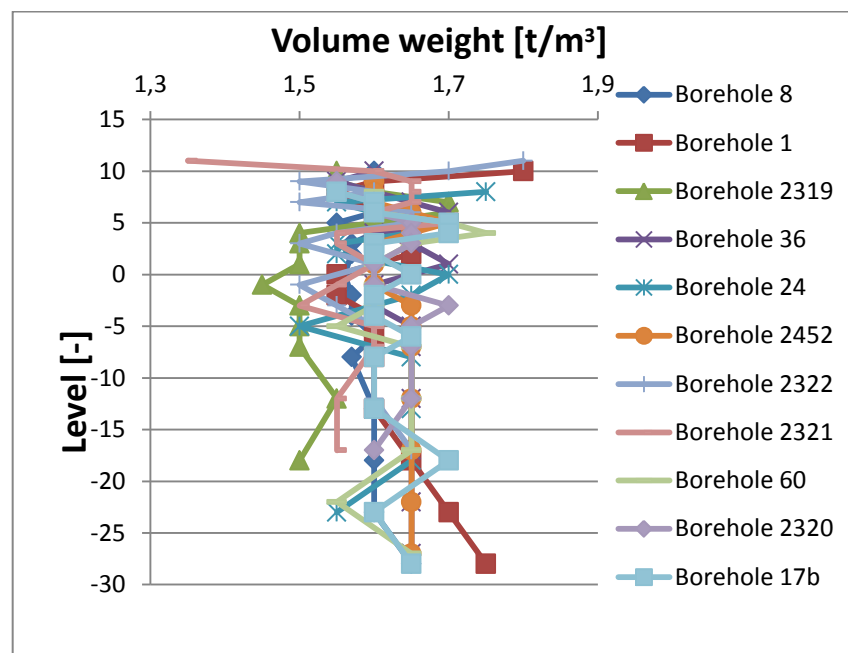


Figure C 2 Volume weight plotted versus level.

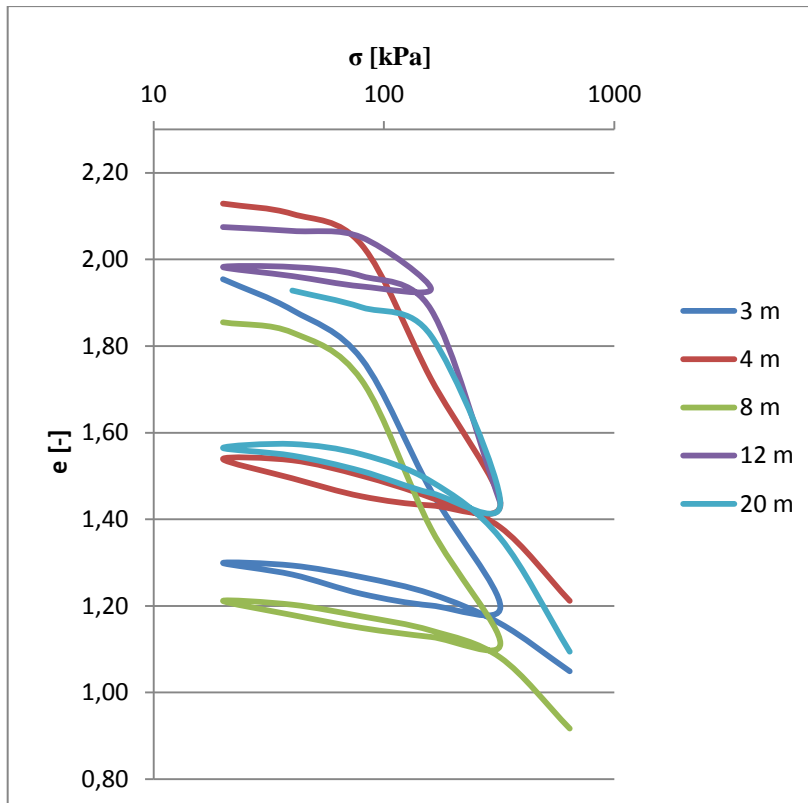


Figure C 3 Oedometer tests for borehole 1. Stress plotted versus void ratio.

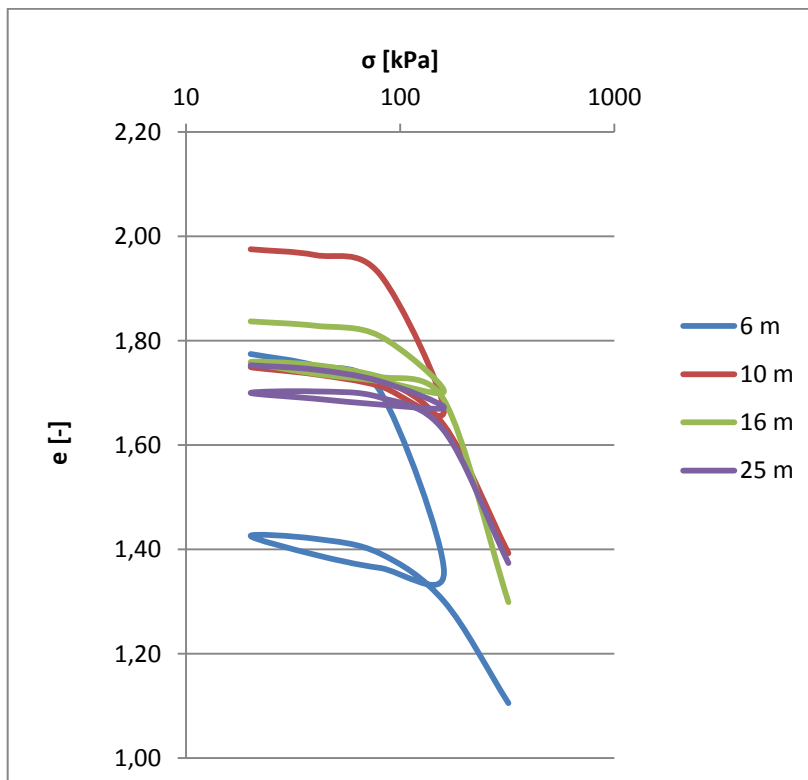


Figure C 4 Oedometer tests for borehole 17b. Stress plotted versus void ratio.

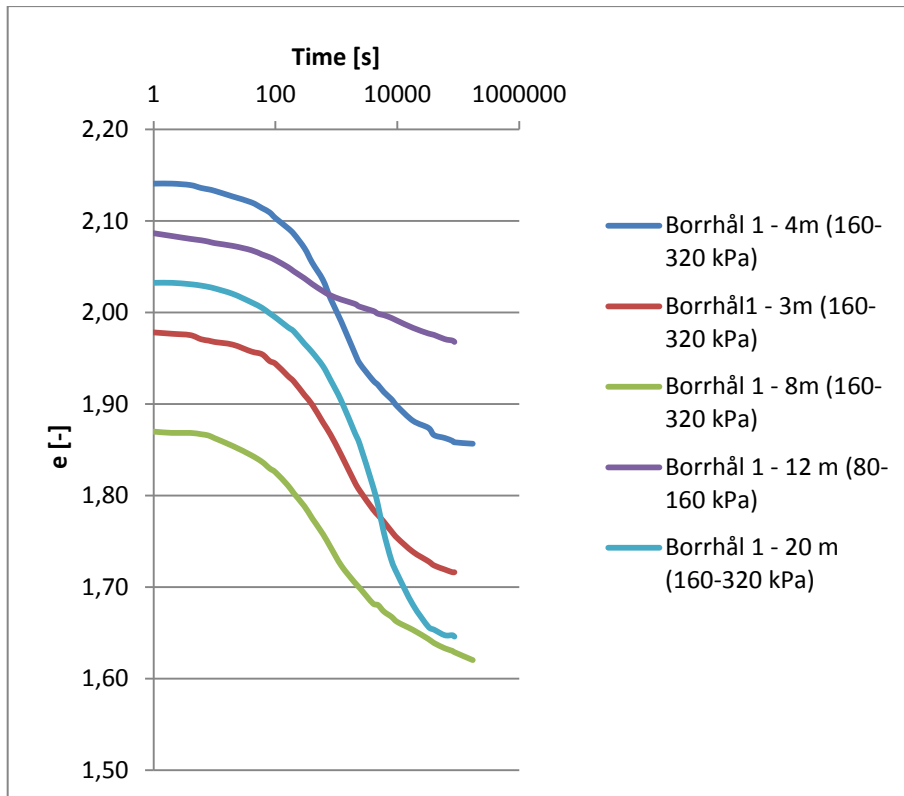


Figure C 5 Oedometer tests for borehole 1. Time versus void ratio plotted for the loading stages used when evaluating C_a .

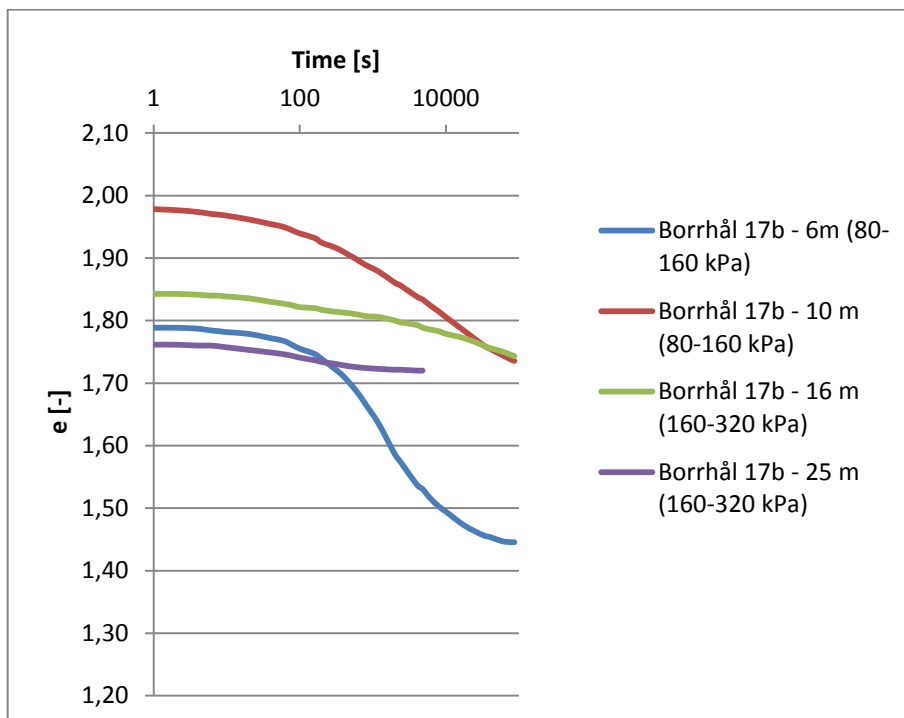


Figure C 6 Oedometer tests for borehole 17b. Time versus void ratio plotted for the loading stages used when evaluating C_a .

Table C 1 Evaluation of permeability for borehole 1

3 m			[m ² /s]	[m ² /kN]		
log(sigma) [kPa]		e1	Cv	mv	ky	kx
	Load					
20		1,95				
40		1,88				
80		1,77				
160		1,47	1,30E-08	1,37E-03	1,78E-10	2,67E-10
320		1,20	1,65E-08	6,79E-04	1,12E-10	1,68E-10
	Unload					
160		1,20				
80		1,23				
40		1,27				
20		1,30				
	Reload					
40		1,29				
80		1,27				
160		1,23				
320		1,16				
640		1,05	1,25E-08	1,59E-04	1,99E-11	2,99E-11
				Average	1,03E-10	1,55E-10
				/day	8,94E-06	1,34E-05

4 m			[m ² /s]	[m ² /kN]		
log(sigma) [kPa]		e1	Cv	mv	ky	kx
	Load					
		0,00				
		2,13				
		2,11				
		2,03				
		1,72	1,50E-08	1,28E-03	1,91E-10	2,87E-10
		1,44	2,00E-08	6,63E-04	1,33E-10	1,99E-10
	Unload					
		0,00				
		1,43				
		1,45				
		1,49				
		1,54				
	Reload					
		0,00				
		1,54				
		1,50				
		1,45				
		1,38				
		1,21	1,90E-08	2,23E-04	4,23E-11	6,35E-11
				Average	1,22E-10	1,83E-10
				/day	1,06E-05	1,58E-05

8 m			[m ² /s]	[m ² /kN]		
log(sigma) [kPa]		e1	Cv	mv	ky	kx
	Load					
20		0				
		1,86				
40		1,83				
80		1,72				
160		1,38	1,90E-08	1,57E-03	2,99E-10	4,48E-10
320		1,11	2,60E-08	6,97E-04	1,81E-10	2,72E-10
	Unload					
		0,00				
160		1,13				
80		1,15				
40		1,18				
20		1,21				
	Reload					
		0,00				
40		1,20				
80		1,18				
160		1,14				
320		1,08				
640		0,92	3,40E-08	0,000246027	8,36E-11	1,25E-10
				Average	1,88E-10	2,82E-10
				/day	1,62E-05	2,44E-05

12 m			[m ² /s]	[m ² /kN]		
log(sigma) [kPa]		e1	Cv	mv	ky	kx
	Load					
		0				
		2,07				
		2,07				
		2,05				
		1,93				
		0,00				
	Unload					
		0,00				
		0,00				
		1,94				
		1,96				
		1,98				
	Reload					
		0,00				
		1,98				
		1,96				
		1,88				
		1,44	1,20E-08	9,68E-04	1,16E-10	1,74E-10
		0,00				
				/day	1,00E-05	1,51E-05

20 m			[m ² /s]	[m ² /kN]		
log(sigma) [kPa]		e1	Cv	mv	ky	kx
	Load					
		0				
20		0,00				
40		1,93				
80		1,89				
160		1,82				
320		1,44	5,00E-09	8,57E-04	4,28E-11	6,43E-11
	Unload					
160		1,46				
80		1,51				
40		1,55				
20		1,56				
	Reload					
40		1,57				
80		1,55				
160		1,49				
320		1,36				
640		1,09	2,50E-08	3,48E-04	8,69E-11	1,30E-10
				Average	6,49E-11	9,73E-11
				/day	5,60468E-06	8,41E-06

Table C 2 Evaluation of permeability for borhehole 17b

6 m						10 m					
			[m ² /s]	[m ² /kN]					[m ² /s]	[m ² /kN]	
log(sigma) [kPa]	e1	Cv	mv	ky	kx	e1	Cv	mv	ky	kx	
0 Load						0 Load					
20	1,775					1,9755114					
40	1,752					1,964357					
80	1,705					1,9281052					
160	1,356	1,30E-08	0,001610825	2,09E-10	3,14E-10	1,6659768	1,00E-08	0,001119	1,12E-10	1,68E-10	
320						0					
0 Unload						0 Unload					
160						0					
80	1,365					1,713383					
40	1,390					1,7356918					
20	1,426					1,7496348					
0 Reload						0 Reload					
40	1,421					1,7468462					
80	1,393					1,727326					
160	1,301					1,6380908					
320	1,105	1,30E-08	0,000530303	6,89E-11	1,03E-10	1,392694	3,50E-08	0,000581	2,03E-10	3,05E-10	
660											
			Average	1,39E-10	2,09E-10			Average	1,58E-10	2,37E-10	
			/day	1,2E-05	1,8E-05			/day	1,36E-05	2,04E-05	

16 m						25 m					
			[m ² /s]	[m ² /kN]					[m ² /s]	[m ² /kN]	
log(sigma) [kPa]	e1	Cv	mv	ky	kx	e1	Cv	mv	ky	kx	
0 Load						0 Load					
20	1,837					1,7531342					
40	1,829					1,7447684					
80	1,809					1,7224596					
160	1,703					1,6722648	1,00E-08	0,00023	2,30E-11	3,46E-11	
320						0					
0 Unload						0 Unload					
160						0					
80	1,723					1,677842					
40	1,737					1,6889964					
20	1,759					1,7001508					
0 Reload						0 Reload					
40	1,754					1,7029394					
80	1,731					1,691785					
160	1,687					1,6276472					
320	1,299	2,20E-08	0,00090172	1,98E-10	2,98E-10	1,3738846	3,50E-08	0,000604	2,11E-10	3,17E-10	
660											
			/day	1,71E-05	2,57E-05			Average	1,17E-10	1,76E-10	
								/day	1,01E-05	1,52E-05	

Table C 3 Hand calculated stress analysis

Nivå	Depth [m]	z from y=5.8	σ_v [kPa]	u [kPa]	σ'_o [kPa]	σ'_c [kPa]	OCR	KoOC	KoNC	σ'_c creep [kPa]	σ'_z	$\Delta\sigma_z$	$\sigma'_z + \Delta\sigma_z$
12,1	0		0		0					0			
10,1	2		36	0	36					0			
9,1	3		52	10	42	80	1,90	0,69	0,5	64			
8,1	4		68	20	48	90	1,88	0,68	0,5	72			
6,1	6		100	40	60	84	1,40	0,59	0,5	67,2			
5,8	6,3	0	104,8	43	61,8	75	1,21	0,55	0,5	60	0	53	53
4,1	8	1,7	132	60	72	82	1,14	0,53	0,5	65,6	10,2	51,0	61,2
2,1	10	3,7	164	80	84	94	1,12	0,53	0,5	75,2	22,2	48,8	71,0
0,1	12	5,7	196	100	96	110	1,15	0,54	0,5	88	34,2	46,7	80,9
-3,9	16	9,7	260	140	120	140	1,17	0,54	0,5	112	58,2	42,9	101,1
-7,9	20	13,7	324	180	144	170	1,18	0,54	0,5	136	82,2	39,5	121,7
γ_{clay} [kN/m ³]	16			width [m]	79,2								
γ_{fill} [kN/m ³]	18			length [m]	96								
				q [kPa]	96								
				q' [kPa]	53	(load without uplifting water pressure)							

Table C 4 Hand calculations for design limits

	Edge	Middle	
Length	1,5	2,4	[m]
Width	1,5	1,9	[m]
Area	2,25	4,56	[m ²]
q_new_b	9,6	9,6	[MP/m ²]
q_ground	5,1	5,1	[MP/m ²]
q_pile	45,9	45,9	MP
q_water_now	3,9	3,8	[MP/m ²]
q_water_org. Design	5	5	[MP/m ²]
q_excavated	10,4	10,4	[MP/m ²]
q_piles	20,4	10,1	[MP/m ²]

Appendix D – Continuous beams with uniformly distributed loads – Sectional forces




load case	max. field moment (factor: qL^2)					support moment (factor: qL^2)					reaction forces (factor: qL)				
	M_1	M_2	M_3	M_4	M_5	M_B	M_C	M_D	M_E	A	B_v B_h	C_v C_h	D_v D_h	E_v E_h	
2 spans 	0,0703 0,0703					-0,1250					0,3750				
	0,0957					-0,0625					0,4375				
3 spans 	0,0800 0,0250 0,0800					-0,1000 -0,1000					0,4000				
	0,1013					-0,0500 -0,0500					0,4500				
	0,0750					-0,0500 -0,0500					-0,0500				
	0,0735 0,0535					-0,1167 -0,0333					0,3833				
	0,0939					-0,0667 +0,0167					0,4333				
4 spans 	0,0772 0,0364 0,0364 0,0772					-0,1071 -0,0714 -0,1071					0,3929				
	0,0996					-0,0536 -0,0357 -0,0536					0,4464				
	0,0720 0,0610					-0,1205 -0,0179 -0,0580					0,3795				
	0,0561 0,0561					-0,0357 -0,1072 -0,0357					-0,0357				
	0,0940					-0,0665 +0,0179 -0,0045					0,4335				
	0,0737					-0,0491 -0,0536 +0,0134					-0,0491				

Figure D 1 Force distribution for pillars supporting a continuous beam.

Appendix E – Settlement limits

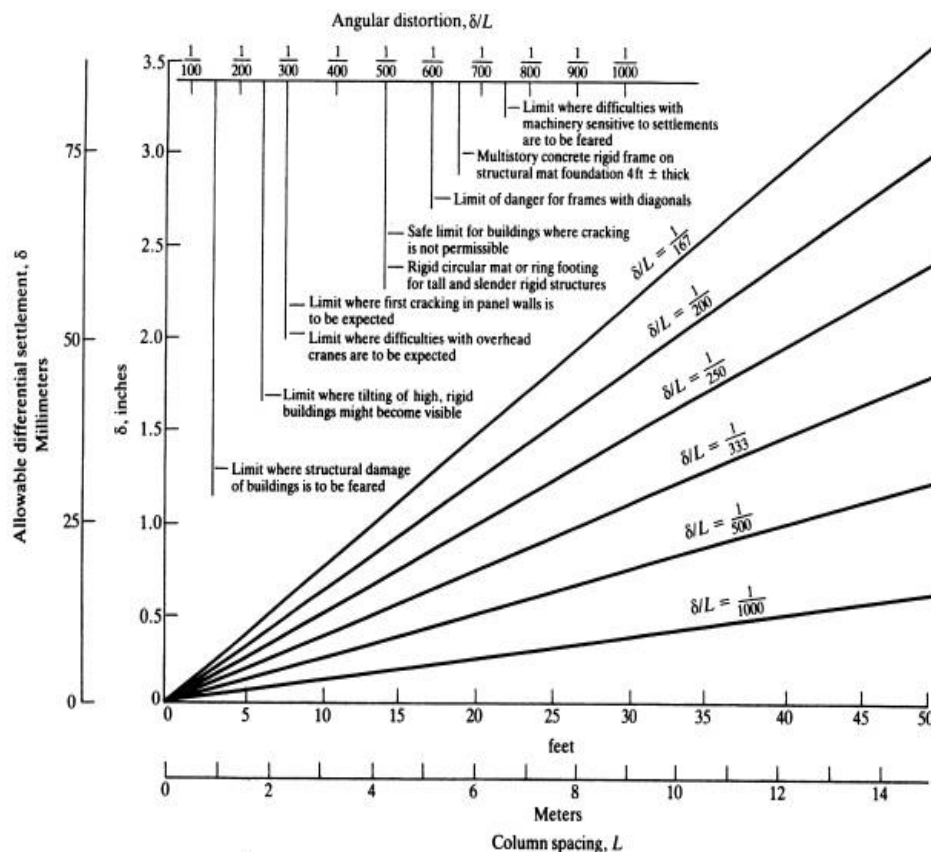


Fig. 5.59 Tolerable settlements for buildings. (Bjerrum, 1963; U.S. Navy, 1982.)

TABLE 5.13 LIMITING SETTLEMENTS FOR STRUCTURES*.

Type of Movement	Limiting Factor	Maximum Allowable Settlement or Differential Movement
Total settlement	Drainage	6 to 12 in
	Access	12 to 24 in
	Probability of nonuniform settlement	
	Masonry-walled structure	1 to 2 in
	Framed structures	2 to 4 in
	Smokestacks, silos, mats	3 to 12 in
Tilting	Stability against overturning	Depends on height and weight
Most maintain B.C. safety	Tilting of smokestacks, towers	$0.004h$
	Rolling of trucks, etc.	$0.01L$
	Stacking of goods	$0.01L (\sim 1/100)$
	Machine operation—cotton loom	$0.003L$
	Machine operation—turbogenerator	$0.0002L$
	Crane rails	$0.003L$
	Drainage of floors	$0.01L$ to $0.02L$
Differential movement	High continuous brick walls	$0.0005L$ to $0.001L (\sim 1/300)$
	One-story brick mill building, wall cracking	$0.001L$ to $0.02L$
	Plaster cracking (gypsum)	$0.001L (1/600)$
	Reinforced-concrete building frame	$0.0025L$ to $0.004L (\sim 1/150$ to $1/170)$
	Reinforced-concrete building curtain walls	$0.003L$
	Steel frame, continuous	$0.002L$
	Simple steel frame	$0.005L$

* After Sowers (1962), Perloff and Baron (1976, p. 517).

Note: L = distance between adjacent columns that settle different amounts, or between any two points that settle differently. Higher values of allowable settlement are for regular settlements and more tolerant structures. Lower values are for irregular settlements and critical structures.

Figure E 1 Settlement limitations for structures (Holtz, 1991).

Appendix F – Settlement readings

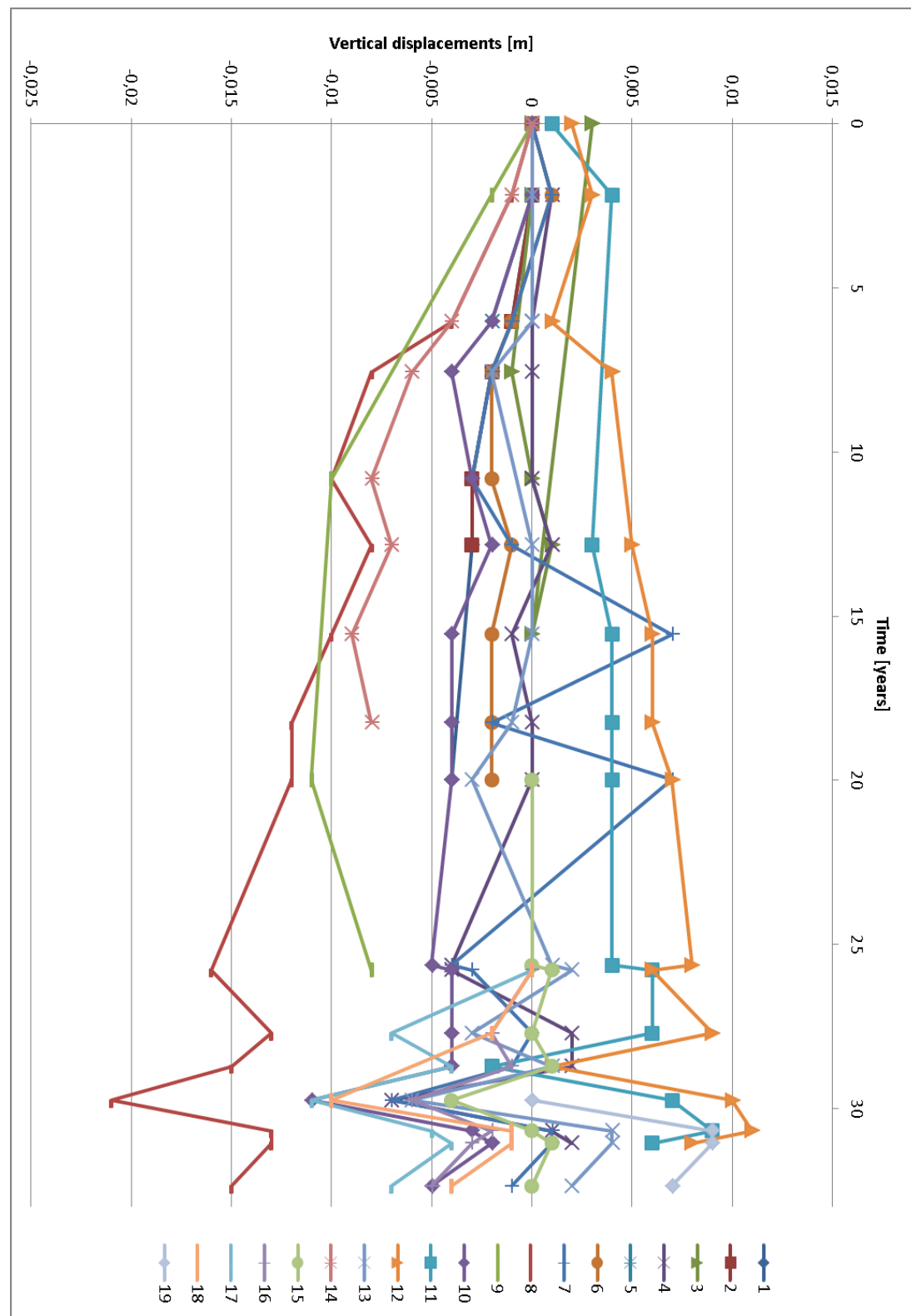


Figure F 1 Reading of settlement targets for Nordstaden 8:27 between 1978-2010.

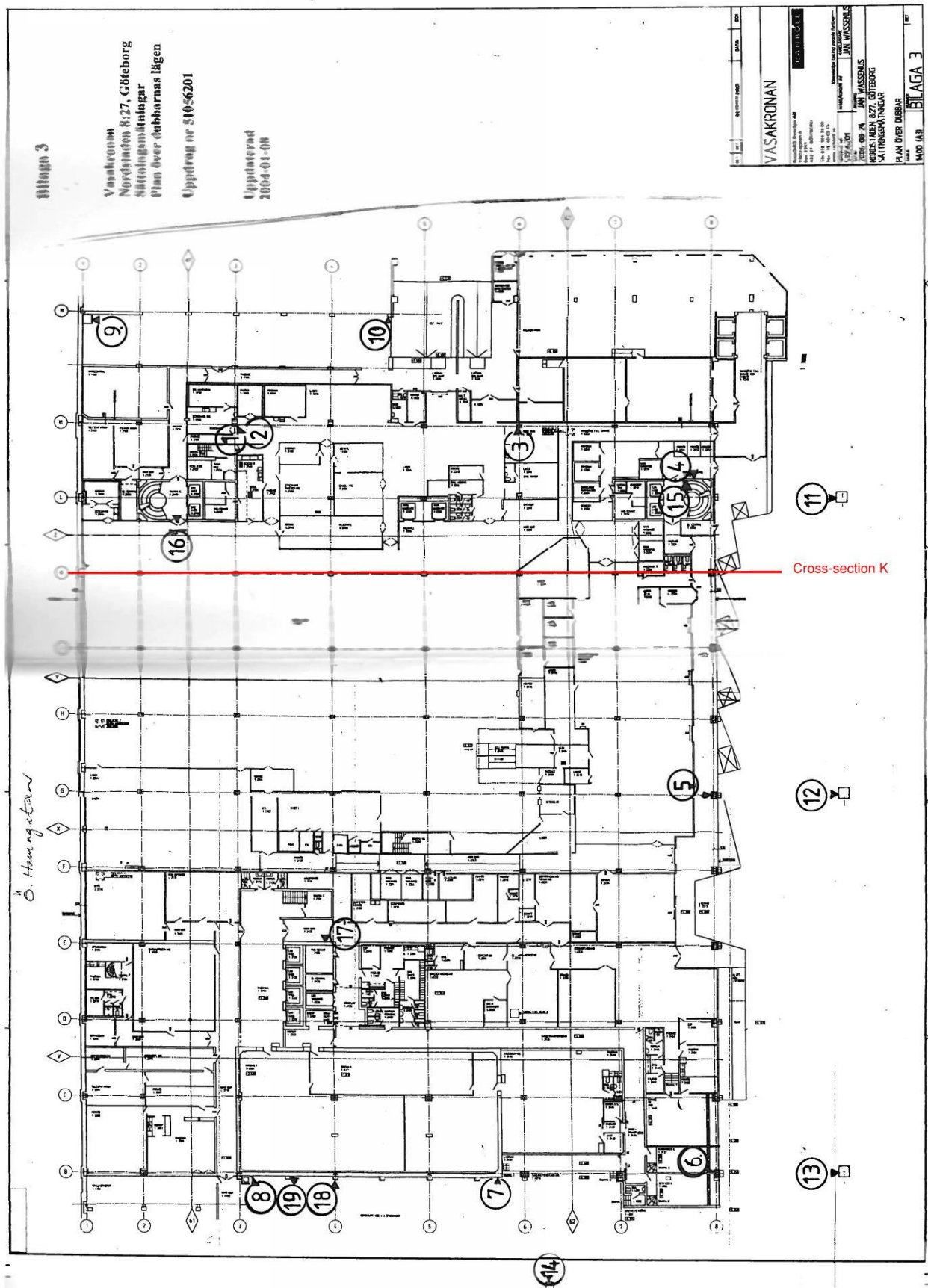


Figure F 2 Location of settlement targets at Nordstaden 8:27.